DESIGN OF A SATELLITE RF RECEIVER AT KU-BAND FOR TROPICAL REGION

BY

ARAFAT A.A. SHABANA

INTERNATIONAL ISLAMIC UNIVERSITY
MALAYSIA

2011

DESIGN OF A SATELLITE RF RECEIVER AT KU-BAND FOR TROPICAL REGION

BY

ARAFAT A.A. SHABANA

A dissertation submitted in partial fulfilment of the requirements for the degree of Master of Science in Communication Engineering

Kulliyyah of Engineering

International Islamic University
Malaysia

FEBRUARY 2011

ABSTRACT

Receivers designed at Ku-Band are very critical and challenging. Satellite signals travel a very long path and consequently losses and noises are high. Hence, the design of low noise amplifier, bandpass filter, and downconverter need careful consideration at satellite receivers, especially at Ku-Band. A Low Noise Amplifier (LNA) is designed with 8.90 dB gain and 2.188 dB noise figure at Ku-Band. Bandpass filter is designed with operating frequency ranges from 11.966GHz to 12.052GHz and bandwidth of 86MHz. Downconverter is also designed to converts 12GHz to 1GHz at Ku Band with bandwidth of 475MHz. All designs are based on Microwave Office Simulator (AWR) 2006 version and optimized through many simulation and analysis of results. Tropical region suffers from high humidity, high temperature, and heavy rainfall. These factors critically affect the captured signal especially when the frequency goes above 10GHz. Three characteristics of atmospheric losses at Ku-Band link budget are investigated: scintillation, Cross-Polarization Depolarization (XPD), and rain fade attenuation. All designed components (LNA, BPF, DC) are also simulated in system level using Visual Simulation System (VSS). The performance of the designed receiver at clear air and raining condition are investigated using various modulation schemes. The performance during raining condition using vertical, horizontal, and circular polarizations with different availabilities is also investigated and presented in this thesis. A comparison between 16-PSK and 16-QAM is done and presented in this work. The 16-PSK values for the availability $A_{0.1\%}$, $A_{0.01\%}$, and $A_{0.001\%}$ in vertical polarization are found to be better than the results in 16-QAM. The designed satellite receiver at $A_{0.1\%}$ availability gives the best BER with vertical polarization. At the same time, the values of the bit error rate are proportional with the availability.

ملخص البحث

يُعتَبرُ جهازُ المستقبِلِ في الأقمارِ الصِّناعيةِ منَ المكوّناتِ الحسّاسة و المهمّةِ في نظامِ المايكروويف اللّاسلكيِّ (RF). يعرفُ التّشتّتُ الناتجُ عنِ المطرِ أنّهُ امتصاصُ أو تبددُ إشارةِ المايكروويف بسببِ قطراتِ الماءِ، وهذا التشتتُ يُصبحُ مسألةً حرجةً عندَ ترددٍ أعلى من 10 جيجا هرتز. تعاني المناطقَ الاستوائيةَ من ظاهرةِ التَّشتتِ بشكلٍ كبير وذلك نظراً لارتفاعِ نسبةِ الأمطارِ وغزارتِها والرطوبةِ العاليةِ ودرجاتِ الحرارةِ المرتفعةِ أيضاً، وهذهِ العواملُ تؤثرُ على الإشاراتِ المستقبَلَةِ ممّا يؤدي إلى ضَعفِها وردائتِها، وهذهِ المسألةُ تعتبرُ قضيةً حساسةً ومصدراً للمشاكلِ في المناطقِ الاستوائيةِ. يقعُ المستقبِلُ في بدايةِ أجهزةِ الاتصالِ، وتحدَّدُ وظيفتُه بشكلٍ عام في أنَّهُ يستقبلُ الإشاراتِ من اللّاقطِ الهوائيِّ الموجودِ في مقدمةِ نظامِ الاتصالاتِ، وبعدَ استقبالِهِ للإشاراتِ يعملُ على تنقيتِها من التّشويشِ غيرِ اللّازمِ أو الزائدِ عن الحدِّ، ويعالجُها مروراً بباقي أجزاءِ المستقبِلِ. ويتكونُ المستقبِلُ للأقمارِ الصناعيةِ من "مضخِّمِ الإشارةِ و مُخفِّفِ التشويشِ"(LNA)،والمنقِّحِ للإشارةِ الملتَقَطَةِ(BPF)، ومحوّلِ التّرددِ (DownConverter).يعملُ مضخمُ الإشارةِ على تضخيمِ الإشارةِ الضعيفةِ والقادمةِ من اللّاقط الهوائيِّ والتّخفيفِ من حدةِ التّشويشِ فيها، أمّا المنقّحُ أو (الفلتر) فإنّه يقومُ بتنقيةِ الإشارةِ من الشوائبِ والتّشويشِ الزّائدِ فيها حتى تكونَ صالحةً للاستعمالِ دونَ مشاكل، فيما يقومُ محولُ التّرددِ بتحويلِ التّرددِ العالِي من 12 جيجا هيرتز إلى 1 جيجا هيرتز وذلكَ لجعلِ الإشارةِ صالحةً للاستخدامِ. هناكَ ثلاثةُ عواملٍ تمَّ حسابُها باعتبارِها مُؤَثِّرةً بشكلٍ مباشرٍ على الإشارةِ، وهذهِ الخصائصُ هيَ الوميضُ والاستقطاب المتقاطعُ والتَّشويشُ الذي تسبّبُه كثافةُ المطرِ. في هذهِ الدراسةِ تمَّ تصميمُ ومناقشةُ نتائجِ المستقبِلِ، وذلكَ باستخدامِ AWR وتمَّ الحصولُ على نتائجَ ممتازةٍ. علاوةً على ذلكَ تمَّتْ مراقبةُ وفحصُ التغيّرِ في معدلِ الخطأ(BER) لهذا المستقبل عندَ الإشاراتِ 16-PSKو 16-QAM في الهواءِ النَّقيِّ ومعَ الهواءِ الذي يحتوي على التّشويشِ في حالة هطول الامطار وذلكَ بواسطةِ VSS.وفي النهايةِ أوجدَ هذا البحثُ نظاماً ونوعيةً جديدةً من المستقبِلِ للأقمارِ الصِّناعيةِ قادراً على التعامل والتخفيفِ من المشاكلِ التي تواجهُ أجهزةَ الاستقبالِ في المناطقِ الاستوائيةِ مثلَ ماليزيا والعملِ على تحسينِ نوعيةِ الإشارة الملتَقَطةِ.

APPROVAL PAGE

I certify that I have supervised and read this study and that in my opinion; it conforms to acceptable standards of scholarly presentation and is fully adequate, in scope and quality, as a thesis for the degree of Master of Science (Communications Engineering)

……
MD Rafiqul Islam
Supervisor

I certify that I have read this study and that in my opinion it conforms to acceptable standards of scholarly presentation and is fully adequate, in scope and quality, as a thesis for the degree of Master of Science (Communications Engineering)

……
Rashid Abdelhaleem Saeed
Examiner

This dissertation was submitted to the Department of Electrical and Computer Engineering and is accepted as a partial fulfilment of the requirements for the degree of Master of Science (Communications Engineering)

……
Othman O. Khalifa
Head, Department of
Electrical and Computer
Engineering

This dissertation was submitted to the Kulliyyah of Engineering and is accepted as partial fulfilment of the requirements for the degree of Master of Science (Communications Engineering)

……
Amir Akramin Shafie
Dean, Kulliyyah of
Engineering

DECLARATION

I hereby declare that this dissertation is the result of my own investigations, except where otherwise stated. I also declare that it has not been previously or concurrently submitted as a whole for any other degrees at IIUM or other institutions.

Arafat A.A Shabana

Signature …… Date ……..

INTERNATIONAL ISLAMIC UNIVERSITY MALAYSIA

DECLARATION OF COPYRIGHT AND AFFIRMATION OF FAIR USE OF UNPUBLISHED RESEARCH

DESIGN OF A SATELLITE RF RECEIVER AT KU-BAND FOR TROPICAL REGION

1. No part of this unpublished research may be reproduced, stored in a retrieval system, or transmitted, in any form or by any means, electronic, mechanical, photocopying, recording or otherwise without prior written permission of the copyright holder except as provided below

2. Any material contained in or derived from this unpublished research may only be used by others in their writing with due acknowledgement.

3. IIUM or its library will have the right to make and transmit copies (print or electronic) for institutional and academic purposes.

4. The IIUM library will have the right to make, store in a retrieval system and supply copies of this unpublished research if requested by other universities and research libraries.

Affirmed by Arafat A.A Shabana

---------- ----------

Signature Date

ACKNOWLEDGEMENTS

In the name of Allah, the Most Merciful, the Most Compassionate

Praise and thanks are due to Allah, the Lord and the Creator. His bounties on me are countless. This work would not have been complete without His guidance and support. I pray to Allah that He accepts from me this humble work and account it in my good deeds.

The advice and directions of Assoc. Prof. Dr. MD Rafiqul Islam, my advisor, can never be forgotten. He pushed me to reach my limits in a very genteel and polite way. His continuous encouragement, invaluable comments, fruitful suggestions and consistent guidance are highly appreciated. I have learned a lot from working with him; I owe my thanks to him for all that.

I would like to express my deep and grateful thanks to my co-supervisor Assoc. Prof. Dr. A.H.M. Zahirul Alam for his excellent help, timely suggestions, guidance and active support.

Special sincere thanks are also extended to every person who cooperated with me to finish this study, especially; Alhareth Zyoud**,** Haytham Shabana, Marwan Badran, Belal Salhab, Aladdin Assaiqeli and Ibrahim Zyoud May Allah reward them all.

Finally special heartfelt thanks are due to my mother, the pure soul of my father, my beloved brother (Abbas) may Allah release him from the Israeli jail, my sisters and their husbands, for being there, giving me the strength and much needed moral support, and consistently motivating me to further my higher studies.

TABLE OF CONTENTS

LIST OF TABLES

LIST OF FIGURES

LIST OF ABBREVIATIONS

AF	Audio Frequency
AM	Amplitude Modulation
ASK	Amplitude-Shift Keying
AWGN	White Gaussian Noise Channel
AWR	Microwave Office Simulator
AWRDE	Applied Wave Research Design Environment
BER	Bit Error Rate
BJT	Bipolar Junction Transistor
BPF	Bandpass Filter
CAD	Computer Aided Design
dB	Decibel
dBm	Decibel Mili Watt
DBS	Direct Broadcast Satellite
DC	Downconverter
ECM	Edge Coupled Microstrip
EM	Electromagnetic
FET	Field-Effect Transistor
GaAs	Gallium Arsenide
HEMT	High Electron-Mobility Transistor
IF	Intermediate Frequency
ITU-R	International Telecommunication Union Radiocommunication Sector
LNA	Low Noise Amplifier
LNB	Low Noise Block

LO	Local Oscillator
MBEND	Bend Mitered Arbitrary Angle
MCFIL	Coupled Line Section for Filters
MESFET	Metal Semiconductor Field Effect Transistor
MIM	Metal-Insulatormetal
MLIN	Microstrip Transmission Line
MMIC	Monolithic Microwave Integrated Circuits
NF	Noise Figure
PHEMT	Pseudomorphic High Electron Mobility Transistor
PTH	Parathyroid Hormone
QAM	Quadrature Amplitude Modulation
QPSK	Quadrature Phase Shift Keying
RF	Radio Frequency
SNR	Signal-to-Noise Ratio
SWR	Stand Wave Ratio
USM	University Sains Malaysia
VSS	Visual Simulating System
VSWR	Voltage Standing Wave Ratio
XPD	Cross-Polarization Depolarization

LIST OF SYMBOLS

B	Bandwidth
C_σ	Canting angle-dependent
D	Antenna Diameter
D_{eff}	Effective antenna diameter
F	Frequency
f_B	Filter bandwidth
G	Gain
H	Humidity
h	Distance from the surface of the earth to the satellite orbit
h_L	Height of turbulent layer
h_s	Height of earth surface above sea level
h_0	Isometric height for Malaysia
K	Stability
k	Boltzmann's constant
L_E	Effective path length
L_G	Horizontal projection
L_s	Slant-path length
R_e	Earth radius
T	Absolute temperature of the load or the system
σ	Standard deviation
ζ	Fade slope
φ	Elevation angle

Θ	Elevation angle
Φ	Latitude of earth station
λ	Difference in longitude
η	Antenna Efficiency
γ_R	Specific attenuation
ε_r	Relative dielectric constant

CHAPTER ONE

INTRODUCTION

1.1 BACKGROUND

The use of microwave satellite receivers in communications systems is a part of everyday life and can sometimes be out-matched by natural factors. It is a phenomenon known as signal attenuation which weakens the microwave signal as it passes through a satellite receiver. This project aims to design, simulate, and investigate the satellite receiver performance for tropical region. This research concentrates on receivers designed at Ku-Band and performance analysis in tropical regions. Satellite receivers contain Low Noise Amplifier (LNA), Downconverter (DC), and Band-pass Filter (BPF). The function of the receiver is to receive the signal from the satellite by the antenna as an input, and then it processes and filters it from the noise. This research highlights the design of a satellite RF receiver (low noise amplifier, bandpass filter, and downconverter) to cope with high frequency and investigate the problems with the heavy rainfall that affect the captured signals in tropical regions.

Developing satellite services resulted in the emergence of a need to develop new equipment with improved performance to compete the requirements markets and service suppliers. So, the demand on the evolution of the millimeter- wave elements increases for the broadband communication services. Therefore the receiver is a very important element that is situated in the front step of the communication system. In satellite communication systems, a message signal is transmitted from an earth station via an uplink to a satellite, amplified in a transponder on board of the satellite and then

retransmitted from the satellite via a downlink to another earth station. These earth stations are provided with transmitters and receivers (Scappaviva el at., 2008; Chang el at., 2003).

The Low Noise Block (LNB) consists of Low Noise Amplifier (LNA), mixer, Local Oscillator (LO), Intermediate Frequency (IF) amplifier and image rejection filter. The microwave amplifier usually completes the Low Noise Block (LNB), and is connected to the indoor element using coaxial cable. Low noise amplifiers are found in many applications of microwave and communication circuits and it is one of the most important element blocks in RF front end circuit. In receiver applications, the low noise amplifiers are used in order to amplify the received low power signal and retain low noise. Thus an amplification method for all communication systems is needed because the signal received in real world standard is low in power. As known, the signals are corrupted by internal and external noise. Low noise amplifier receives signals and amplifies them to a suitable level while minimizing the noise it adds. The main function of a low noise amplifier is to give enough gain and introduce as little noise as possible (Dafalla el at., 2004; Abbas and Bin Ihsan, 2005; Long, 2007).

The second device in satellite receiver is the filter, a significant component that is widely used in satellite and terrestrial communications applications. Filters are crucial RF and Microwave components. Modern satellite receiver focuses on the filters for filtering the signals and separates them from its noise level. The third important part in receiver is the downconverter. The function of the downconverter is to convert or change the high frequency signal into low frequency signal.

The use of the Ku-Band for satellite communications in tropical regions like Malaysia is becoming more frequent especially in broadcasting. Many satellites above Malaysia have Ku-Band transponders. The most popular microwave band exploited

for satellite communication is the Ku-Bands. In satellite receiver applications, Ku-Band ranges from 12 to 18 GHz. It is also used for backhauls and particularly for satellites from remote locations back to a television network's studio. The band is divided into multiple segments that vary according to geographical regions identified by the International Telecommunication Union (ITU) (Elbert, 2008).

The tropics are the geographic areas of the earth centered on the equator and limited in latitude by the Tropic of Cancer in the northern hemisphere, at approximately 23°30' (23.5°) N latitude, and the Tropic of Capricorn in the southern hemisphere at 23°30' (23.5°) S latitude as shown in Figure1.1. This area occupying approximately forty percent of the land surface of the earth includes all the areas of the earth where the sun reaches a point directly overhead at least once during the solar year. In the temperate zones, north of the Tropic of Cancer and south of the Tropic of Capricorn, the sun never reaches an angle of 90° or become directly overhead. The word "tropics" comes from the Greek word *tropos,* meaning "turn", because the apparent position of the sun oscillates between the two tropics with a period that defines the average length of a year. Along the equator is the intertropical convergence zone, characterized by high temperatures and year-round heavy rainfall. Due to active vertical uplift or convection of air, precipitation is quite frequent in this area that is accompanied with thunderstorms almost every day. The climate in tropical regions is usually common in places like Kuala Lumpur in Malaysia (Rene el at., 2001).

From the previous features of the tropical regions, there are a lot of factors that affect the received signals from satellites by antennas, so that attenuates the signals with noise and corrupts it.

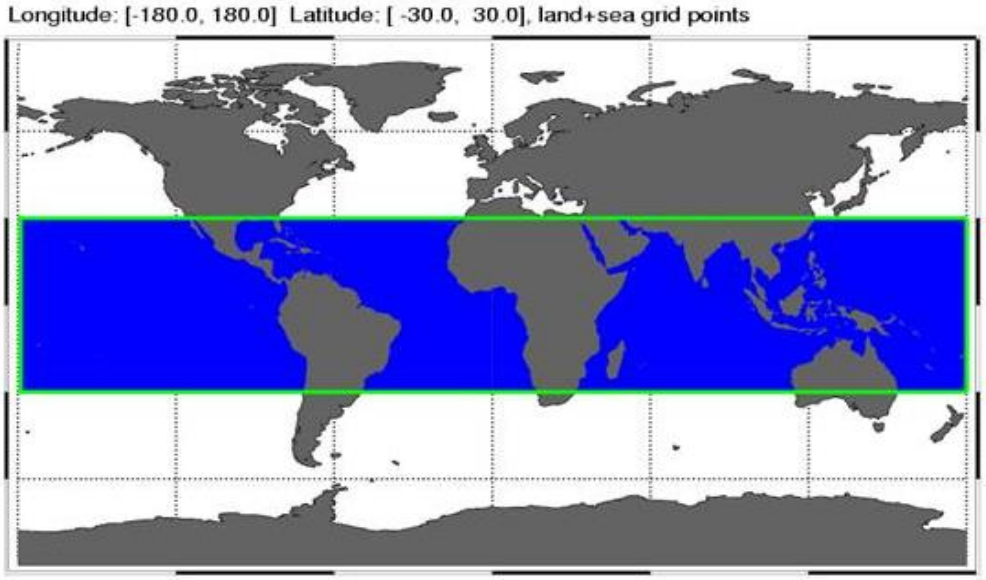

Figure 1.1: Tropical region (www.ecmwf.int, 2010)

1.2 PROBLEM IN EARTH-TO-SATELLITE LINK IN TROPICAL REGION

Rain attenuates the signal such that the signal received is very low, to handle this, a proper Low Noise Amplifier (LNA) should be designed. Attenuation due to rain at frequencies above 10 GHz, may lead to outages that compromise the availability and/or quality of service, making it one of the critical factors in satellite link design. Designing a new telecommunication system requires knowledge of rain attenuation in order to optimize the system capacity, quality and reliability criteria. The tropical regions have higher rain attenuation. Hence, the receiver model has to be improved in order to cope with tropical regions (Pratt el at., 2003).

Investigate the performance of satellite receiver with rain attenuation is the best way. Simulation is the best way or method to prove that it is possible to design a receiver for the earth station that receives the signal with less noise (rain, air, high humidity), and also less effects of attenuation. Furthermore, elements such as low noise amplifier, bandpass filter, and downconverter will be designed through Microwave office simulator. All components will be investigated using Visual System

Simulator (VSS) to check their performance in tropical environment (Abbas and Bin Ihsan, 2005; Pratt el at., 2003).

1.3 PROBLEM STATEMENT AND ITS SIGNIFICANCE

Tropical regions where excessive rain fall is a common phenomenon throughout the year, knowledge of rain attenuation at the frequency of operation becomes extremely required for designing a satellite receiver at Ku-Band. When the signal is received from a satellite to the earth station by antenna, it is usually attenuated and corrupted with noise due to the features of tropical regions such as; heavy rainfall, high humidity, and high temperature (Rene el at., 2001). So, designing an optimized satellite receiver at this high frequency is the best way to minimize and solve this problem, with the aim of enhances the output of the signals with less noise.

Most of the available researches discuss the design of satellite receiver at high frequency; however, this thesis considers the criteria of tropical regions to evaluate the performance of a receiver structure (LNA, BPF, DC). The designed satellite receiver is simulated in tropical environment with a transmitter, in order to observe the performance and the changes of BER for 16-PSK and 16-QAM at different availability with vertical, horizontal, and circular polarizations.

1.4 RESEARCH OBJECTIVES

The main objectives of this research can be summarized as follows:

a) To design a low noise amplifier, based on estimated rain fade for 99.9% availability at Ku-Band in Table 3.1 with vertically polarization, the minimum gain is 8.8dB has been targeted for low noise amplifier design,

and based on available low noise amplifier designs, the noise figure for low noise amplifier must be less than or equal 2.0dB.

b) To design a downconverter with bandwidth around 500MHz, very high gain, and converted high frequency to intermediate frequency such as 12 GHz downconverted to 1GHz.

c) To design a bandpass filter with bandwidth around 86MHz.

d) To estimate the rain fade at Ku-Band for $A_{0.1\%}$, $A_{0.01\%}$, and $A_{0.001\%}$ availability.

e) To evaluate the performance of the designed satellite receiver using estimated rain fade for different modulation schemes with different availabilities.

1.5 RESEARCH METHODOLOGY

In this research, the following steps will take place in order to achieve the objectives required of this study, and the methodology flowchart is shown in Figure 1.2.

a) Study the satellite receiver parameters (low noise amplifier, bandpass filter, and downconverter) at Ku-Band.

b) Familiarize the modules with RF simulator Microwave Office Simulator (AWR), and familiarize the receiver with Visual Simulating System (VSS) simulator 2006 version.

c) Design and simulate the LNA, BPF, and DC at Ku-Band using RF simulator.

d) Optimize the designed parameters of the satellite receiver design.

e) Estimate the rain fade using the available data from ITU-R at Ku-Band for Malaysia.

f) Simulate the receiver in system level using estimated rain to investigate the performance of the receiver with different modulations schemes with different availabilities.

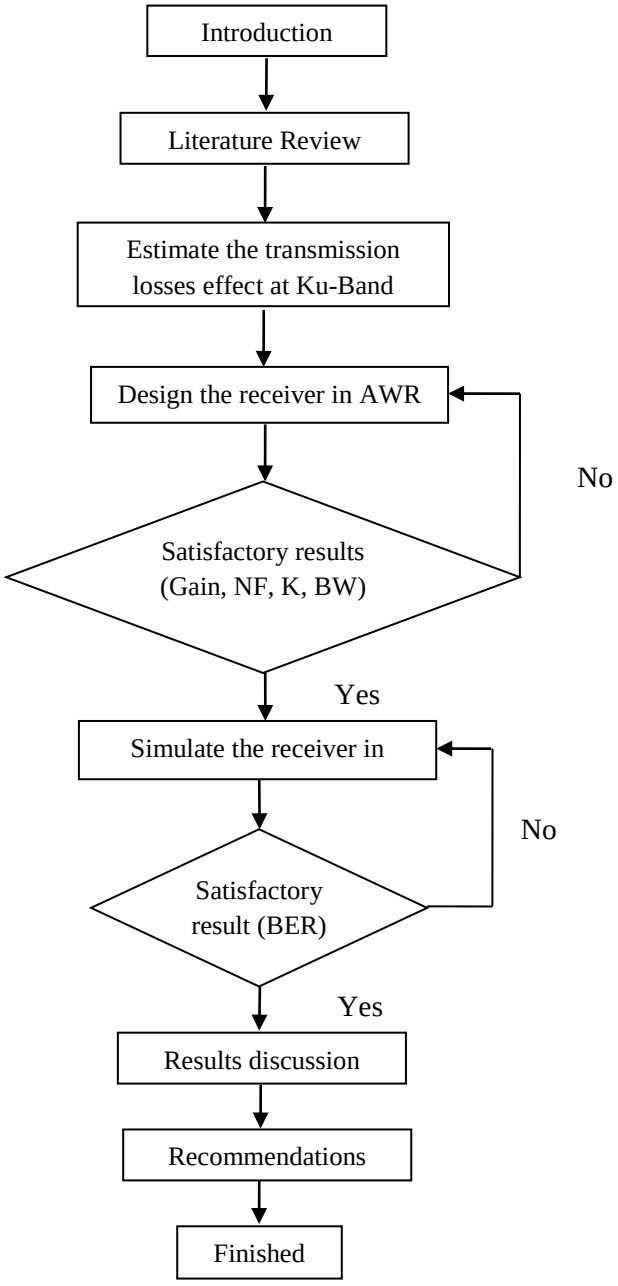

Figure 1.2: Methodology Flowchart

1.6 RESEARCH SCOPE

This project would be essential for communication systems design. Three important design aspects are analyzed and discussed. Low noise amplifier is important to amplify the captured signals and retains low noise figure. Bandpass filter is significant to determine bandwidth and to filter the signal from the noise. Downconverter is consequential to convert the input frequency from 12GHz to 1GHz using oscillator frequency. The scope is to design a satellite receiver at Ku-Band and test the performance in tropical regions to evaluate the BER for different modulation schemes with numerous availabilities.

1.7 THESIS ORGANIZATION

In this thesis, satellite receiver characteristics and their effects are being studied as they are important to the stability of any communication system. Satellite receiver properties of a low noise amplifier, downconverter and bandpass filter design are highlighted. The goal is to design and simulate a new model of receiver that can be used in tropical countries such as Malaysia.

Chapter One is an introduction to the project and its significance, in addition to the methodology used in this work.

Chapter Two is a review of designing models that describe the low noise amplifier, downconverter and bandpass filter. It gives a summary about gain, bandwidth, stability and noise. Definition of these three elements is presented in this chapter.

Chapter Three describes the atmospheric losses that affect the signals at Ku-Band calculations, which include the scintillation, Cross-Polarization Depolarization (XPD), and rain fade attenuation.

Chapter Four studies and discusses the design and results of simulating a low noise amplifier, downconverter and bandpass filter for satellite receivers at Ku-Band, which can handle the signals captured by the antenna.

Chapter Five presents the performance evaluation of receiver in VSS to observe the bit error rate. The presented design, in this chapter is combined with the data in Chapter Three (link budget calculations for Ku-Band) and the design in Chapter Four (receiver design at Ku-Band).

Chapter Six presents the conclusions found and the results of the simulation of the satellite receiver design. Future works and recommendations are also included in this chapter.

CHAPTER TWO

LITRATURE REVIEW

2.1 INTRODUCTION

This chapter highlights the previous studies that were done in the research area. This is in order to give the reader an idea about the design of satellite receiver components at Ku-Band. Three of these parts, namely low noise amplifier, downconverter, and bandpass filter are presented. The next Section presents the design of low noise amplifier. Then, the downconverter design is discussed in Section 2.3. Whereas Section 2.4 discusses the bandpass filter design, and the last Section 2.5 highlights the conclusions of this chapter.

2.2 LOW NOISE AMPLIFIER DESIGN

A Low Noise Amplifier (LNA) is an electronic device used to amplify the input signals received at the front ends of communication systems and retains low noise. Low Noise Amplifiers (LNA) are used in a wide variety of applications such as RF communication systems, including wireless computer networks, mobile phones, navigation use and satellite receivers (Abbas and Bin Ihsan, 2005).

A Low Noise Amplifier (LNA) is the first stage of RF and microwave receivers, so it is a very important element in communication systems. In the assembling process of Direct Broadcast Satellite (DBS) converters, the input matching network is usually tuned by cutting and pasting strip lines in order to optimize their noise figure (Wang el at., 2008).

Most of the available designs of low noise amplifier have low gain with big size. Designing low noise amplifier at Ku-Band needs a lot of issues to be taken care of. Circuits at this high frequency deviate from their normal behavior and are not very easy to implement. Abbas and Bin Ihsan (Abbas and Bin Ihsan, 2005) designed and implemented a LNA at 16 GHz. Different issues regarding simulations and implementations which related to the low noise amplifier design have been discussed. They have explained the design at 16 GHz with noise figure around 2.0 dB and a gain of 10 dB per stage. The design of a low noise amplifier was optimized using momentum for input and output matching networks' simulations. They have resolved two main issues that compromise the accomplishment of LNA design. Furthermore, they discussed the parasitic behaviors of the capacitors at Ku-Band and the solution to this problem was found and implemented.

The amplifier discriminates the relatively weak microwave signals received by the antenna from background noise, and amplifies it to a reasonable required working level. Ain and his team (Ain el at., 2007) designed three stages with PHEMT ATF-36077 LNA at 11GHz. The amplifier is manually designed using conventional techniques. Smith chart was used to do a matching of the input and output of the amplifier. A completed design of the amplifier was optimized using Hewlett-Packard Advanced Design System (HP-ADS) software. The layout of 11 GHz Ku-Band Amplifier design was generated by the software simulation. Microwave amplifier is usually integrated in the Low Noise Block (LNB) and connected to the indoor equipment using a coaxial cable. The DC power supply is fed to the downconverter block using the same cable and typically 12 Volt. Microwave amplifier normally calls for the negative power supply for biasing the Gate of the PHEMT.

The first stage of the amplifier is typically the primary demand of the device that reduces the noise figure, and the second stage provides required gain at reasonable noise figure. A High Electron-Mobility Transistor (HEMT) exhibits lower noise figure and higher gain at microwave frequencies up to 70 GHz. The Hewlett Packard ATF-36077 PHEMT is capable of noise figures and it has very low noise resistance. Through reducing the sensitivity of noise performance to variations in input impedance match, it can be considered the ideal and perfect choice for use in first stage of extremely low noise cascades. However, the second and third stages are also designed using the same device. The designing method presented is based on the manufacturer S-parameters of the device.

New software packages have been developed since the demand for fast and accurate designs appeared, especially with the growth of required for Microwave Monolithic Integrated Circuits (MMTC). The development of new software simulation tools was necessary. Stratakos and his team (Stratakos, and Uzunoglu, 1995) designed a MMIC Low Noise amplifier at 10 GHz using Computer Aided Design Techniques (CAD). The method used for the LNA design is quite simple; two similar stages with source peaking at each stage are used. The advantage of source peaking is that stability occurs in the full frequency range of operation as well as good input matching with corresponding low noise figure. The only disadvantage here is that the gain of each stage is reduced by a certain amount. That is why two stages are used in order to obtain the final 10 dB overall gain at 10 GHz. The maximum unilateral transducer gain is given by Equation 2.1 in dB. The transistor used for the design of both stages is the 6x50 μm of the F20 process. A six fingered MESFET is used in order to minimize the parasitic in the gate pad due to their parallelism, and at the same time succeed an adequate gain suitable for the design specifications. A plot

of Equation 2.1 for Vds= 5 Volts and Ids=0.2 Idss is shown in Figure 2.1. Also in Figure 2.1 the minimum noise figure is plotted for the band from 1 to 20GHz.

$$G_{max} = 10.\log (|S_{21}|^2 / ((1- |S_{11}|^2) (1- |S_{22}|^2))) \quad (2.1)$$

This process has an associated gain of 10 dB with minimum noise figure of 1.6 dB at 12 GHz as shown in Figure 2.1. The area of the chip is $2mm^2$, the gain is 5dB per stage at 10GHz, the noise figure obtained is almost 2dB and the input and output return loss is better than 10dB. The chip is designed to work at a low noise radar receiver. Experimental results are also presented on wafer measurements using a CASCADE wafer probe station concerning both linear (S-parameters, Noise Figure) and nonlinear measurements (Power, Gain, Spectrum). The simulation for experimental results was noted using Microwave Design System (MDS) (Stratakos, and Uzunoglu, 1995).

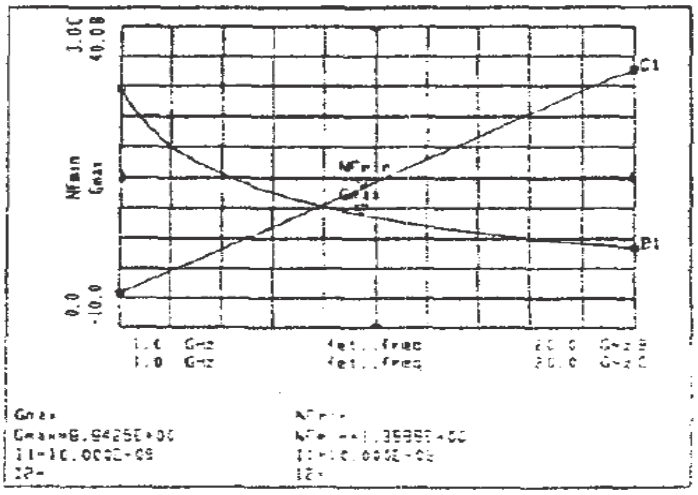

Figure 2.1: G_{max} and NF_{min} versus frequency for the 6x50μm (Stratakos, and Uzunoglu, 1995)

Remarkable improvements in the performance of GaAs power MESFET's have been seen. The GaAs power MESFET is one of particularly attractive features; compared with other solid-state microwave power devices. It has large bandwidth potential. An equivalent circuit of the GaAs MESFET was developed and used in the final design of the matching networks. The result was found between the measured small-signal gain of the single-ended modules, and the gain computed using the equivalent circuit of GaAs MESFET, as shown in Figure 2.2. Final tuning of the amplifiers was performed at output power levels close to the 1.5 dB compression points of the unit whose original matching networks were based on small-signal analysis. The attendant gain was 4.6 ± 0.6 dB and the maximum NF amounted to 1.4 dB across the Ku-Band. These results demonstrate the outstanding broad-band power capability of the GaAs MESFET up to 18 GHz (Niclas el at., 1978).

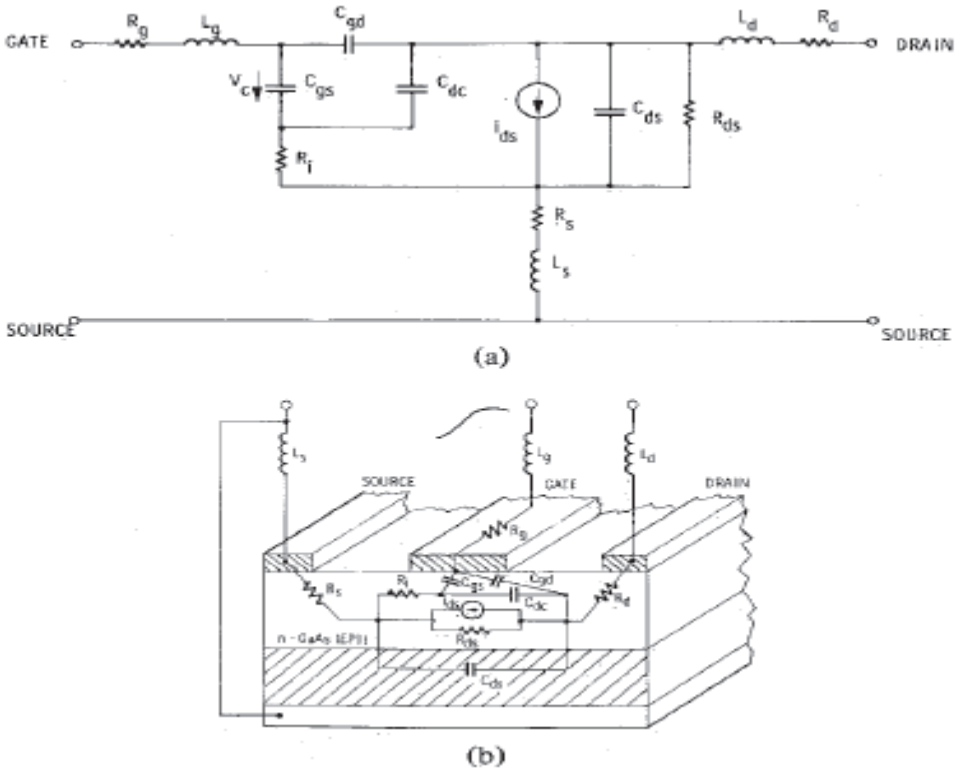

Figure 2.2: GaAs MESFET (a) Schematic RF equivalent circuit. (b) Physical origin of the circuit elements (Niclas el at., 1978)

A monolithic four-stage low-noise MMIC amplifier was described in (Shiga el at., 1992).This was based on 0.3 µm gate pulse-doped GaAs MESFET's for Direct Broadcast Satellite (DBS). Downconverters were testified possessing both productivity and not bad low noise performance. Using a simple MESFET processing technology, the most specific result of this project is that a practically sufficient low-noise performance can be achieved. VSWRs of below 1.5: l as well as a noise figure of 1.1 dB and a gain of 6 dB at 12 GHz per stage was obtained. In power characteristics, a 1 dB compression point (P_{ldB}) of 10 dBm and a third order intercept point (IP_3) of 19 dBm were shown. The LNA design and the test results are presented in this study. Figure 2.3 shows the simulation results where matching networks are synthesized so that the amplifier per stage had a minimum noise figure, namely noise-matched amplifier as shown in Figure 2.3.

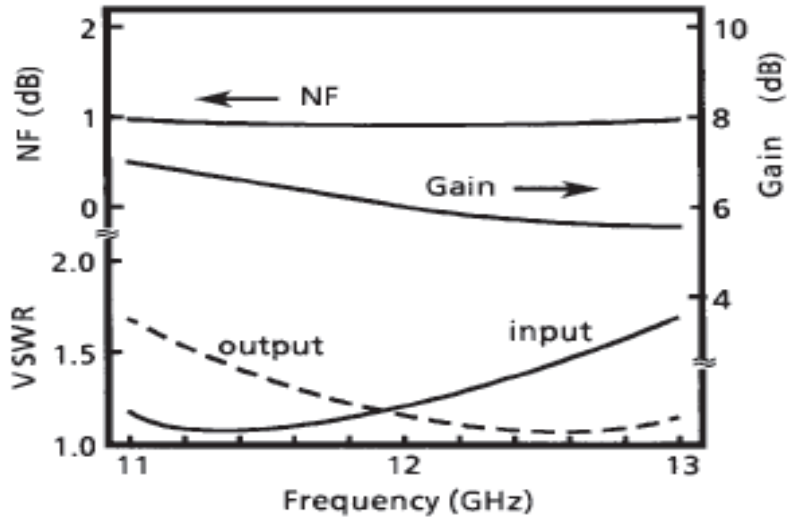

Figure 2.3: Simulation results of noise figure and gain (Shiga el at., 1992)

In this thesis the design of low noise amplifier is discussed in Chapter Four. Referring to Table 2.1, a comparison among the previous studies are shown the gain

and noise figure. Table 2.1 summarizes the design parameters of other researcher works for a MMIC low noise amplifiers working at 10-18 GHz. This table shows that the gain per stage and the noise figure for previous studies ranges between 10-18 GHz.

Table 2.1
Comparison of 10-18GHz MMIC low noise amplifier design

Study	Process	Frequency (GHz)	Gain (dB)	Min NF (dB)	NF (dB)	Area
B. Hughes el at.,(1993)	PMODEF	12	8.2	0.86	1.6	0.31 mm^2
K. Sakuno el at.,(1992)	FET GaAs	12	8.3	-	2.5	0.72 mm^2
N. Shiga el at.,(1992)	MESFET GaAs	12	6.5	0.7	1.1	1.2 mm^2
M. Yamane el at.,(1990)	2DEGFET	12	7.7	1.1	1.3	1.5 mm^2
H. Tsukada el at.,(1990)	HEMT	12	8.2	0.5	1.2	1.63 mm^2
N. Ayaki el at.,(1988)	HEMT	12	7	1	1.6	1.96 mm^2
H. Itoh el at.,(1983)	CSEFET GaAs	12	8	1.7	2.8	0.65 mm^2
S. Hori el at.,(1983)	FET GaAs	12	6.6	1.9	3.4	1.5 mm^2
N. Shiga el at.,(1991)	MESFET GaAs	12	6	1.2	1.6	2.25 mm^2
L. Boglione el at.,(1999)	PHEMT	13	4.5	-	1.3	800x800µm
J. Gil el at.,(2003)	CMOS	10	4.9	-	4.67	0.1023 mm^2
C.S. Wang el at.,(2006)	CMOS	10	12	-	6	0.696mm^2
G. Stratakos el at.,(1995)	MESFET GaAs	16	10	-	2	2 mm^2
K.-B. Schad el at.,(2000)	SiGeHBT	12-18	8	-	4	1x0.8x25 μm^2
K. Niclas el at.,(1978)	MESFET GaAs	12-18	4.8	-	1.5	350x500 µm

2.2.1 LNA Parameters

The important design considerations in a microwave transistor amplifier design are stability, gain and noise. Among these factors, the most important ones, in the design of LNA, are stability and noise. These factors are very significant in choosing the right transistor for a low noise amplifier design (Pozar,1998).

2.2.2 Noise Figure

Noise Figure (NF) is a measure of degradation of the Signal-to-Noise Ratio (SNR), caused by components in a Radio Frequency (RF) signal chain. It can be said that noise figure is the noise factor of merit that does not truly exist in the same sense as current, power or voltage. As a consequence, its measurement is necessarily indirect. Noise figure is defined as the ratio of the output noise power of a device, to the portion thereof attributable to thermal noise in the input termination, at standard noise temperature T_0 (usually 290 K). The noise figure is accordingly the ratio of actual output noise to which it would remain if the device itself did not introduce noise. It is a number by which the performance of a radio receiver can be specified (Gilbert, 2008).

The noise figure between the noise output of the actual receiver and the noise output of an ideal receiver is measured in decibels (dB), with the same overall gain and bandwidth when the receivers are connected to sources at the standard noise temperature T_0. The noise power (N) from a simple load as in Equation 2.2 is equal to

$$N = kTB \tag{2.2}$$

where k is Boltzmann's constant, T is the absolute temperature of the load or the system, and B is the measurement bandwidth.

This makes the noise figure very important to be measured and a useful figure of merit for terrestrial systems where the antenna effective temperature is usually near the standard 290 K. Conversely, in the electrical devices of satellite communication systems, where the antenna is pointed out into humidity space, the antenna effective temperature is frequently colder than 290 K. As a result, a 2 dB improvement in receiver noise figure results in more than 2 dB improvement in the output signal to

noise ratio. Therefore, the related figure of effective noise temperature is then used, instead of the noise figure, for characterizing satellite communication receivers and low noise amplifiers (Gilbert, 2008).

The lowest noise figure can be achieved by obtaining maximum gain, based on Equation 2.1 for a low noise amplifier design. In LNA applications, it is often required to have a preamplifier with as low noise figure as possible. The noise factor and noise figure of a system are defined as in Equations 2.3-2.8 (Monstein, 2002).

$$F = SNR_{in}/SNR_{out} \tag{2.3}$$

where SNR_{in} and SNR_{out} are the input and output power signal-to-noise ratios, respectively. The noise figure is defined as:

$$NF = 10 \log (SNR_{in}/SNR_{out}) = SNR_{in,dB} - SNR_{out,dB} \tag{2.4}$$

where $SNR_{in,dB}$ and $SNR_{out,dB}$ are in decibels (dB). The noise figure is the noise factor, given in dB:

$$NF= 10 \log (F) \tag{2.5}$$

These formulas are only valid when the input termination is at standard noise temperature T_0, even though in practice small differences in temperature do not much affect the values.

The noise factor of a device is related to its noise temperature T_e:

$$F=1+ (T_e/ T_0) \tag{2.6}$$

Devices with no gain such as attenuators have a noise figure equal to their attenuation L (absolute value, not in dB) when their physical temperature equals T_0. Moreover, for an attenuator at a physical temperature T, the noise temperature is $T_e = (L - 1) T$, giving a noise factor of:

$$F=1+ ((L - 1) T/ T_0) \quad (2.7)$$

If several devices are cascaded, the total noise factor can be found with Friis' Formula:

$$F = F_1 + \frac{F_2-1}{G_1} + \frac{F_3-1}{G_1G_2} + \frac{F_4-1}{G_1G_2G_3} + \cdots + \frac{F_n-1}{G_1G_2G_3\ldots G_{n-1}} \quad (2.8)$$

where F_1 is the noise factor of the first stage, which dominates the overall noise performance if $G_1$is sufficiently high. F_n is the noise factor for the n-th device, and G_n is the power gain (linear, not in dB) of the n-th device. In a good designed receiving chain, only the noise factor of the first amplifier should be significant (Monstein, 2002; Long, 2007).

2.2.3 Stability

As in section 2.2, the design of a low noise amplifier method presented in (Ain el at., 2007) is based on the manufacturer S-parameters (Scattering parameters) of the device ATF-36077 PHEMT transistor. The transistor can be modeled by the block diagram, as shown in Figure 2.4, to represent the S-parameters.

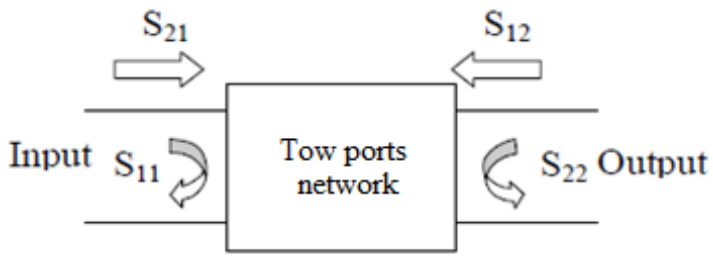

Figure 2.4: Scattering parameters of two ports network (Ain el at., 2007)

S_{11} is the input port voltage reflection coefficient at port 1 when port 2 is matched.

S_{21} is the transmission coefficient voltage gain at port 1when port 2 is matched.

S_{12} is the reflection coefficient voltage gain at port 2 when port 1 is matched.

S_{22} is the output port voltage transmission coefficient at port 2 when port 1 is matched.

The stability of an amplifier as in Equations 2.9-2.13, i.e. the resistance to oscillate, is a very important to be considered in the design of a low noise amplifier in microwave amplifiers. It can be determined from the S-parameters, the matching networks, and the terminations. The transistor is unconditionally stable if K is greater than 1 and conditionally stable if K is less than 1. In Figure 2.5, where a matching network is used on both sides of the transistor, the reflection coefficients on the input and output sides of the transistor are defined. Oscillations are possible when either the input or output port presents a negative resistance. This occurs when $|\Gamma_{in}| > 1$ or $|\Gamma_{out}| > 1$. This is due to Γ_{in} and Γ_{out}. Furthermore, amplifiers behave differently when the frequencies are high due to parasitic effects, S-parameter dependence on frequency, stability, etc.

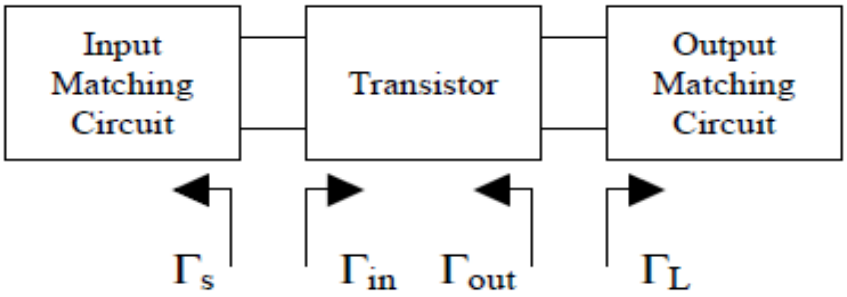

Figure 2.5: General microwave transistor amplifier block diagram (Ain el at., 2007)

Matching networks depend on the source and the load circuits, while the stability of the amplifier depends on Γ_S and Γ_L, as presented by the matching networks. Alternatively, it can be noted that the amplifier can be unconditionally stable if the following necessary and sufficient conditions are met (Ain el at., 2007; Sahoolizadeh el at., 2009).

$$K = \frac{1-|S_{11}|^2-|S_{22}|^2+|\Delta S|^2}{2|S_{21}S_{12}|} \geq 1 \quad (2.9)$$

$$|\Delta s| < 1 \quad (2.10)$$

where

$$\Delta s = S_{11}.S_{22}\text{-}S_{12}.S_{21} \quad (2.11)$$

and

$$\Gamma_{in} = S_{11} + \left(\frac{S_{12}S_{21}\Gamma_L}{1-S_{22}\Gamma_L}\right) \quad (2.12)$$

$$\Gamma_{out} = S_{22} + \left(\frac{S_{12}S_{21}\Gamma_s}{1-S_{11}\Gamma_s}\right) \quad (2.13)$$

where $|\Gamma_S|$ and $|\Gamma_L|$ are the magnitudes of the source and load reflection coefficients. Γ_S and Γ_L are less than or equal to 1, which means that the corresponding impedances have positive real parts (Ain el at.,2007;Davis, and Agarwal, 2001).

2.2.4 Gain

In electronic devices, gain is a measure of the ability of a circuit often an amplifier as shown in Equation 2.1. In order to increase the power or amplitude of a signal, maximum gain is needed. It is typically defined as the mean ratio of the signal output of a system to the signal input of the same system. It may also be defined on a logarithmic scale, in terms of the decimal logarithm of the same ratio (dB gain) (Pratt el at.,2003; Davis, and Agarwal, 2001).

To investigate the power gain is defined by the 10 log rule in decibels (dB), as follows:

$$\text{Gain} = 10\log (P_{out}/P_{in})\ \text{dB} \tag{2.14}$$

where P_{in} and P_{out} are the input and output powers, respectively. A similar calculation can be done using a natural logarithm instead of a decimal logarithm. Then the result is in nepers instead of decibels. Voltage gain is also a very important aspect to simulate and test the design of low noise amplifier. This is when power gain is calculated using voltage instead of power, making the substitution ($P=V^2/R$), the formula is:

$$\text{Voltage Gain} = 10\log (V^2_{out}/R_{out})/ (V^2_{in}/R_{in}) = 20\log (V_{out}/V_{in}) \tag{2.15}$$

where R_{in} and R_{out} are the input and output impedances, respectively. V_{in} and V_{out} are the input and output voltage, respectively. In many cases, the input and output impedances are equal, so the above equation can be simplified to:

$$\text{Gain} = 10 \log (V_{out}/V_{in})^2 \text{ dB} \quad (2.16)$$

This simplified formula is used to calculate a voltage gain in decibels for low noise amplifier design, and is equivalent to a power gain only if the impedances at input and output are equal. Finally, as a conclusion, gain is one of the most important and significant characteristics of low noise amplifier design, as well as increasing the gain in the microwave circuit design absolutely, it would increase the efficiency of that circuit.

2.3 DOWNCONVERTER DESIGN

Downconverter is a basic RF downconverter system that is designed to convert high frequency to low frequency or other wideband signals. The Ku-Band downconverter consists of a preamplifier, a double-balanced mixer, and an IF amplifier as shown in Figure 2.6.

Lee and his team (Lee el at.,2005) used a number of technologies, such as High Electron Mobility Transistor (HEMT), silicon Bipolar Junction Transistor (BJT), and GaAs Metal-Semiconductor- Field-Effect-Transistor (MESFET) process for developing a Ku-Band Microwave Monolithic Integrated Circuit (MMIC) downconverters. These downconverters do not meet the requirement of low power consumption and simultaneous high Radio-Frequency (RF) performance, because of the limitations of each technology. GaAs-based Heterojunction Bipolar Transistors (HBTs) possess many advantageous properties, such as higher values of and with relaxed lithographic dimension, better device matching, higher current density, higher transconductance, low noise, lower output conductance, no parasitic substrate capacitance, and greater radiation hardness relative to those of Field-Effect Transistors

(FETs), and the excellence of RF performance, including high gain, linearity, and efficiency, relative to that of homojunction BJTs. Therefore, GaAs technology is becoming widely used in commercial applications because it offers high efficiency, and it works with high frequency.

In their study the RF input signal of 11.7–12.75 GHz is down-converted to an L-band IF frequency of 0.95–2 GHz by using a local oscillator at 10.75 GHz. This figure displays a generic Ku-Band Low Noise Block (LNB) system, which usually requires a conversion gain of 50–62 dB, a noise figure of 1.1 dB, a gain flatness within 5 dB, a $P_{1dB,\ OUT}$ of 0 dBm, and an IF output power range from 37 to 8 dBm. In their study, the design and fabrication of a Ku-Band MMIC downconverter was reported. It can be applied for a given Ku-Band LNB system, using InGaP–GaAs HBT technology. The preamplifier employs a two-stage of common-emitter configuration having a resistive load as indicated in Figure 2.7. To block the effectiveness of RF signal, 1.5 and 2.2 kΩ NiCr resistors were used for base voltage biasing, rather than using a quarter-wave transformer. Microstrip short stubs were applied, instead of a spiral inductor, for the input and output matching networks, to keep the chip area (Lee el at., 2005).

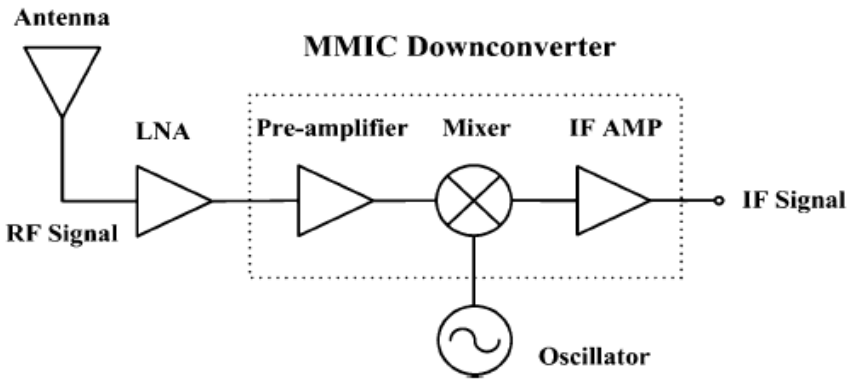

Figure 2.6: Block diagram of an MMIC downconverter (Lee el at., 2005)

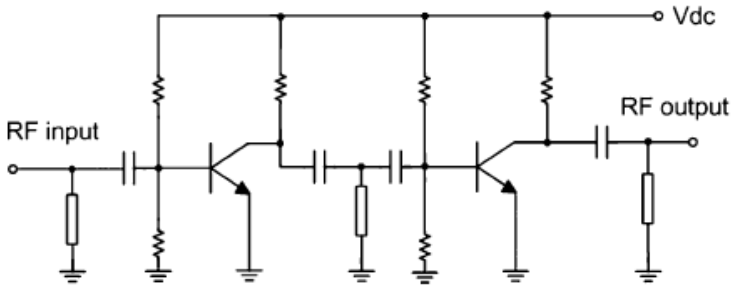

Figure 2.7: Circuit schematic of the preamplifier (Lee el at., 2005)

A GaAs MMIC downconverter for commercial Ku-Band broadcast satellite receiver's applications has been developed (Sakuno el at., 1992). The MMIC downconverter receives 11.7 - 12.2 GHz signals and converts them down in frequency to 1.0 - 1.5 GHz. The size of the mixer is 0.73 mm X 0.93 mm. The measured RF performance of the mixer is shown in Figure 2.9. Less than 6.5 dB noise figure and more than 0 dB conversion gain have been achieved in the frequency range from 11.7 to 12.2 GHz and the corresponding IF frequency ranges from 1.0 to 1.5 GHz. The LO frequency and input power were 10.7 GHz and 8 dBm, respectively.

The mixer has a drain LO injection configuration, which does not require an RF-LO combiner and consumes no DC current. The circuit schematic of the MMIC mixer is shown in Figure 2.8. To reduce the size of the mixer, the RF, IF, and LO matching circuits contain lumped LC elements, including spiral inductors and metal-insulatormetal (MIM) capacitors. Self-resonance of the spiral inductor (Ll) has been intentionally used to improve the LO-IF isolation and the LO injection efficiency. The IF signal is effectively transmitted to the IF port owing to the series resonance of L1 and C1 (Sakuno el at., 1992).

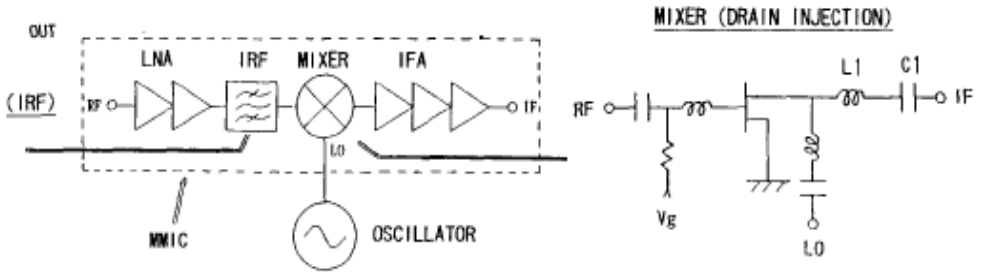

Figure 2.8: Circuit schematic of the mixer downconverter (Sakuno el at., 1992)

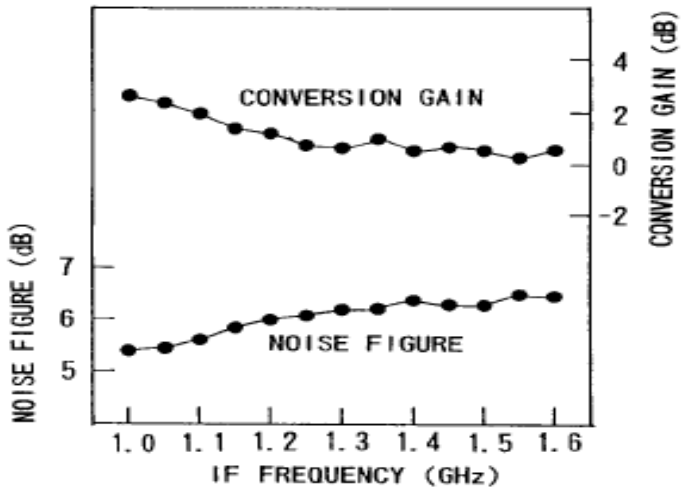

Figure 2.9: Measured frequency response of the mixer (Sakuno el at., 1992)

In (Jeong el at., 2002) a Ku-Band downconverter at the frequency range from 14-14.5GHz to 12.252-12.752GHz was presented. The key performance parameters of the receiver downconverter for satellite transponders are linearity, not bad quality of temperature, stability, and low noise figure. Using a hybrid technology, all RF components were assembled with 15-mil thinfilm substrate. The components of a receiver downconverter consist of a low noise amplifier module, a downconverter module driven from a local oscillator that accepted the development of this project, and an IFAMP module. The receiver downconverter module input and output is to provide the waveguide interface and coaxial output port, respectively.

In Ku-Band systems, the local oscillator frequency value (f_{LO}) is lower than the frequency value of the input RF signals (f_{RF}) coming from the geostationary satellite (low-sind injection). This is shown in Equation 2.17 (Lee el at., 2004).

$$f_{1/IF} = f_{RF} - f_{LO} \quad \text{MHZ} \tag{2.17}$$

2.4 BANDPASS FILTER DESIGN

The microwave filter design requirements of high performance, small size, and low-cost are inevitable for market competition. One of the most important components in a satellite receiver is the filter, the preselected choice of filter in the RF is to fine the radio signal and get rid of most of the noise out of the signal band. In this section, three studies have been discussed.

The development of miniaturized and high performance microwave and millimeter wave systems is important to cover the increasing demand on telecommunication applications. Higher frequency of microwave communication systems are growing quickly and can provide many advantages over conventional wireless links such as X-band or Ku-Band, for example, the larger bandwidth and smaller device size. The design of RF circuits on micromachined substrate materials is lead to integrate the entire communication system on a single chip. Waveguide components are widely used at these frequencies, they offer very good performance. It has two main disadvantages, namely high production costs and bulky systems. The structures of conventional planar filter suffer from radiation thus is caused by the resonators into the substrate, and from high ohmic loss, therefore, give high insertion loss and poor filter rejection. In recent times, removing the dielectric material up to a thin membrane that suspends the planar filters the micromachined techniques is

available. It is shown to enhance filter performance by reducing the radiation, ohmic and dielectric losses of resonators. However, lowering the cost of the commercial RF micromachined device is still a challenge since the devices are fabricated in semiconductor-like process (Islam el at., 2007).

Bandpass Filters (BPFs) often use the parallel-coupled microstrip technique at microwave frequencies. Two or more resonators are cascaded such as the coupled multiresonator BPF. Each individual resonator is affected by reactive loading from adjacent couplings and open-ended capacitive fringing. In (Islam el at., 2007) the wireless Ku-Band operating in parallel coupled microstrip, BPF was presented; this design is used for RF filter for Ku-Band receiver aboard a telecommunication satellite. Generally, it is easy to fabricate microstrip or stripline bandpass coupled line filters with bandwidths less than about 20%. However, very tightly coupled lines are needed wherever wider bandwidth filters are desired. This can be achieved by reducing the substrate height used, where the required track separation, realizing the coupled line filter, becomes smaller. However, in terms of manufacturability, a problem of this small track separation can be noted. In addition, the characteristic impedances of the stub resonator are in reality difficult to realize also. As a result, the trade-offs between substrate height, minimum coupling gap, realizable characteristic impedances and overall loss must be addressed to gain the required filter performance. Figure 2.10 shows the receiver schematic as well as the location of the RF filter. Coupled line filters can be designed to produce either a maximally flat or equi-ripple response. In this design, using coupled half-wave resonators that give maximally flat response a 4^{th} order bandpass filter has been designed with a center frequency of l6GHz and a 3dB bandwidth of 5.8GHz. The design procedure that is based on the even- and odd-mode impedances of the coupled lines to design bandpass filter, and is further optimized

using IE3D. Figure 2.11 demonstrates the top structure view of the simulated bandpass filter.

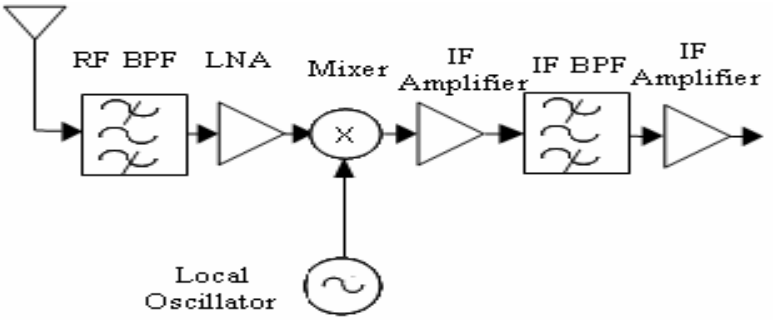

Figure 2.10: Schematic circuit of the Ku-Band receiver (Islam el at., 2007)

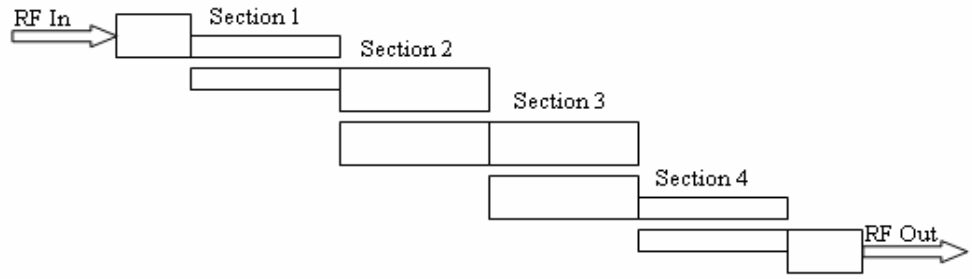

Figure 2.11: The top structure view of the simulated bandpass filter (Islam el at., 2007)

By using microstrip technology, a 16GHz filter has been demonstrated. On 600 μm-thik inexpensive commercial FR4 (ε_r=4.3) substrate the filter was designed. Figure 2.12 displays the simulation performances of the bandpass filter with frequency. This kind of filter development suggests the feasibility of building highly Standard Operating Procedure (SOP) integrated microwave and millimeterwave radio front ends (Islam el at., 2007).

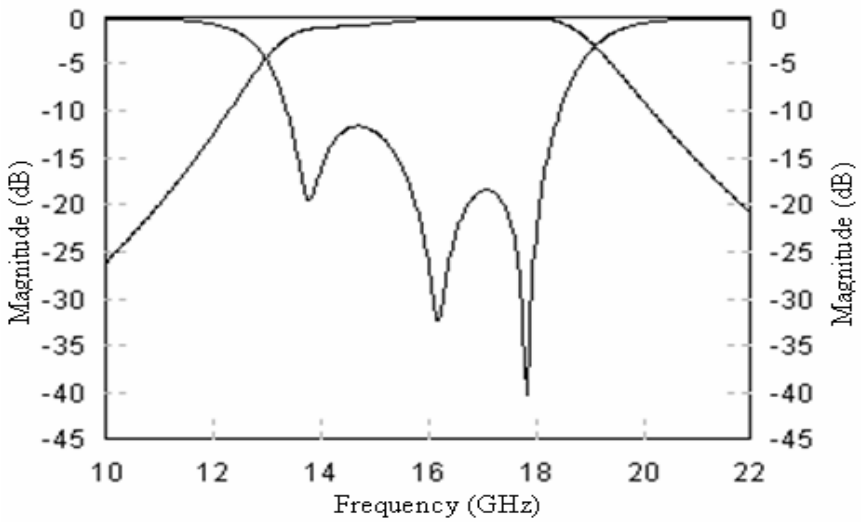

Figure 2.12: Simulation performances of the bandpass filter (Islam el at., 2007).

Microstrip interdigital filters have been widely used in microwave systems due to their easy processing, reliability and consistency. Changing coupled structure increases the effective coupling area of the microstrip line, and can make the structure of filter more compact. In (Jia el at.,2009) study, by adjusting coupled structural or increasing the effective coupling area of the microstrip line some more compact filter was achieved. The L-band band-pass interdigital filter was studied, a large number of experimental data showed that bandwidth narrowed, with the increasing of resonator width and the center frequency, becomes larger with the reduction of the resonator length. The bandwidth widens when the distance between resonators was reduced. Based on these conclusions, a new type of filter was designed; the size of the filter was only 71.4% of that of the original one, compared with the traditional interdigital filter. The conventional design of interdigital microstrip bandpass filter is based on a classical network synthesis method. First step is to find out the lumped element low-pass prototype, and then get the frequency transform of band-pass filter lumped parameters, through the existing formula design to approximate the elf-capacitance of each stroke, besides the mutual capacitance between the adjacent poles, obtain the

cross- finger capacitor filter network parameters, and then the microstrip parameters is achieved. Finally, Figure 2.13 shows the band-pass filter simulations with respect to the frequency.

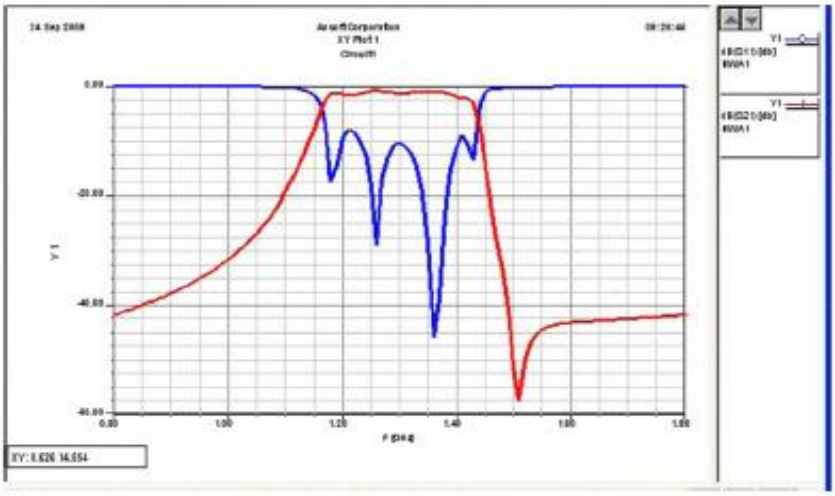

Figure 2.13: The band-pass filter simulations (Jia el at., 2009)

In the last study, it is difficult to realize the filter using lumped elements, because the frequency is over 500MHz, and the dimensions of the electronic component are comparable with the wave length of the signal, as in (Hao el at., 2008). Recently the method usually adopted is called “prototype filter design”. It begins at the low-pass filter prototype, and confirms the stage of the filter according to the attenuation required in a specified frequency, after the type like butterworth, Chebyshev, ellipse, etc is chosen, then the unitary resistances in an experiential table and derive the length, width, gap of the coupled microstrip in different stages by calculation on a set of equations. Microstrip filters have many features, Such as their smart layout in microwave circuit design broad-band application, in addition to convenience of match work with the circuit. That is why they are widely used. The performance of such filters is usually dissatisfactory because of their parameters,

especially when calculating the approximation of conventional formulas. Hence, in engineering, the design is carried out using microwave Electronic Design Automatic (EDA). For high frequency circuit design Advanced Design System (ADS), a good software tool is produced by Agilent Corporation. It can make thorough analysis from circuit design to circuit realization. The most serious interference was faced when the down-mix carry out by alias interference. To restrain the interference, a preselect filter is needed before mixing. Thus, the performance of the preselect filter is crucial to the RF design. The intermediate frequency after the first step of mixing is set to 91.5MHz, while the alias frequency is 2308.25MHz in the RF circuit design for a satellite receiver, then the requirement for the filter can be derived (Hao el at., 2008).

The alias interference is the most troublesome signal that can produce the same intermediate frequency. This means that it would degrade the Signal to Noise Ratio (SNR) deeply of the signal and raise the error rate of demodulation. In RF receivers, a band-pass filter is usually located behind the Low Noise Amplifier (LNA) to choose the particular band radio signal and decrease the energy in the alias frequency. However, the signal is very weak after being received by the antenna in the microwave communication system. Therefore, added strict requests are needed on the indexes of the preselect filter, such as Stand Wave Ratio (SWR), insert loss and alias frequency attenuation. The OPTIM controller is adopted to adjust the parameters of the coupled microstrip; the requested simulations show numerous elements to the filter, such as centre frequency: 2491.75±4.08MHz, insert loss is less than 5dB, ripple is less than 0.5dB, bandwidth is 100MHz. The goals are well realized after the optimization, and it is amended to deviate and distort the response curve and meet the demand bitterly. Figure 2.14 shows the layout of the microstrip filter design (Hao el at., 2008).

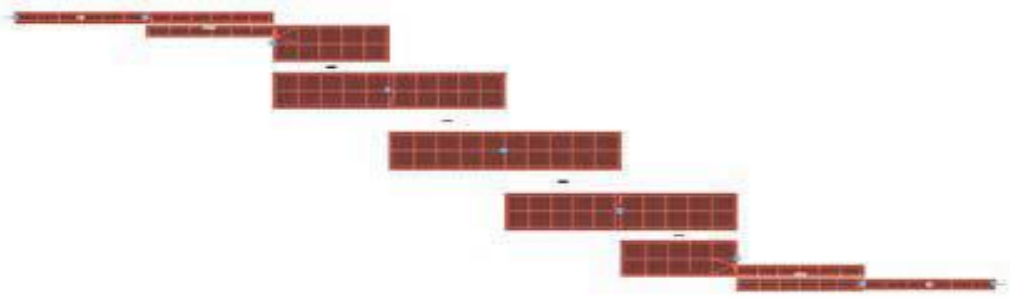

Figure 2.14: The layout of the microstrip filter (Hao el at., 2008)

2.5 SUMMARY

Previous studies show that designing a low noise amplifier, downconverter, and bandpass filter at Ku-Band in microwave communication systems requires a lot of concerns to be taken care of, especially at this high frequency. The architecture of a satellite receiver consists of a low noise amplifier, downconverter, and bandpass filter. Therefore, designing the component with respect to gain, noise figure, and stability, is crucial for the low noise amplifier design. Focusing on the bandwidth and converted frequency is important to design the downconverter. Yet getting suitable bandwidth, size, insertion loss, and return loss is significant to design the bandpass filter.

CHAPTER THREE

LINK BUDGET CALCULATIONS FOR KU-BAND

3.1 INTRODUCTION

In this chapter, the effects of scintillation, Cross-Polarization Depolarization (XPD), and rain fade attenuation will be highlighted in order to calculate the link budget of transmission losses at Ku-Band.

MEASAT-2 is an acronym of Malaysia East Asia Satellite and was launched on November 13, 1996 to the 148°East Geostationary Orbit. For the calculations in this chapter the earth station used is located in University Sains Malaysia (USM), Penang (5.17°N, 100.4°E) with 2.4m antenna diameter. The next Section presents the scintillation, XPD, and rain fade estimation for MEASAT-2 at Ku-Bands characteristics. Information on the MEASAT-2 at Ku-Band analysis is calculated in Section 3.3. Section 3.4 shows the results of the calculations. And Section 3.5 is the conclusion.

3.2 SCINTILLATION, XPD, AND RAIN FADE ESTIMATION FOR MEASAT-2 AT KU-BAND

A link budget is the most important tool for system-level design of wireless systems. It is the total amount of all of the gains and losses from the transmitter, through the medium (free space, cable, waveguide, fiber, etc.) to the receiver in a telecommunication system. It calculates the attenuation of the transmitted signal due to propagation, as well as the antenna gains, feedline and miscellaneous losses. Randomly varying channel gains, such as fading, are taken into account by adding

some margin. This depends on the anticipated severity of its effects (Buettrich, and Pascual, 2005).

A simple link budget equation looks as follows:

Received Power (dBm) = Transmitted Power (dBm) + Gains (dB) –Losses (dB) (3.1)

However, the recommended and the measured $R_{0.01}$ in Malaysia does not fit exactly, rather it underestimates the rain attenuation, so the Malaysian ITU-R rain map needs further investigation. In order to observe the differences through long term measurements of the dynamic rain attenuation, this is due to the different climatic conditions in Malaysia. Therefore, the ITU-R model has to be improved in order to agree with other regions (Recommendation ITU-R P.837-4, 2003).

3.2.1 Scintillation

"Scintillation" refers to a fast fluctuation of signal amplitude and phase. It is caused by atmospheric turbulence. This effect is due to turbulent irregularities in temperature, humidity and pressure, which is reflected into small-scale variations in refractive index. The result, in a multipath effect, is an electromagnetic wave passing through this medium, and then encountering various refractions and scattering effects. In the microwave region, the result is random degradation and enhancement in signal amplitude and phase, which is received on a satellite-earth link, where humidity fluctuations are more important (Van de Kamp el at., 1998).

According to (Recommendation ITU-R P.618-8T, 2003), the magnitude of the tropospheric scintillations depends on the magnitude and structure of the refractive index variations. It increases with frequency and with the path length through the

medium, and decreases as the antenna beam-width decreases because of aperture averaging. The wet term, N_{wet}, which is the wet term of the radio refractivity depends on the water vapor content of the atmosphere and can cause the monthly average r.m.s. fluctuations. The calculations for the scintillation are based on the monthly or longer averages of temperature T (°C), relative humidity H, and reflect the specific climatic conditions of the site.

To calculate the Scintillation effect on the frequency bands stated above, there is a need to know the elevation angle from the earth station selected to the satellite using the formula given below:

$$\cos\theta = (R_e + h)\sqrt{\frac{1-\cos^2\varphi.\cos^2\Delta\lambda}{h^2+2R_e(R_e+h)\left(1-\cos^2\varphi.\cos^2\Delta\lambda\right)}} \tag{3.2}$$

where:

Θ = Elevation angle (°)

Φ = Latitude of earth station

$\Delta\lambda$ = Difference in longitude between the earth station and the satellite location

R_e = Earth radius

h = Distance from the surface of the earth to the satellite orbit

After this angle is obtained, the calculation for scintillation can be done by following the ITU-R P.618-8T recommendation (2003) which will be shown later in this chapter.

3.2.2 Rain Fade

Various atmospheric components such as gases, water vapour, clouds, and rain, generally cause attenuation on radio propagation paths. One of the most fundamental limitations to the performance of satellite communication links in the Ku-Band is rain attenuation. It is caused by scattering and absorption by water droplets, and causes large variations in the received signal power, with little predictability and many sudden changes. This kind of signal fading is also prevalent on earth-space links in the C and Ku-Bands. Nonetheless, the depth of fades in those frequency bands is small enough to be compensated in order to maintain the desired performance for a small fixed fade margin in the link budget (Rahman el at., 2008).

The calculation is based on the relationship between the slant path and the rain height as shown in the following Figure 3.1:

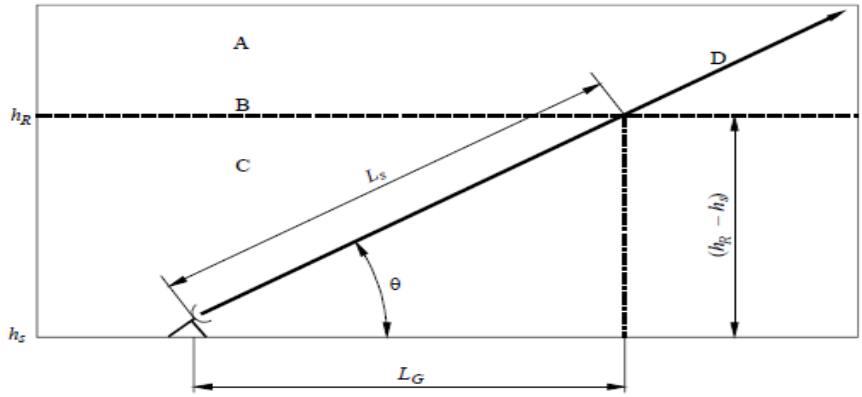

A: frozen precipitation
B: rain height
C: liquid precipitation
D: Earth-space path

Figure 3.1: Schematic presentation of an Earth-space path giving the parameters to be input into the attenuation prediction process (Recommendation ITU-R P.618-8T, 2003)

Figure 3.2 used to obtain the rain fall rate, R_p, the rain rate in millimeter per hour exceeds the percentage 0.01% of the average year, p, for Malaysia. Then calculation for estimation is done following the ITU-R recommendations.

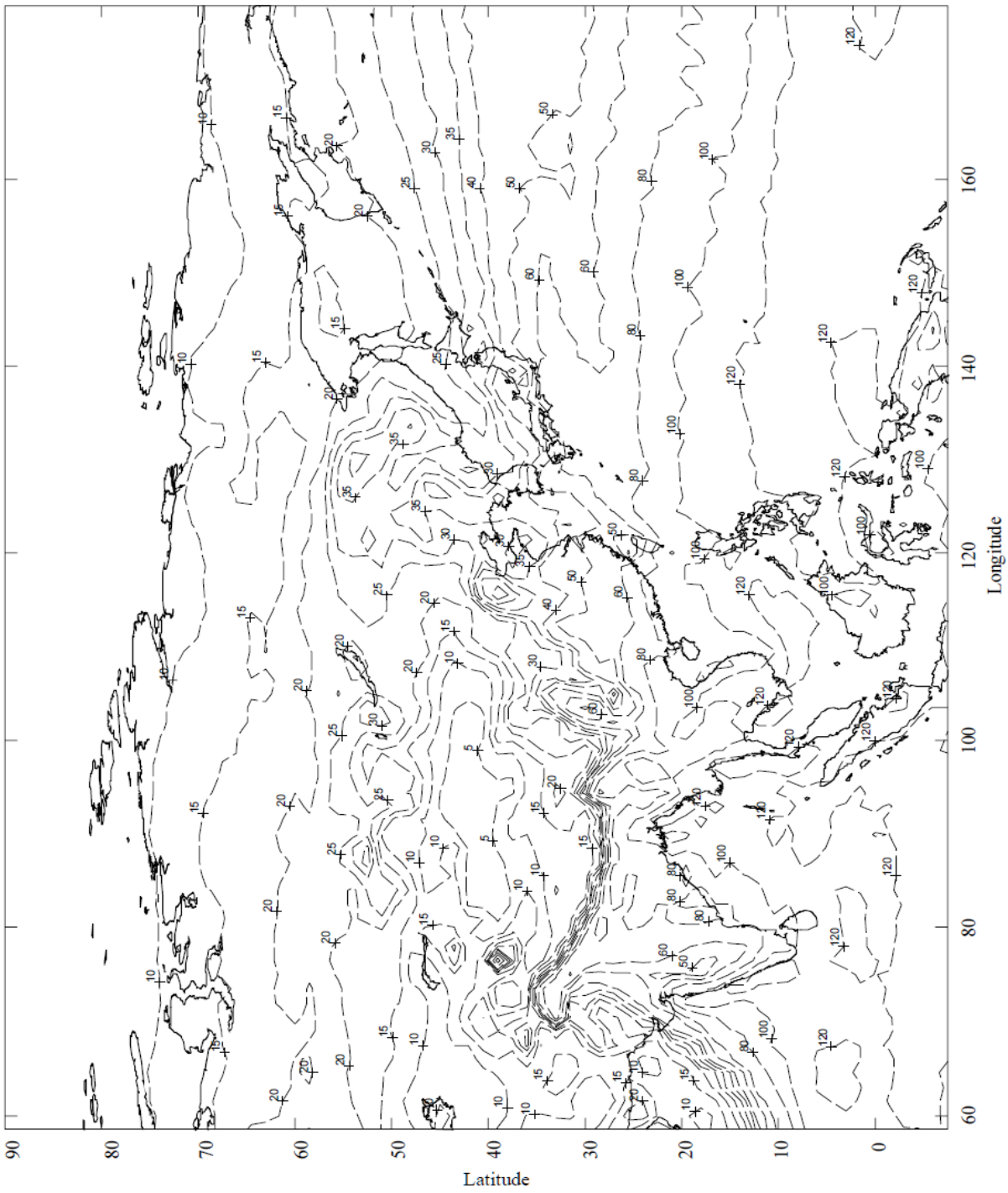

Figure 3.2: Rain rate (mm/h) exceeds 0.01% of the average year (Recommendation ITU-R P.837-4, 2003)

3.2.3 Cross-Polarization Depolarization

Two independent channels using the same frequency band can be transmitted over a single link by using orthogonal polarizations. To increase the available spectrum, this technique is effectively used in satellite communication systems. Some degree of interference between the orthogonally polarized channels is inevitable whereas they are completely isolated in theory. On the propagation path, the main sources of this depolarization at millimeter wave frequencies are absorption and scattering by hydrometers in the troposphere, most commonly in rainstorms. The anisotropical raindrops in the storm cause anisotropy in the propagation medium. A different attenuation and phase shift cause these two polarization directions, which normally cause the polarization of an incident wave, and arbitrarily polarized. The medium then has two principal planes (Bazak el at., 1994).

Frequency reuse by means of orthogonal polarization is used to increase the capacity of the space telecommunication systems. The system is restricted by depolarization on atmospheric propagation paths. The calculation is based on the value of the rain attenuation. However, the tilt angle needs to be obtained first for this procedure using the formula below:

$$\tau = \tan^{-1}\left(\frac{\tan\varphi}{\sin\lambda}\right) \tag{3.3}$$

where:

Φ = Latitude of earth station

λ = Difference in longitude

3.3 MEASAT-2: ELEVATION ANGLE CALCULATION

MEASAT 2 location: 148°E.

Earth Radius, $R_e = 6378.14\text{km}$

Distance from surface of the earth to satellite, h = 35790km

Earth station location, USM (Penang) = 5.17°N, 100.4°E

Difference in Longitude, $\Delta\lambda$ =148°-100.4° = 47.6°

Calculation to obtain elevation angle, θ, from the earth station with latitude, φ, of 5.14°:

$$\cos\theta = (R_e + h)\sqrt{\frac{1-\cos^2\varphi.\cos^2\Delta\lambda}{h^2+2R_e(R_e+h)(1-\cos^2\varphi.\cos^2\Delta\lambda)}} \quad (3.4)$$

$$\cos\theta = (6317.14 + 35790)\sqrt{\frac{1-\cos^2(5.17°).\cos^2(47.6°)}{35790^2+2(6317.14)(6317.14+35790)(1-\cos^2(5.17°).\cos^2(47.6°))}}$$

$$\cos\theta = 42107.14\sqrt{\frac{0.549}{1.281\times10^9+(532\times10^6)(0.549)}}$$

$$\cos\theta = 42107.14(1.8682\times10^{-5}) = 0.7866$$

$$\theta = 38.13°$$

3.4 MEASAT-2: KU-BAND ANALYSIS

This Section aims to calculate and analyze the link budget losses. Section 3.3.1 Part 1calculates Scintillation for MEASAT-2 at Ku-Band, Section 3.3.2 Part 2 displays Rain Fade Estimation Calculation for MEASAT-2 at Ku-Band, and Section 3.3.3 Part 3 demonstrates XPD calculation for MEASAT-2 at Ku-Band.

3.4.1 Part 1: Scintillation Calculation for MEASAT-2 at Ku-Band

Scintillation is calculated based on the recommendation by ITU-R P.618-8T, (Recommendation ITU-R P.837-4, 2003).

Parameters:

Elevation Angle, θ = 38.13°

Wet Term for Malaysia, $N_{wet} = 0.1$ppm

Frequency, f = 12GHz

Antenna Diameter, D = 2.4m

Antenna Efficiency, $\eta = 0.5$

Height of turbulent layer, $h_L = 1000\text{m}$

Step 1: For the value of average surface ambient temperature (t), calculate the saturation water vapour pressure, e_s, as specified in Recommendation ITU-R P.453-9 (2003).

Step 2: Compute the wet term of the radio refractivity, N_{wet}, corresponding to e_s, t and the average surface relative humidity (H) as given in Recommendation ITU-R P.453-9 (2003).

Since, the N_{wet} value has been obtained, step 1 and 2 are skipped. (Steps 1 and 2 are not needed because N_{wet} is obtained directly from Recommendation ITU-R P.453-9, 2003).

Step 3: Standard deviation of the signal amplitude, σ_{ref}

$$\sigma_{ref} = 3.6 \times 10^{-3} + 1 \times 10^{-4} \times N_{wet} \quad (3.5)$$

$$\sigma_{ref} = 3.6 \times 10^{-3} + 1 \times 10^{-4} \times 0.1$$

$$\sigma_{ref} = 3.61 \times 10^{-3}\text{dB}$$

Step 4: The effective path length, L, is calculated

$$L = \frac{2h_L}{\sqrt{\sin^2\theta + 2.35\times10^{-4}} + \sin\theta}\text{m} \quad (3.6)$$

$$L = \frac{2(1000)}{\sqrt{\sin^2(38.13°) + 2.35\times10^{-4}} + \sin(38.13°)}\text{m}$$

$$L = 2001.08\text{m}$$

Step 5: The effective antenna diameter, D_{eff} is estimated from the geometrical diameter, D, and the antenna efficiency, η.

$$D_{eff} = D\sqrt{\eta} \tag{3.7}$$

$$D_{eff} = 2.4\sqrt{0.5}$$

$$D_{eff} = 1.697$$

Step 6: The antenna averaging factor is calculated by

$$g(x) = \sqrt{3.86(x^2+1)^{11/12}.\sin\left[\frac{11}{6}\tan^{-1}\frac{1}{x}\right] - 7.08x^{\frac{5}{6}}} \tag{3.8}$$

$$x = 1.22D_{eff}{}^2.\frac{f}{L} \tag{3.9}$$

$$x = 1.22(1.697)^2.(\frac{12}{2001.8})$$

$$x = 0.021$$

$$g(x) = \sqrt{3.86(0.021^2+1)^{11/12}.\sin\left[\frac{11}{6}\tan^{-1}\frac{1}{0.021}\right] - 7.08\times 0.021^{5/6}}$$

$$g(x) = 0.86$$

Step 7: The standard deviation of the signal

$$\sigma = \sigma_{ref} f^{7/12}\frac{g(x)}{(\sin\theta)^{1.2}} \tag{3.10}$$

$$\sigma = (3.61\times 10^{-3})(12)^{7/12}\frac{0.86}{(\sin 38.13)^{1.2}}$$

$$\sigma = 0.023594$$

Step 8: Time percentage factor, a (p), for the time percentage, p, of concern in the range $0.01 \leq p < 50$ is calculated.

Assume p = 0.01

$$a(p) = -0.061(\log_{10}p)^3 + 0.072(\log_{10}p)^2 - 1.71\log_{10}p + 3.0 \tag{3.11}$$

$$a(p) = -0.061(\log_{10}0.01)^3 + 0.072(\log_{10}0.01)^2 - 1.71\log_{10}0.01 + 3.0$$

$$a(p) = 0.356$$

Step 9: The scintillation fade depth for time percentage 0.01 is

$$A_s(p) = a(p).\sigma \quad (3.12)$$

$$A_s(p) = (0.356)(0.023594)$$

$$A_s(p) = 0.0084\text{dB}$$

3.4.2 Part 2: Rain Fade Calculation for MEASAT-2 at Ku-Band

Parameters:

According to the table of Rain Climatic Zone P, rain fall rate of 0.01% of an average year for Malaysia, $R_{0.01}$ = 125mm/h

Height of earth surface above sea level, h_s=0.057km

Elevation Angle, $\theta = 38.13°$

Latitude of earth station located at USM, Penang, $\varphi = 5.17°N$

Downlink Frequency = 12GHz

Effective radius of earth, R_e=6317.14km

Polarization: Vertical

Coefficient: $K_V = 0.02455$; $\alpha_V = 1.1216$

h0: isometric height for Malaysia

Step 1: Determine the rain height, h_R, as given in Recommendation ITU-R P.839-3, (2001).

$$h_R = h_0 + 0.36\text{km} \quad (3.13)$$

$$h_R = 4.5 + 0.36\text{km}$$

$$h_R = 4.86\text{km}$$

Step 2: For $\theta \geq 5°$ compute the slant-path length, L_s, below the rain height from:

$$L_S = \frac{(h_R - h_S)}{\sin\theta}\text{km} \quad (3.14)$$

$$L_S = \frac{(4.86-0.057)}{\sin(38.13°)}\text{km}$$

$$L_S = 7.78\text{km}$$

Step 3: Calculate the horizontal projection, L_G, of the slant-path length from:

$$L_G = L_S\cos\theta\text{km} \tag{3.15}$$

$$L_G = (7.78)\cos(38.13)\text{km}$$

$$L_G = 6.12\text{km}$$

Step 4: Obtain the rain fall rate, $R_{0.01}$, exceeded for 0.01% of an average year with an integration time of 1 min, given in Recommendation ITU-R P.837.

$$R_{0.01} = 125\text{mm/hr}$$

Step 5: Obtain the specific attenuation, γ_R, using the frequency-dependent coefficients given in Recommendation ITU-R P.838-2 (2003) and the rain fall rate, $R_{0.01}$, determined from Step 4, by using:

$$\gamma_R = k_v(R_{0.01})^{\alpha_v}\text{dB/km} \tag{3.16}$$

$$\gamma_R = (0.02455)(125)^{1.1216}\text{dB/km}$$

$$\gamma_R = 5.52\text{dB/km}$$

Step 6: Calculate the horizontal reduction factor, $r_{0.01}$, for 0.01% of the time:

$$r_{0.01} = \frac{1}{1+0.78\sqrt{\frac{L_G\gamma_R}{f}}-0.38(1-e^{-2L_G})} \tag{3.17}$$

$$r_{0.01} = \frac{1}{1+0.78\sqrt{\frac{(6.12)(5.52)}{12}}-0.38(1-e^{-2(6.12)})}$$

$$r_{0.01} = 0.52$$

Step 7: Calculate the vertical adjustment factor, $v_{0.01}$, for 0.01% of the time:

$$\zeta = \tan^{-1}\left(\frac{h_R-h_S}{L_G r_{0.01}}\right)° \tag{3.18}$$

$$\zeta = \tan^{-1}\left(\frac{4.86-0.057}{6.12(0.52)}\right)^{\circ}$$

$$\zeta = 56.57^{\circ}$$

For $\zeta > \theta$,

$$L_R = \frac{L_G \cdot r_{0.01}}{\cos\theta}\text{km} \tag{3.19}$$

$$L_R = \frac{(6.12)(0.52)}{\cos 38.13^{\circ}}\text{km}$$

$$L_R = 4.04\text{km}$$

For $|\varphi| < 36^{\circ}$,

$$\chi = (36 - |\varphi|)^{\circ} \tag{3.20}$$

$$\chi = (36 - |5.17|)^{\circ}$$

$$\chi = 30.83^{\circ}$$

$$v_{0.01} = \frac{1}{1+\sqrt{\sin\theta}\left(31\left(1-e^{-\left(\frac{\theta}{1+\chi}\right)}\right)\frac{\sqrt{L_R\gamma_R}}{f^2}-0.45\right)} \tag{3.21}$$

$$v_{0.01} = \frac{1}{1+\sqrt{\sin 38.13^{\circ}}\left(31\left(1-e^{-\left(\frac{38.13}{1+30.83^{\circ}}\right)}\right)\frac{\sqrt{4.04\times 5.52}}{12^2}-0.45\right)}$$

$$v_{0.01} = 0.90$$

Step 8: The effective path length is:

$$L_E = L_R v_{0.01} \tag{3.22}$$

$$L_E = (4.04)(0.90)$$

$$L_E = 3.63\text{km}$$

Step 9: The prediction attenuation exceeded for 0.01% of an average year is:

$$A_{0.01} = \gamma_R L_E \text{dB} \tag{3.23}$$

$$A_{0.01} = (5.52)(3.63)\text{dB}$$

$$A_{0.01} = 20.0376\text{dB}$$

Step 10: The estimated attenuation for other percentage of an average year, in the range of 0.001% to 50%, is determined from the attenuation to be exceeded for 0.01% for an average year:

Assume p=0.001%,

For p<1% and $|\varphi|<36°$ and $\theta \geq 25°$,

$$\beta = -0.005(|\varphi| - 36) \tag{3.24}$$

$$\beta = -0.005(|5.17| - 36)$$

$$\beta = 0.15415$$

$$A_p = A_{0.01}\left(\frac{p}{0.01}\right)^{-(0.655+0.033\ln(p)-0.045\ln(A_{0.01})-\beta(1-p)\sin\theta)} \text{ dB} \tag{3.25}$$

$$A_p = (20.0376)\left(\frac{0.001}{0.01}\right)^{-(0.655+0.033\ln(0.001)-0.045\ln(20.0376)-0.15415(1-0.001)\sin 38.13°)} \text{ dB}$$

$$A_p = 31.54406\text{dB}$$

The previous calculation steps are for vertical polarization. The same steps are applied for horizontal and circular polarizations. The results are presented in Table 3.1.

Table 3.1 summarizes the transmission losses results for the rain attenuation of $A_{0.1\%}$, $A_{0.01\%}$, and $A_{0.001\%}$ availability 99.9%, 99.99%, and 99.999%, respectively. These are calculated for vertical, horizontal, and circular polarizations in dB. The worst calculated outcome of the transmission losses occurs in horizontal polarization, the best and lowest outcome happen in the vertical polarization, and the calculated values of circular polarization are in the middle between the values of the vertical and horizontal polarization. These calculated results are used with different availabilities in Chapter five, Section 5.6.2 (Simulation Results in Rain Fade), in order to obtain the Bit Error Rate (BER) for 16-PSK and 16-QAM, and to evaluate the performance of the designed receiver in tropical environment.

Table 3.1
The rain attenuation availabilities for vertical, horizontal, and circular polarizations

Availability	99.9%	99.99%	99.999%
Rain fade	$A_{0.1\%}$	$A_{0.01\%}$	$A_{0.001\%}$
Vertical-polarization	8.81436 dB	20.0376 dB	31.54406 dB
Horizontal-polarization	10.1626 dB	22.87972 dB	35.52207 dB
Circular-polarization	9.460446 dB	21.44257 dB	33.51535 dB

3.4.3 Part 3: XPD calculation for MEASAT-2 at Ku-Band

Parameters:

Rain attenuation exceeded for the required percentage of time, A_P= 20.0376dB

Frequency = 12GHz

Path Elevation Angle, $\theta = 38.13°$

Difference in Longitude, $\lambda = 148° - 100.4° = 47.6°$

The tilt angle of the linearly polarized electric field vector w.r.t. horizontal is obtained from:

$$\tau = \tan^{-1}\left(\frac{\tan\varphi}{\sin\lambda}\right) \quad (3.26)$$

$$\tau = \tan^{-1}\left(\frac{\tan 5.14°}{\sin 47.6°}\right)$$

$$\tau = 6.95°$$

Step 1: The frequency-dependent term is calculated:

For $8 \leq f \leq 35$GHz

$$C_f = 30\log f \quad (3.27)$$

$$C_f = 30\log(12)$$

$$C_f = 32.37$$

Step 2: The rain attenuation dependent term is calculated:

$$C_A = V(f)\log A_p \quad (3.28)$$

For 8≤f≤35GHz;

$$V(f) = 12.8(f)^{0.19} \quad (3.29)$$

$$V(f) = 12.8(12)^{0.19}$$

$$V(f) = 20.52$$

$$C_A = (20.52)\log 20.03$$

$$C_A = 26.71$$

Step 3: The polarization improvement factor:

$$C_\tau = -10\log[1 - 0.484(1 + \cos(4\tau))] \quad (3.30)$$

$$C_\tau = -10\log[1 - 0.484(1 + \cos(4(6.95)))]$$

$$C_\tau = 10.56\text{dB}$$

Step 4: The elevation angle-dependent term is calculated:

$$C_\theta = -40\log(\cos\theta) \quad (3.31)$$

$$C_\theta = -40\log(\cos 38.13°)$$

$$C_\theta = 4.17$$

Step 5: The canting angle-dependent term is calculated:

$$C_\sigma = 0.0052\sigma^2 \quad (3.32)$$

For p=0.01%, σ=10°

$$C_\sigma = 0.0052(10°)^2$$

$$C_\sigma = 0.52$$

Step 6: The rain XPD not exceeded for p% of the time:

$$XPD_{rain} = C_f - C_A + C_\tau + C_\theta + C_\sigma \quad (3.33)$$

$$XPD_{rain} = 32.37 - 26.71 + 10.56 + 4.17 + 0.52$$

$$XPD_{rain} = 20.91\text{dB}$$

Noting that, there is no need to calculate step 7 and step 8 because there is no ice in Malaysia. So, ($XPD_{rain} = 20.91dB$)=($XPD_{p} = 20.91dB$).

3.5 CALCULATION RESULTS

Table 3.2 summarizes the calculation results of the three aspects of the atmospheric losses, namely scintillation, Cross-Polarization Depolarization (XPD), and the rain fade attenuation at different band frequencies: C-Band, Ku-Band, and Ka-Band. This table shows that XPD values are the worst, the values of scintillation are the best at all frequencies, and the rain fade calculations are in the middle between XPD and scintillation. This thesis focuses on Ku-Band link budget calculations, and the results are used as transmission losses parameters by Additive White Gaussian Noise Channel (AWGN) in Sections 5.6.2-5.6.4 in order to test the performance of BER with respect to transmission losses in tropical environment.

Table 3.2
The results for different band frequencies with atmospheric losses for $A_{0.01\%}$ availability

Frequency	Scintillation (dB)	Rain Fade (dB)	XPD (dB)
C-Band	0.0032 dB	4.41 dB	25.40 dB
Ku-Band	0.0084 dB	20.03 dB	20.91 dB
Ka-Band	0.0911 dB	34.64 dB	17.69 dB

3.6 SUMMARY

Three parameters (losses), namely scintillation, Cross-Polarization Depolarization (XPD) and rain fade attenuation, have been estimated using MEASAT-2 downlink (12GHz) at Ku-Band frequency. For the above calculations, the medium results of the

three aspects for atmospheric losses are at Ku-Band. This means that the problem of high attenuation starts from this frequency. Attenuation by atmospheric losses, which is entirely caused by absorption, depends mainly on frequency, elevation angle, altitude above sea level and water vapour density (absolute humidity). At frequencies below 10 GHz, it may normally be neglected. Its importance increases with frequency above 10 GHz, especially for low elevation angles. The estimated results show the transmission losses for the rain fade of $A_{0.1\%}$, $A_{0.01\%}$, and $A_{0.001\%}$ availability, which are calculated for vertical, horizontal, and circular polarizations.

CHAPTER FOUR

RECEIVER DESIGN AT KU-BAND

4.1 INTRODUCTION

This chapter highlights the design of a satellite RF receiver, which includes low noise amplifier, downconverter, and bandpass filter. The design of these components was constructed by using Microwave Office Simulator (AWR) Ver. 2006. The next Section presents the properties of Microwave Office Simulator. Section 4.3 shows the architecture of the receiver. Section 4.4 displays the design of low noise amplifier. The design of bandpass filter is presented in Section 4.5. Section 4.6 shows the design of downconverter and the last Section 4.7 is the conclusion of this chapter.

4.2 MICROWAVE OFFICE SIMULATOR

The AWR® Applied Wave Research Design Environment (AWRDE) suite comprises powerful tools that can be used together to create an RF integrated system. Microwave Office enables users to design circuits composed of schematics and Electromagnetic (EM) structures from an extensive electrical model database, and then generate layout representations of these designs. The powerful tools are fully integrated in the AWR Design Environment. They suite and allow the users to incorporate circuit designs into system designs without leaving the AWR Design Environment. The simulation performs using one of AWR's simulation engines, a linear simulator, an advanced harmonic balance simulator for nonlinear frequency-domain simulation analysis, a 3D-planar EM simulator (the EMSight™ tool), the APLAC simulator or an optional HSPICE simulator, and displays the output in a wide variety of graphical forms based

on the analysis needs. The tune of the designs keeps changes automatically and immediately and is reflected in the layout. At the center of the AWR Design Environment capability is advanced objectoriented technology. The results of this technology in software are compact, fast, reliable, and easily enhanced with new technology as it becomes available (Applied Wave Research, 2007).

4.3 RECEIVER ARCHITECTURE

The receiver is the most critical component of a wireless communication system. The purpose of the receiver is to reliably recover the desired signal from a wide spectrum of transmitting sources interference, and noise. As the Satellite receiver at C-band becomes more congested, it needs to use higher frequency bands for additional application services. The microwave satellite receiver contains low noise amplifier, downconverter, and bandpass filter. Low noise amplifier is the first element of the satellite receiver in the communications system as shown in Figure 4.1(a) and (b) (Pozar, 2001).

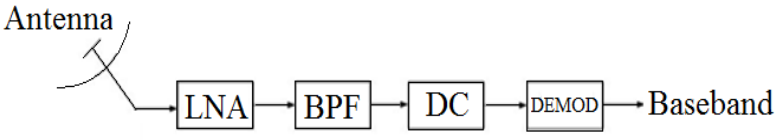

(a)

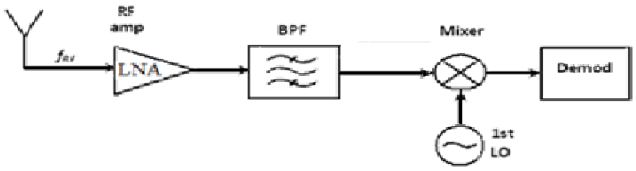

(b)

Figure 4.1: a) The general block diagram of microwave receiver. b) The block diagram of superheterodyne receiver (Pozar, 2001)

4.4 DESIGN OF A LOW NOISE AMPLIFIER

It is undoubted that Low Noise Amplifier (LNA) plays a very important role in the receiver design. Its main function is to amplify extremely low signals without adding noise, so that it preserves the required Signal-to-Noise Ratio (SNR) of the system at extremely low power levels.In communications system, LNA is a special type of electronic amplifier. It is used to amplify distinguishes rewardingly weak microwave signal, captured by the antenna, from the first level of the noise to believable working level. It is often located very close to the antenna, so that losses in the feedline become less critical. Designing a low noise amplifier at Ku-Band requires dealing with a lot of concerns. Circuits at this high frequency (12 GHz) deviate from their normal behavior and are not very easy to implement or fabricate. The design specifications for this amplifier are very demanding, compared to industry and to the communication applications (Abbas and Bin Ihsan, 2005).

The first step of designing amplifiers is typically the device that reduces the noise figure. The second step is to give the required materials to the Gain at a certain noise figure. As a result, the best low noise figure and high associated Gain make it probable for commercial communication systems and industrial applications. Figure 4.2 shows the general block diagram of low noise amplifier circuit which includes the N76038a transistor, RF input, RF output, input matching network, and output matching network.

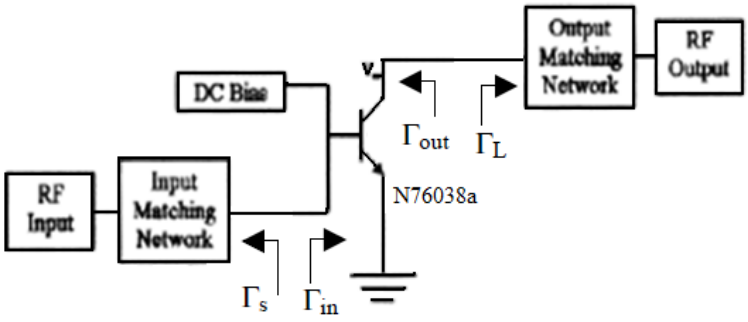

Figure 4.2: General block diagram of LNA circuit (Abbas and Bin Ihsan, 2005)

4.4.1 Circuit Design and Simulations Discussion

The important design considerations in designing a microwave transistor amplifier are stability, gain and noise. Among these factors, the most important for designing LNA are stability and noise. These factors help to choose the right transistor for low noise amplifier design. Besides stability and gain, another important design consideration for a microwave amplifier is its noise figure. In receiver application particularly, it is often required to have a preamplifier with as low noise figure as possible (Pozar, 2001).

Design blocks and simulation results are presented in this Section. As mentioned above, the most important element in low noise amplifier design is the transistor. The principle player among the FET devices is the metal semiconductor field-effect transistor, MESFET or also known as Schottky barrier transistor. It is made with a metal-to-semiconductor junction at the gate. Figures 4.3 and 4.4 show the N76038a GaAs MESFET transistor, which is used in this design, and the noise figure and associated gain versus frequency for N76038a transistor, respectively. GaAs is the most cost effective and widely used material in the family of engineering ceramics. The raw materials from which this high performance technical grade ceramic is made are readily available and reasonably priced, resulting in good value for the cost in

fabricated alumina shapes. With an excellent combination of properties and an attractive price, it is no surprise that fine grain technical grade alumina has a very wide range of applications. Furthermore, it also provides an excellent size and shape capability and high strength and stiffness.

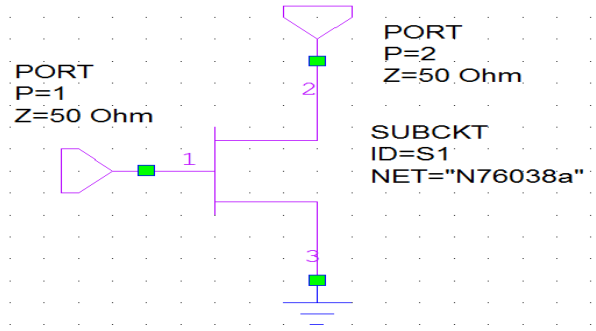

Figure 4.3: N76038a Transistor

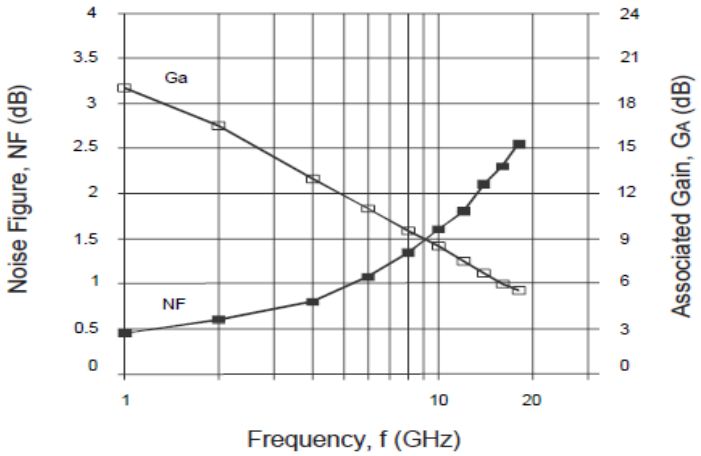

Figure 4.4: Noise figure & associated Gain vs. Frequency (V_{DS} = 3V, I_{DS} = 10mA)

The features of the transistor are low noise figure is 1.8 dB typical at 12 GHz, high associated gain is 7.5 dB typical at 12 GHz, low cost plastic packaging and L_G = 0.3 mm, W_G = 280 mm. (For more details see Appendix A). It is important to determine the main steps or blocks of the first stage of low noise amplifier design. This leads to Figure 4.5 that shows the general block diagram of a low noise amplifier

as configured by AWR Microwave Office Simulator. It includes two ports, and stable amplifier.

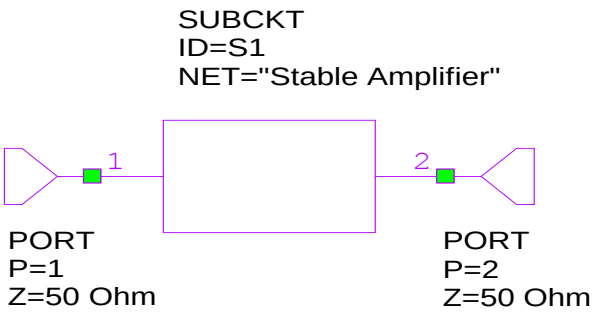

Figure 4.5: General block diagram of a low noise amplifier design

A stable amplifier (final low noise amplifier design) is shown in Figure 4.6 as blocks from which the LNA was designed. Figure 4.6 shows the diagram structure of stable amplifier presented in blocks, this design consists of major electrical elements such as microstrip, ports, ground, capacitors, microstrip I cell, microstrip transmission line, and lumped element series inductors and resistors (Applied Wave Research, 2006).

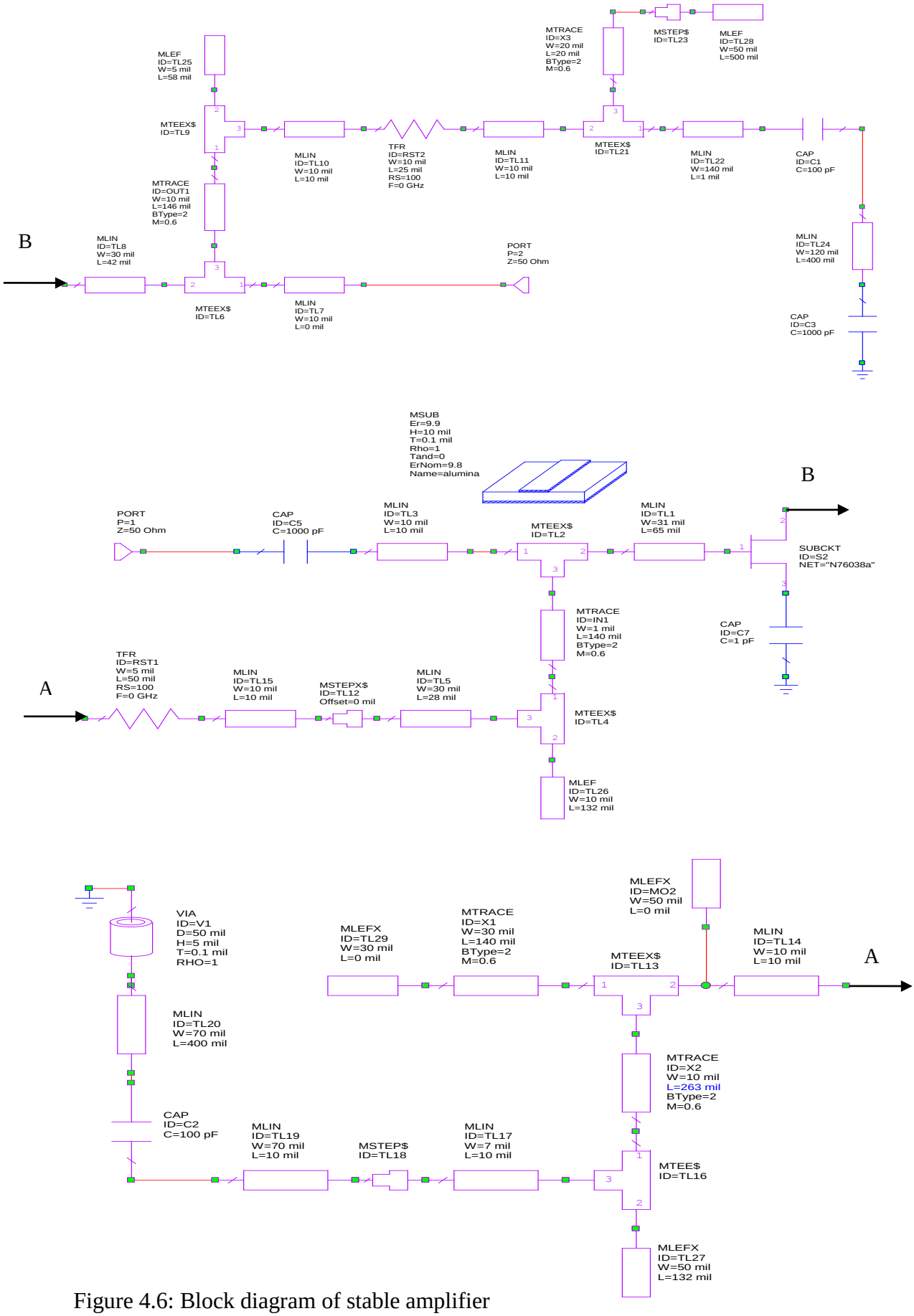

Figure 4.6: Block diagram of stable amplifier

After building the circuit design and running the simulations, the following figures and results appeared. Figure 4.7 shows the gain and the return loss for the overall design of the low noise amplifier. It is found that the amplifier gain is 8.9044 dB and S_{22} is -23.09 dB at 12GHz which gives comparatively better results comparing with other designs with gain of 4.8dB, 6dB, and 6.5 dB low noise amplifiers (Niclas el at., 1978; Shiga el at., 1991; Shiga el at., 1992), respectively at the same frequency 12GHz, and using the same process of MESFET GaAs as observed in Table 2.1.

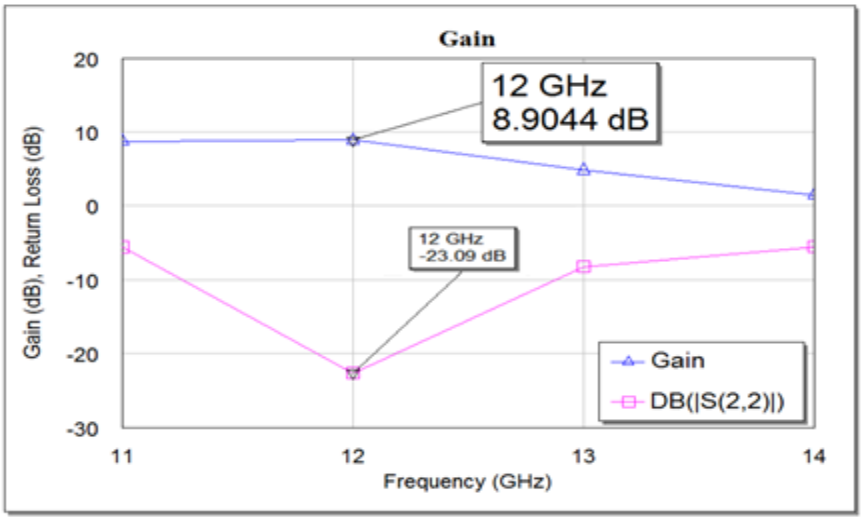

Figure 4.7: Gain and output match of LNA design

Figure 4.8 shows the frequency with the stability factor which is K is more than 1 (1.8264) at 12 GHz. When K is greater than 1, then the device is unconditionally stable for any combination of source and load impedances.

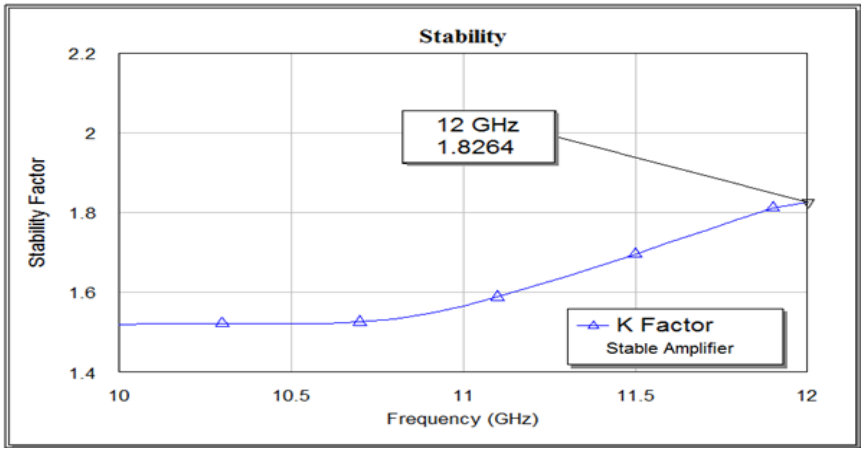

Figure 4.8: The frequency vs. the stability factor for LNA

Figure 4.9 shows the simulation results of Noise Figure (NF) with the frequency at 12GHz, which is 2.188 dB. The NF, which was studied by other researchers and was compared in Table 2.1, is more than the designed LNA. Figure 4.9 shows also the minimum Noise Figure (NF) for the low noise amplifier, which is 1.6278 at 12 GHz.

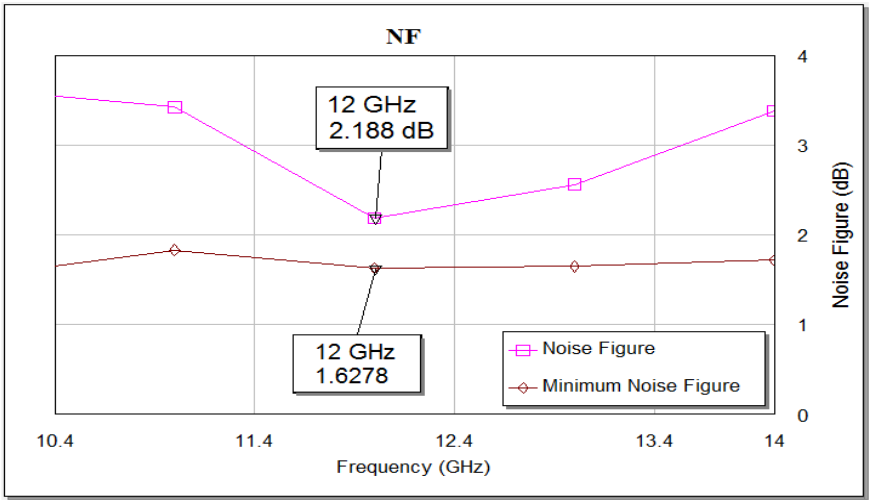

Figure 4.9: Noise Figure (NF) of LNA

Furthermore, Figure 4.10 displays the return loss for the stable amplifier S_{22}, which is -23.09 dB at 12 GHz.

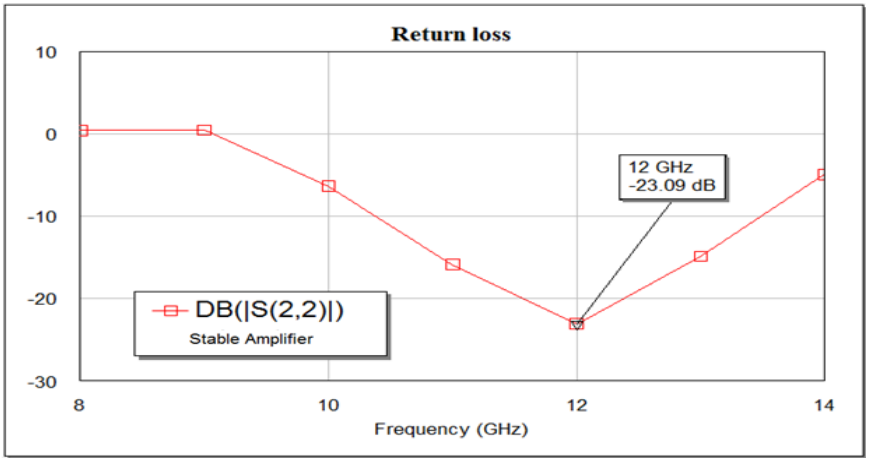

Figure 4.10: Return loss for the final amplifier

To make the design very clear and effective at Ku-Band, Figure 4.11 shows the simulation for the insertion-loss at 12GHz frequency, the low noise amplifier S_{21} represents 8.9 dB.

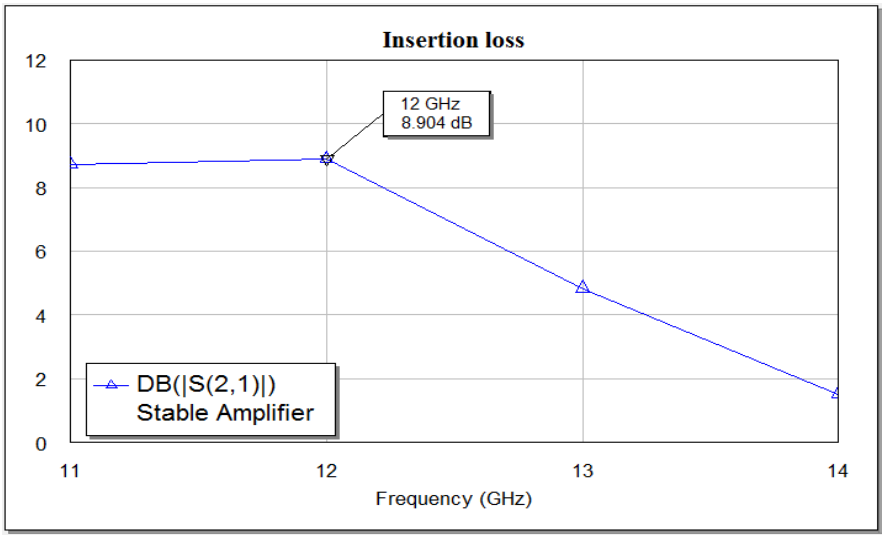

Figure 4.11: Insertion-loss at (12GHz) frequency

The phase shift of S_{11} and that of S_{22} are shown in Figure 4.12. For the low noise amplifier, S_{11} phase shift is -71.39^o and S_{22} phase shift is -0.3884^o at 12GHz.

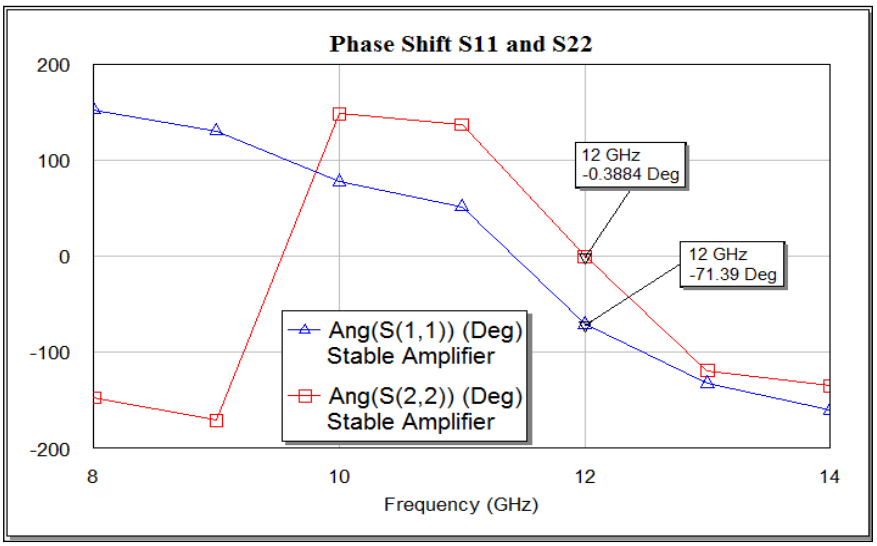

Figure 4.12: Phase shift of $S_{11}$and S_{22}

Figure 4.13 shows that the phase shift for the final amplifier S_{21} and S_{12} are -155.2^{o} and 138.4^{o}, respectively, at 12GHz for Ku-Band.

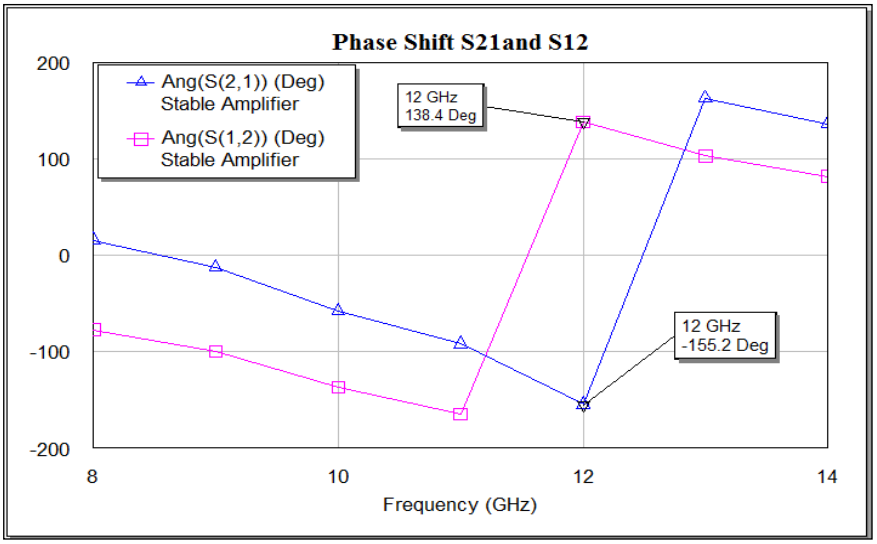

Figure 4.13: Phase shift of $S_{21}$and S_{12}

Table 2.1 summarizes the design parameters of other researcher works for a MMIC low noise amplifiers working at 10-18 GHz. Table 4.1and Table 2.1 show that the gain per stage and the noise figure for this design is better compared with other

studies at 12 GHz. In this work, a LNA has been designed with the highest gain of 8.9044dB at 12 GHz as shown in Table 4.1compared with other works. However, other researchers have got higher noise margin, yet the proposed design can be considered the best candidate for designing the LNA at 12GHz for Ku-Band considering gain and size area.

Table 4.1
The simulated results of 12GHz MMIC low noise amplifier design 1

Study	Process	Frequency (GHz)	Gain (dB)	Min NF (dB)	NF (dB)	Area
This Work	MESFET GaAs	12	8.904	1.6278	2.188	0.316 mm^2

Figure 4.14 represents the layout of a MMIC based proposed low noise amplifier operating at 12GHz Ku-Band, on alumina substrate, using a NEC 76038 GaAs MESFET.

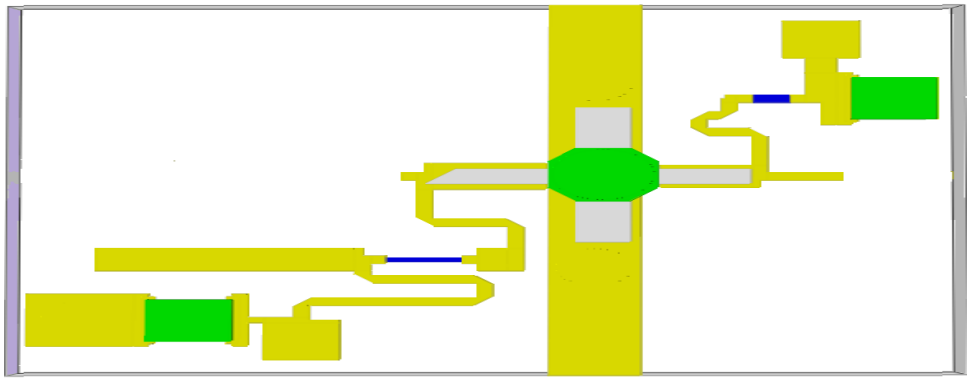

Figure 4.14: The layout of designed MMIC low noise amplifier

Designing a MMIC low noise amplifier at higher frequency, especially at Ku-Band, is very challenging. A low noise amplifier is designed to operate at 12 GHz for Ku Band downlink for satellite receiver. The LNA is designed with 8.90 dB gain and

2.188 dB noise figure at frequency 12GHz as shown in Table 4.2, using the GaAs MESFET transistor on MMIC, with the area of 0.316mm^2. The design of LNA was optimized using AWR (Microwave Office Simulator) 2006 version. The proposed design will enhance the satellite receiver performance.

Table 4.2
Summary results of LNA design

	LNA-Parameters	**Obtained/ simulated results @ 12GHz scale (dB)**	**Expected/ targeted result (dB)**
1.	NF_{min}	2.188 dB	Smaller the better
2.	Gain	8.90 dB	Larger the better

4.5 DESIGN OF BAND PASS FILTER

Filters are widely used in satellite and terrestrial communications applications. Filters are essential RF and microwave components. Modern receiver satellite communication demands tunable filters for flexible and adaptive operations over wide frequency range. Microwave communication systems are expanding rapidly to higher frequency such as Ku-Band since it can provide many advantages over conventional wireless links, for instance, larger bandwidths and smaller device sizes. The goal of this design is to develop a band pass filter to use in satellite receiver using microstrip coupled line which works at 12GHz (Anerao el at., 2009).

Microstrip coupled line filters are convenient for compact designs of wireless communications tools. Depending on the type of transmission line used, transmission line filters can be easy to implement. The parallel coupled-line, i.e. edge-coupled band-pass filter, is widely used in microwave microstrip circuits because of its simple configuration and ease of fabrication. Its analytical development and design procedures for Butterworth and Chebyshev models achieve less than 20% bandwidths.

Thus, the characteristic impedance and precise lengths are two important characteristics of transmission lines; those parameters are used to investigate which transmission line to use to implement filters. BPF is considered one of the most significant devices in satellite receiver, and this filter is designed at Ku-Band frequency (Moradian and Oraizi, 2007).

4.5.1 Circuit Design and Simulations Discussion

Microstrip interdigital filters are widely used in microwave communication systems. The requirements for designing a microwave filter with high performance, small size, and low cost are important for commercial industry, along with the features of ease of processing, reliability and consistency.

The design of BPF can be summarized as an Edge Coupled Microstrip (ECM) filter designed on alumina substrate. The family of engineering ceramics, Alumina is the most cost effective and widely used material. So, it is good value and an attractive price for the cost in fabricated alumina shapes. Several applications used this material for many advantages such as excellent thermal conductivity, good size and shape capability, hard-wear-resistance, high strength and stiffness, and good dielectric properties from DC to GHz frequencies (Farag el at., 2004).

Symmetry is used to simulate two halves of the filter in the "BPF_Half" sub-circuit. Two "BPF_Half" subcircuits are used to make the final "BPF" Filter. Figure 4.15 shows the general blocks of bandpass filter that are designed in AWR. This filter constructed of two sides of BPF (S_1 and S_2), and two ports.

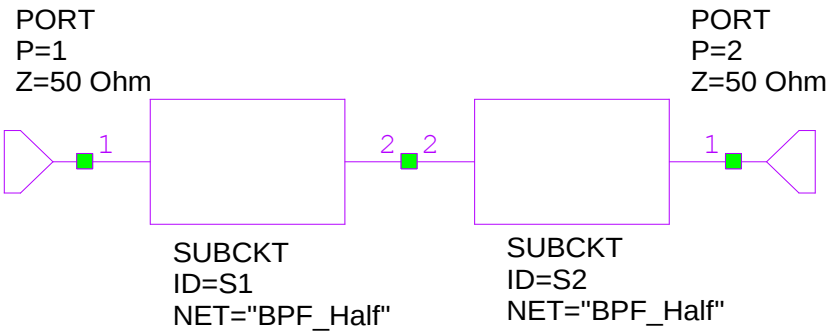

Figure 4.15: General blocks of the bandpass filter

The design of BPF using AWR is shown in Figure 4.16. It consists of microstrip substrate, ports, coupled line section for filters (MCFIL), bend mitered arbitrary angle (MBEND), and microstrip transmission line (MLIN) (Applied Wave Research, 2006).

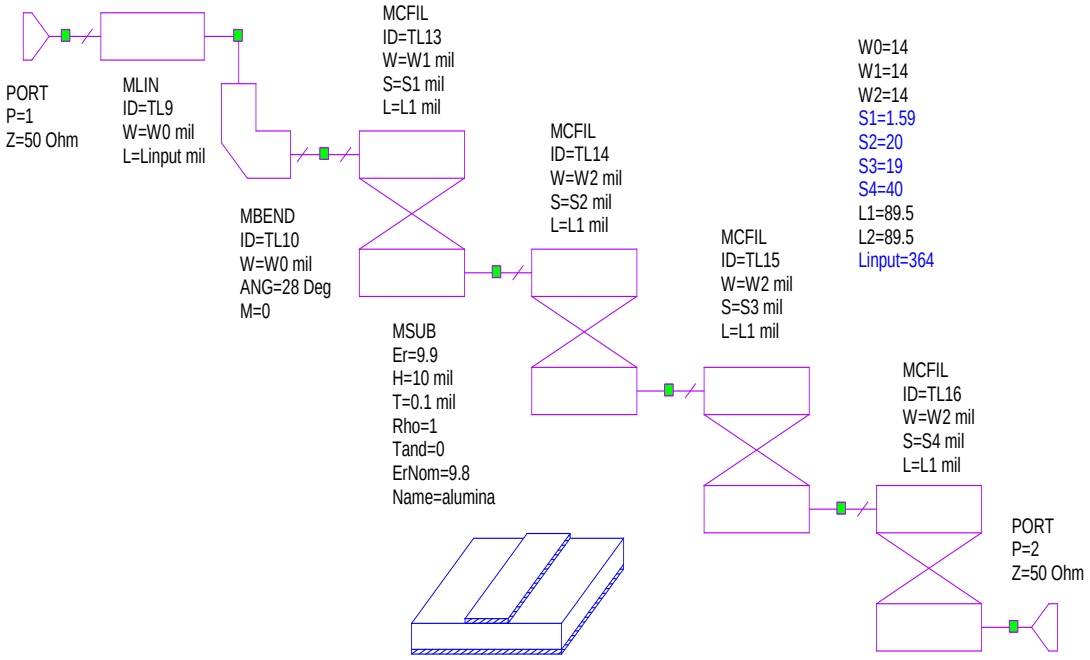

Figure 4.16: The main blocks of the band pass filter design

The variables on the tuner (S1, S2, S3, and S4) change the width of the gaps between the coupled line sections. W0, W1, andW2 are equal 14mil, and they are the conductor width. L1 and L2 are equal 89.5mil, and they are the conductor length.

The optimization goals and simulated results for BPF are shown in Figure 4.17. The plot of the simulated performance of the filter is obtained in the required Ku-Band with very good frequency response and narrow bandwidth. It indicates that the modeling of the filter took into account all necessary parasitic effects and that the manufacturing process is well controlled. The simulated filter has a center frequency of 12GHz with a -6.8415dB insertion loss, -10.053dB return loss, and bandwidth of 86MHz covering the frequency ranges from 11.966GHz to 12.052GHz (around two channels).

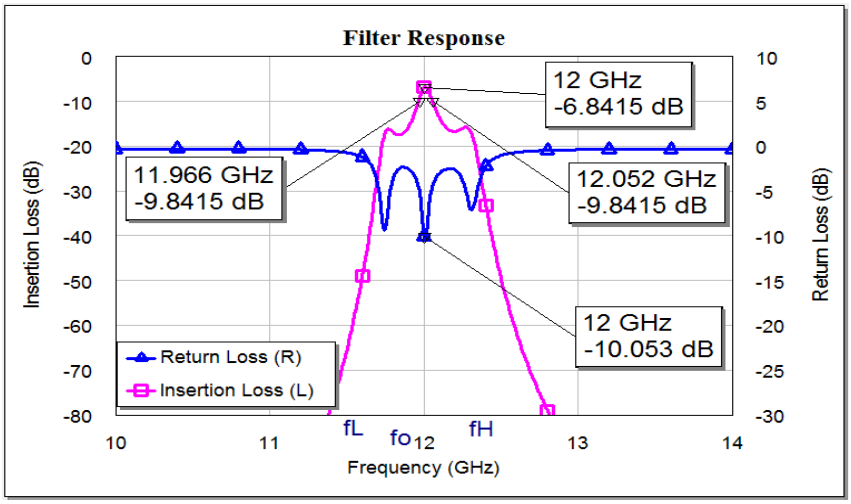

Figure 4.17: Filter response

The bandwidth of an electrical device is usually defined as the difference between the lower and upper half power points. For band pass filter, it passes a specified band of frequencies. The cutoff frequency is the familiar -3dB point on the response curve. This is known as half the maximum value, or −3 dB. Bandwidth, BW

or Δf is the width of the frequency range in which the signal's Fourier transform is nonzero. It is measured in hertz as shown in Equation 4.1.

$$B = f_H - f_L, \text{ Hz} \quad (4.1)$$

Finally, Figure 4.18 displays the layout shape of the first half of the band pass filter from the hand left side, and the second half of the band pass filter from the hand right side. It demonstrates how the elements are arranged.

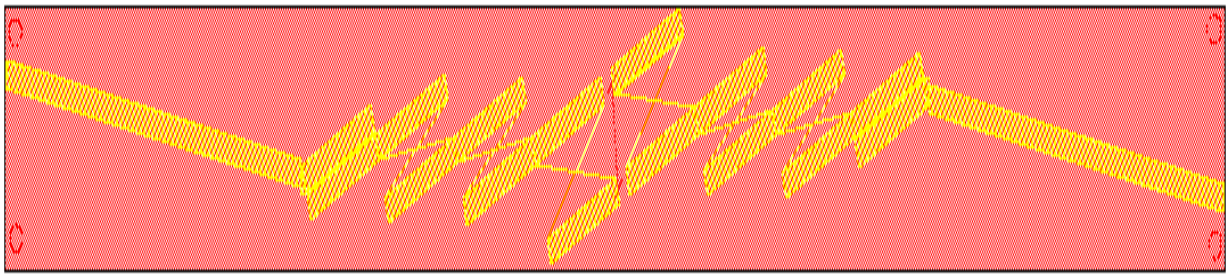

Figure 4.18: The layout of the two halves of the band pass filter

A miniaturized BPF is designed for Ku-Band at12GHz to enhance the satellite receiver performance. The Ku-Band bandpass interdigital filters is studied. Changing the edge coupled microstrip (ECM) structure by increasing the effective coupling area of the microstrip line can make the structure of filter more compact, as well as reduce filter area. Based on these conclusions, a new type of filter is designed. Ku-Band Bandpass Filter (BPF), based on inexpensive commercial (ε_r = 9.9) substrate, is designed. The design and simulation are performed using AWR Microwave Office Simulator. The simulated filter occupies a chip area of 129.16 mm^2. Table 4.3 shows the summary results of BPF design. The filter has a center frequency of 12GHz with a -10.053dB return loss, -6.8415dB insertion loss, and bandwidth of 86MHz, covering

the frequency ranges from 11.966GHz to 12.052GHz. This filter is developed to enhance the telecommunication satellite in the Ku-Band transceivers.

Table 4.3
Summary results of BPF design

	S-Parameters	**Obtained/ simulated results @ 12GHz scale (dB)**	**Expected/ targeted result (dB)**
1.	S_{11}-return loss	-10.053 dB	Smaller the better
2.	S_{21}-insertion loss	-6.8415 dB	Smaller the better

4.6 DESIGN OF DOWNCONVERTER

The second element that is very important and necessary for the receiver design is the downconverter. Mixer translates the signal from the carrier frequency to some intermediate frequency, which is then processed by the baseband circuitry. A new design for the downconverter is built and simulated by AWR 2006 version, which is able to convert the frequency range. It has the ability to optimize and handle with high frequency (12GHz). The downconverter at Ku-Band is the first of its kind to be constructed. This is done in order to develop a basic, 'low-frequency' design for the power of higher-frequency Ku-Band design. Downconverter makes a comparison between two different frequencies: one from the input signal and the other from the oscillator, then it handles and processes the signals, and finally, it creates an output signal.

4.6.1 Circuit Design and Simulations Discussion

After designing the downconverter and running the simulator, the results appeared. This design shows how to simulate a double conversion downconverter using behavioral models. The architecture of double downconverter schematic for this

downconverter/receiver chain, as shown in Figure 4.19, comprises RF1-tone, mixers, nonlinear amplifier system model (NL_AMP2), and bandpass filter (Applied Wave Research, 2006). Referring to the schematic for closer inspection of the configuration of the circuit input port, as well as the LO ports for the mixers, it is noted that the LO power levels of the mixers are made tunable. Therefore, the nonlinearities of the mixers can be adjusted and the variation in the spurious signal output can be observed.

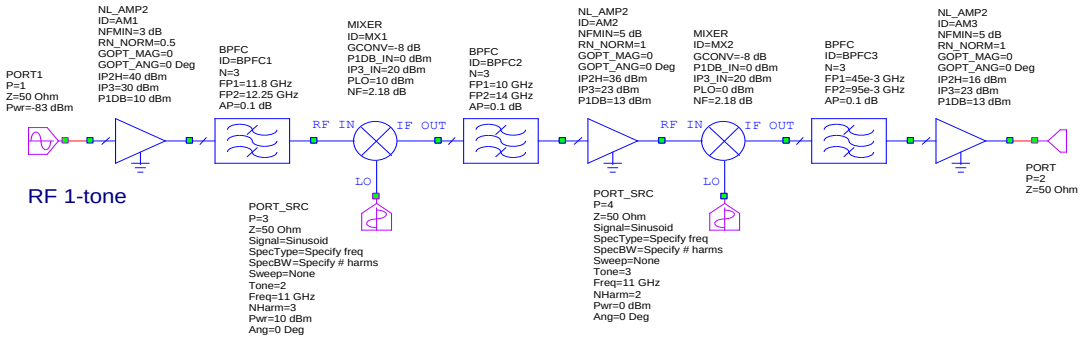

Figure 4.19: The downconverter series

It is now possible to select up to 8 independent tones for circuit simulation. To do this, engineers use the PORT_SRC element. PORT_SRC is an extremely flexible port that allows users to choose the signal shape, the index number of the tone, the frequency of the tone and the number of harmonics for that tone, etc. It even has options for how the frequency and number of harmonics are defined (i.e. as parameters on the port itself, or using the schematic options). PORT_SRC is used for all LO ports in this project. In the double downconverter schematic, a Tone 3 LO source with 2 harmonics is used at the second IF conversion. The NL_Amp2 behavioral amplifier is used. Input and output reflection coefficients can be specified for the NL_Amp2.

Figure 4.20 shows the schematic block of nonlinear amplifier system model (NL_AMP2), which is used to design downconverter at 12GHz for satellite receiver.

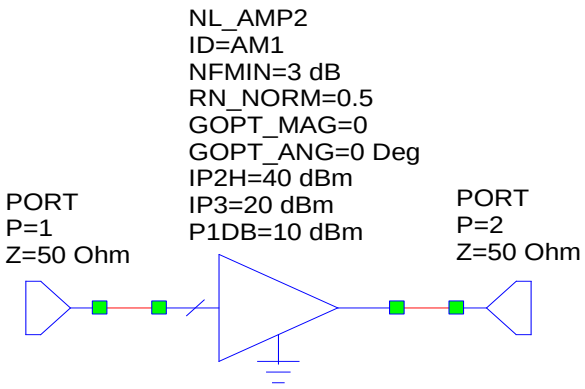

Figure 4.20: The schematic block of nonlinear amplifier system model (NL_AMP2)

Figure 4.21 shows the measured conversion gain performance of the (NL_AMP2), in addition to the noise figure performance of that amplifier. The conversion gain is 9.98dB and the noise figure is 3.01dB at 12GHz.

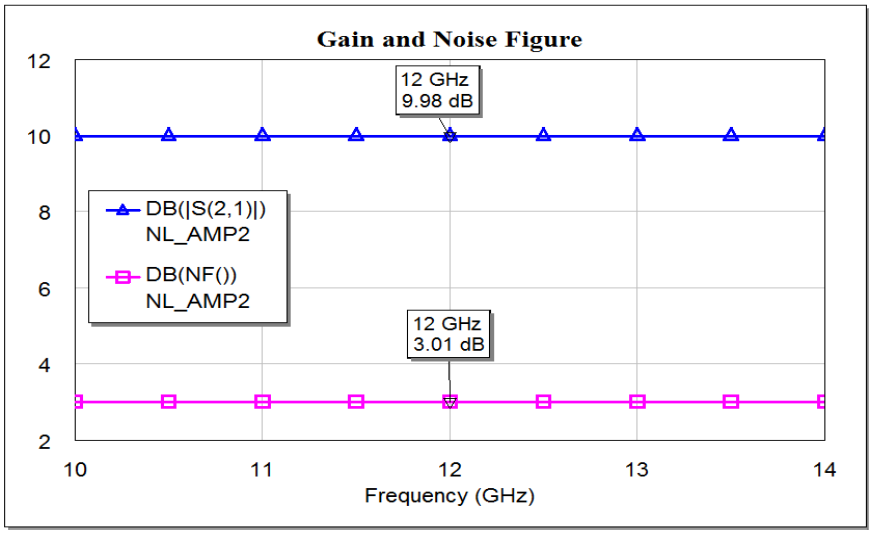

Figure 4.21: The measured gain and NF performance of the (NL_AMP2)

For more investigation, Figure 4.22 shows the schematic circuit block of Chebyshev bandpass filter (BPFC), which is used to design downconverter at 12GHz for satellite receiver.

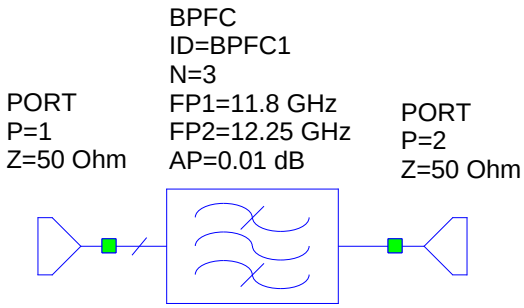

Figure 4.22: The schematic circuit block of Chebyshev Bandpass Filter (BPFC)

To make the simulations of the design clearer, Figure 4.23 demonstrates the range of the bandwidth of BPFC, which is 504 MHz, between 11.807GHz-12.311GHz frequencies. This range of the bandwidth is commonly used for wideband satellite receiver.

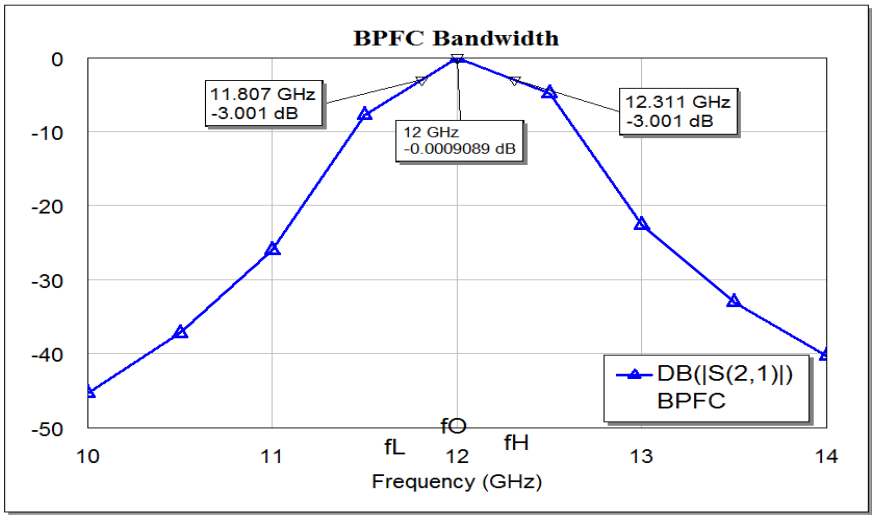

Figure 4.23: The range of the bandwidth of BPFC

Figure 4.24 shows the shape of the oscilloscope signal represented in the graph by voltage (V), and time domain in (ns).

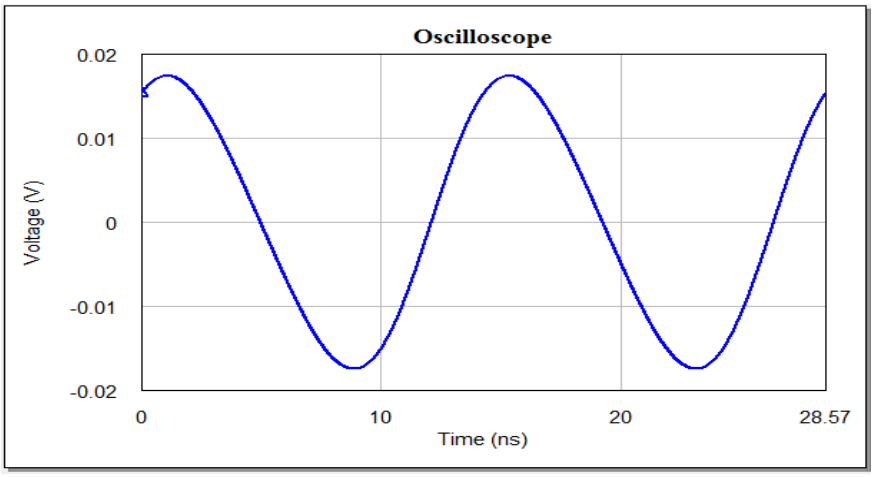

Figure 4.24: The shape of the oscilloscope signal voltage (V) and time domain in (ns)

Finally, downconverter design shows the bandwidth range, which is 475MHz, between 11.776GHz to 12.241GHz frequencies. The center frequency is 12GHz as shown in Figure 4.25.

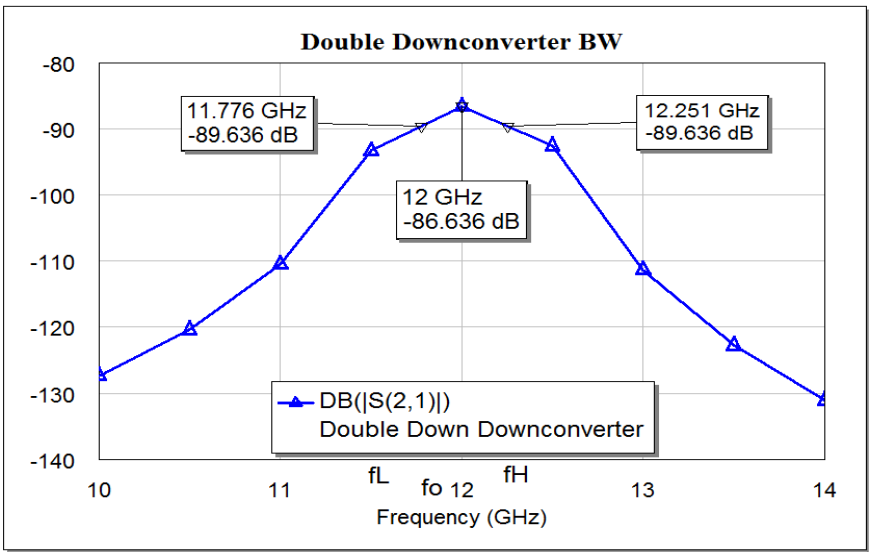

Figure 4.25: Gain and bandwidth range of downconverter

The most important simulated result of this design is shown in Figure 4.26; this figure displays the converted frequency from 12GHz to 1GHz with power 111.4dBm. The design of downconverter is used as a significant component in satellite receiver that converts high frequency to low and believable level work of frequency. Furthermore, Figure 4.27 shows the downconverter return and insertion loss, and the summary results of downconverter design are shown in Table 4.4.

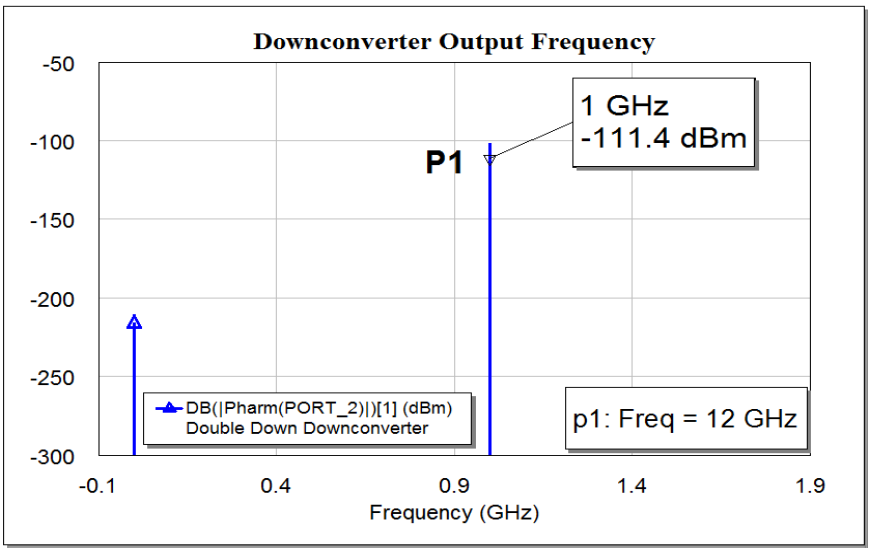

Figure 4.26: The converted frequency from 12GHz to 1GHz with power

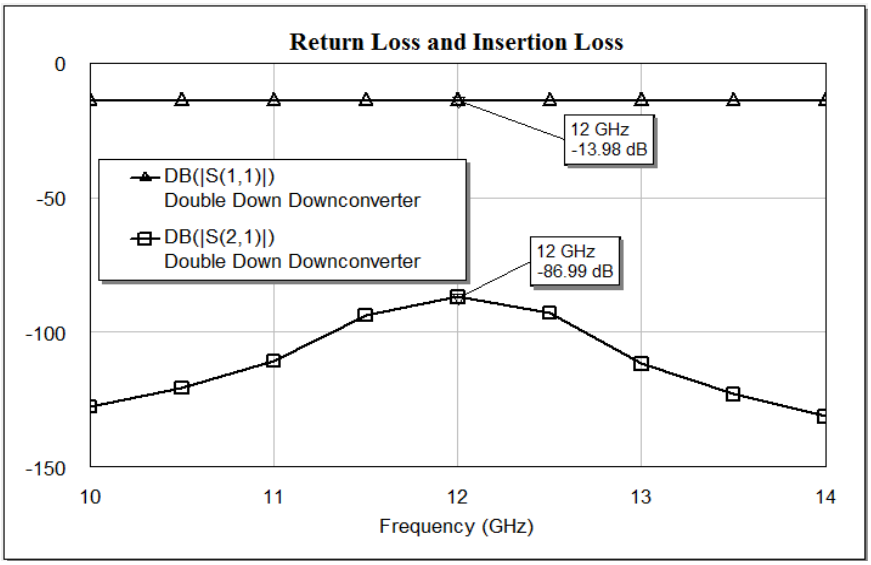

Figure 4.27: Downconverter return and insertion loss

A downconverter is designed to convert 12GHz-1GHz for Ku-Band downlink for satellite receiver. The DC is designed with 86.636 dB gain and bandwidth range 475MHz between 11.776GHz-12.241GHz frequencies, with center frequency as 12GHz, and using NL_AMP2 amplifier and BPFC filter. The design of DC is optimized using Microwave Office Simulator (AWR) 2006 version. The projected design would improve the satellite receiver performances.

Table 4.4
Summary results of downconverter design

	S-Parameters	**Obtained/ simulated results @ 12GHz scale (dB)**	**Expected/ targeted result (dB)**
1.	S_{11}-return loss	-13.98dB	Smaller the better
2.	S_{21}-insertion loss	-86.99dB	Smaller the better

4.7 SUMMARY

Three components of a satellite receiver at 12GHz Ku-Band are designed. The microwave satellite receiver is comprised of low noise amplifier, downconverter, and bandpass filter. Designing a MMIC LNA at a higher frequency, especially at Ku-Band, is very challenging. The LNA is designed with 8.90 dB gain and 2.188 dB noise figure, using the GaAs MESFET transistor on MMIC, with an area of 0.316mm^2. A new type of interdigital miniaturized bandpass filter at Ku-Band is designed. The simulated filter occupies a chip area of 129.16mm^2. The filter has a center frequency of 12GHz with a -6.8415dB return loss, -10.053 insertion loss, and bandwidth of 86MHz, covering the frequency ranges from 11.966GHz to 12.052GHz. A downconverter is designed to convert 12GHz- 1GHz for Ku Band downlink for satellite receiver. The DC is designed with 86.636 dB gain and bandwidth range

475MHz between 11.776GHz-12.241GHz frequencies. The design of the receiver is optimized using Microwave Office Simulator (AWR) 2006 version.

CHAPTER FIVE

PERFORMANCE EVALUATION OF RECEIVER

5.1 INTRODUCTION

At Ku-Band, the environmental effect is the most significant and crucial for designing the microwave communication systems. This chapter discussed the building and simulating of a complete transmitter-channel-receiver chain for Phase Shift Keying (PSK) and Quadrature Amplitude Modulation (QAM) transmission, and focuses on the evaluating performance of satellite receiver based on designing LNA, BPF, and DC in Chapter Four (receiver design at Ku-Band), and using link budget calculations in Chapter Three (link budget calculation for Ku-Band). This design was simulated by using Visual Simulating System (VSS) Ver. 2006. The next Section presents the properties of Visual Simulating System (VSS). Information on PSK and QAM modulation are discussed in Section 5.3, while Section 5.4 discusses the Bit Error Rate (BER) for satellite receiver. Section 5.5 shows the architecture of simulation block design. Section 5.6 displays the simulation results with the discussion of the system, and Section 5.7 presents the conclusion of this chapter.

5.2 VISUAL SIMULATING SYSTEMS

For complex RF communication systems, Visual Simulation System (VSS) is a complete and comprehensive software design. The technology of VSS provides the ability to design the right system construction, and to create suitable specifications for each of the underlying components in the communications designs. VSS is a software that enables the engineer to design and examine end-to-end RF communication

systems. The function of this simulator is to design systems composed of modulated signals, encoding schemes, channel blocks and system level performance measurements. VSS performs simulations predefined of transmitters and receivers. It builds modified transmitters and receivers for customers from basic blocks. The data analysis is needed to demonstrate BER curves, constellations, and power spectrums. VSS provides also a real-time tuner that allows tuning for designs in order to observe the immediately changes in the data display. The time-domain simulator in VSS uses a fixed time step, which is set either by individual blocks inside a system diagram (usually sources) and inherited by subsequent blocks, or by the default system settings for each system chart (Applied Wave Research, 2007).

5.3 PHASE SHIFT KEYING AND QUADRATURE AMPLITUDE MODULATION

Phase Shift Keying (PSK) is a phase modulation version of digital frequency modulation technique, where the phase of the carrier wave is modulated to encode bits of digital information for each phase change. Radio-frequency is a carrier signal that uses four phase states to code two digital bits in QPSK digital modulation. Sometimes QPSK is known as quaternary or quadriphase PSK, 4-PSK, or 4-QAM, QPSK. The function of PSK is sending data over coaxial cable networks. PSK is used mostly for sending data from the cable subscriber upstream to the Internet. This is because it is easy to implement and fairly resistant to noise. Even or odd bits are used to modulate the in-phase element of the carrier, and at the same time are used to modulate the quadrature-phase component of the carrier (Xiong, 2006).

Involving both amplitude and phase coding, QAM is a system that modulates digital signals onto a radio-frequency carrier signal. QAM includes an analog and a

digital modulation format. It conveys some aspect of a carrier signal, the carrier wave of two analog message signals, or two digital bit streams. This is done by modulating the amplitudes of two carrier waves, using the Amplitude-Shift Keying (ASK) digital modulation scheme or Amplitude Modulation (AM) analog modulation scheme. These two waves, usually sinusoids, are out of phase with each other by 90° and are thus called quadrature carriers or quadrature parts. In the digital QAM case, a finite number of at least two phases and at least two amplitudes are used. QAM is used widely as a modulation method for digital microwave telecommunication systems (Xiong, 2006).

5.4 BIT ERROR RATE

In microwave telecommunication transmission, the Bit Error Rate (BER) is the percentage of bits that has errors relative to the total number of bits received in a transmission as shown in Equation 5.1, usually expressed as 10 to a negative power. BER indicates how often a packet or data unit has to be retransmitted because of an error. BER is a unit-less performance measure. High a BER might indicate that a slower data rate would actually recover overall transmission time for a given amount of transmitted data since the BER might be reduced. When data is transmitted over a data link, there is a possibility of errors being introduced into the system. If errors are introduced into the data, then the integrity of the system may be compromised. As a result, it is required to evaluate the performance of the system, and to observe the bit error rate percentage.

$$\text{BER} = \text{number of errors occurred/total number of bits sent} \quad (5.1)$$

When the bit error rate becomes very small, possibly insignificant and having no noticeable effect on the overall system, it means that the medium between the transmitter and receiver is good and that the signal to noise ratio is high. However, if the noise can be detected, then there is a chance that the bit error rate needs to be considered. To achieve a satisfactory bit error rate, it is necessary to balance all the available factors. Normally it is not possible to achieve all the requirements, and some trade-offs are required (Breed, 2003).

The most significant parameter in digital microwave communication or data transmission is E_b/N_0 (the energy per bit to noise power spectral density ratio). It is a normalized Signal-to-Noise Ratio (SNR) measure, also known as the "SNR per bit". It is mainly useful when comparing the bit error rate performance of different digital modulation schemes without taking bandwidth into account (Pearce, 2000).

5.5 THE ARCHITECTURE OF SIMULATION BLOCK DESIGN

A transmitter is an object (source) that sends information to an observer (receiver), which is used in satellite communication and RF microwave wireless systems. Universal sense and vocal cords may also be considered as examples of a transmitter. In a satellite receiver and broadcasting, a transmitter typically consists of a power supply, an oscillator, a modulator, and amplifiers for Audio Frequency (AF) and Radio Frequency (RF). The signal information is modulated by tools or modulators onto the carrier frequency, which then broadcasts.

This system design builds and simulates a complete transmitter-channel-receiver chain for different transmission modulation schemes. VSS blocks able to generate a Quadrature Phase Shift Keying (QPSK) source using elementary blocks or

a “black box” QPSK modulator (called QPSK _SRC). For many common modulation methods, corresponding black boxes already exist in VSS.

Figure 5.1 shows the QPSK _SRC block diagram in order to generate a QPSK source using a “black box” QPSK modulator.

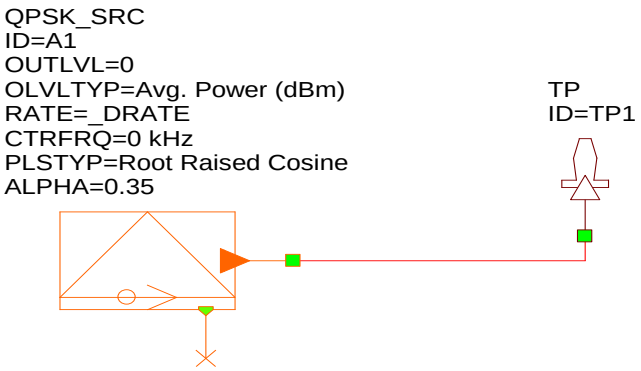

Figure 5.1: QPSK modulator source

The simulation of the power spectrum of the QPSK signal generated by the block (QPSK _SRC) is shown in Figure 5.2.

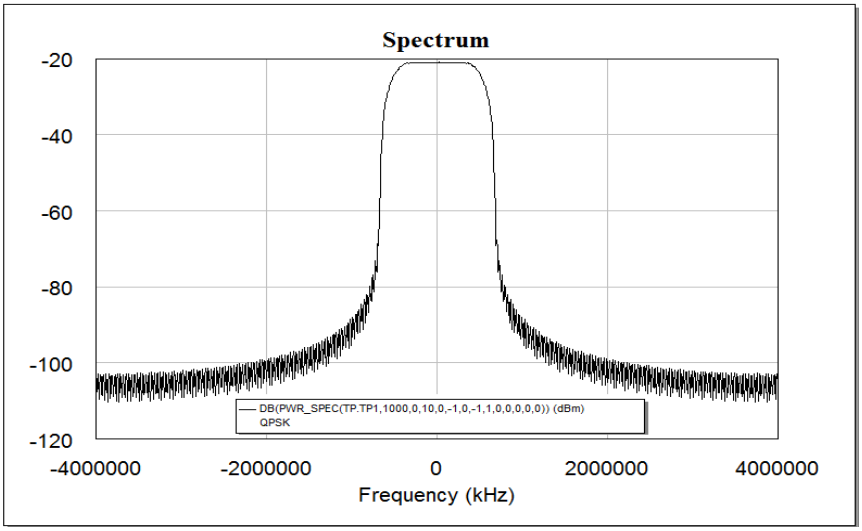

Figure 5.2: The power spectrum of the QPSK modulator

Figure 5.3 shows a complete system design of transmitter-channel-receiver chain. The receiver is built from LNA, BPF, and DC with elementary VSS blocks, in order to estimate the value of BER and evaluating the output performance of the 16-PSK and 16-QAM demodulator with different polarization at several availabilities. The modulated signal (output) of the transmitter is passed through an AWGN channel and then demodulated by the designed receiver mentioned in Chapter Four. The complete receiver chain consists of a filter (PLSSHP), an FM discriminator (FM_DSCRM), an integrate-and-dump block (INTG_DMP), and an ADC block (Applied Wave Research, 2006).

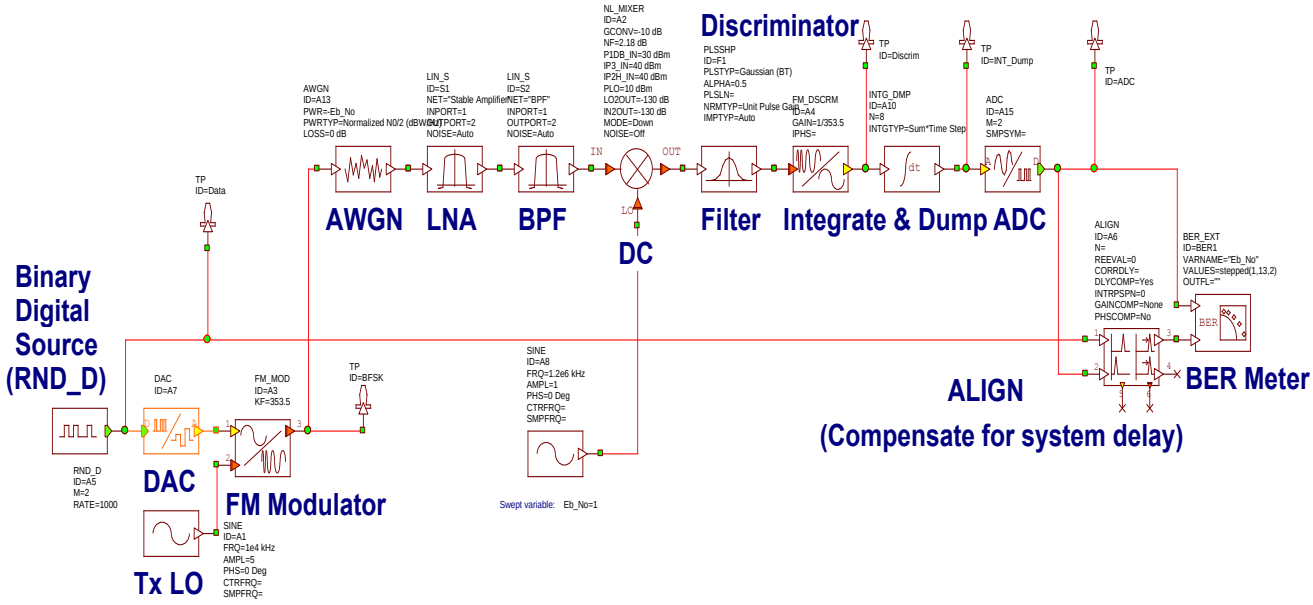

Figure 5.3: Block diagram of simulation system

One of the functions of the transmitter is to generate the power spectrum of PSK and QAM modulation. A rain attenuation loss is assumed to be similar to the White Gaussian Noise Channel in the software Visual Simulator System, therefore

White Gaussian Noise Channel (AWGN) is located between the transmitter and the receiver system, which is used to test the performance of BER for the 16-PSK and 16-QAM demodulator, by considering the changes in the atmospheric losses (which are calculated in Chapter Three) either in clear air or in transmission losses through the parameter (LOSS) in AWGN. The designed receiver by AWR in Chapter Four (LNA, BPF, and DownConverter) is exported in order to simulating the system in Visual Simulating System (VSS) to observe and evaluate the changes in the Bit Error Rate (BER).

5.6 SIMULATION RESULTS

The most important aspect in evaluating the performance of the receiver, as designed in Chapter Four, is the bit error rate. For more useful investigation, the simulated results provide the statistics of BER simulation with E_b/N_0, in clear air and in rain effect with different modulation at various availabilities.

5.6.1 Simulation Results in Clear Air

As shown in the Figures 5.4 and 5.5 .These figures show the 16-PSK_BER in clear air which gives $1e^{-010}$ at 13dB and the 16-QAM_BER in clear air which gives $2.0745e^{-006}$ at 14dB, for the complete transmitter-channel-receiver chain design, respectively.

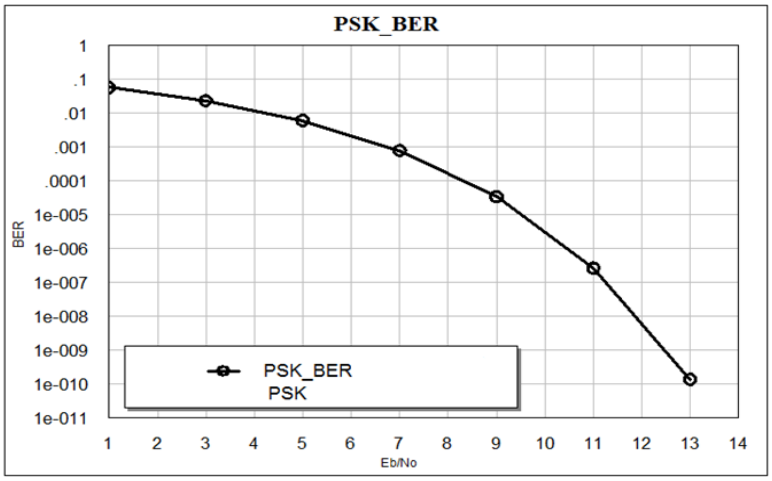

Figure 5.4: The bit error rate for 16-PSK in clear air

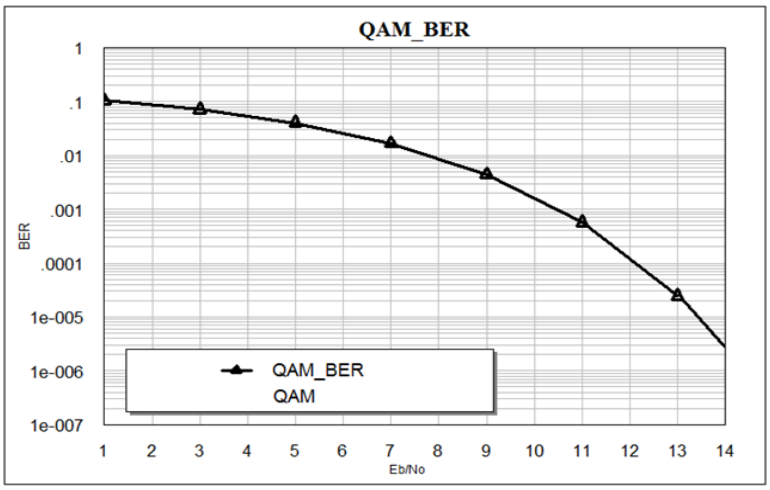

Figure 5.5: The 16-QAM_BER in clear air

5.6.2 Simulation Results in Rain Fade

On the other hand, it is necessary to estimate the bit error rate with respect to the atmospheric losses (estimated rain) as in Section 3.4 (3.4.2 part 2: Rain Fade Calculation for MEASAT-2 at Ku-Band).

Figures 5.6-5.14 show the output relationship between the statistics BER and E_b/N_0 respecting the value of the rain fade (attenuation) for the complete transmitter-channel-receiver chain. These figures display the vertical, horizontal, and circular polarizations for the three elements of the availability which are $A_{0.1\%}$, $A_{0.01\%}$, and

$A_{0.001\%}$, and that means 99.9%, 99.99%, and 99.999%, respectively. Considering the rain fade, transmission losses are calculated for the three availabilities as in Chapter Three, and the calculated results are shown in Table 3.1.

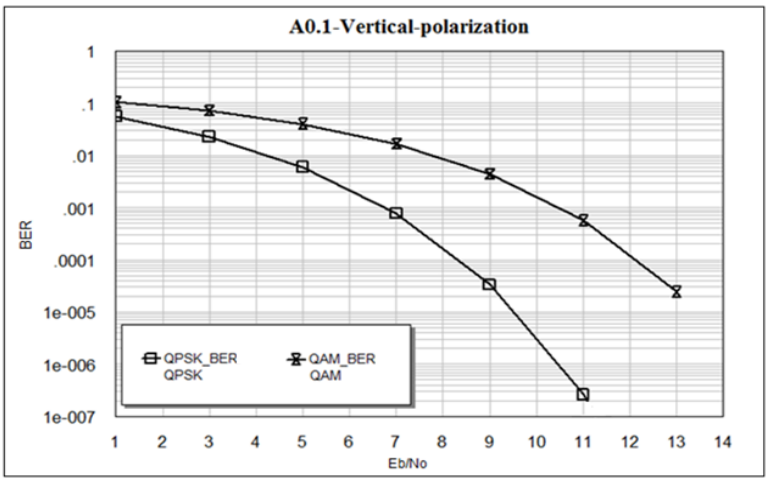

Figure 5.6: Vertical-polarization at $A_{0.1\%}$ for 16-PSK and16-QAM

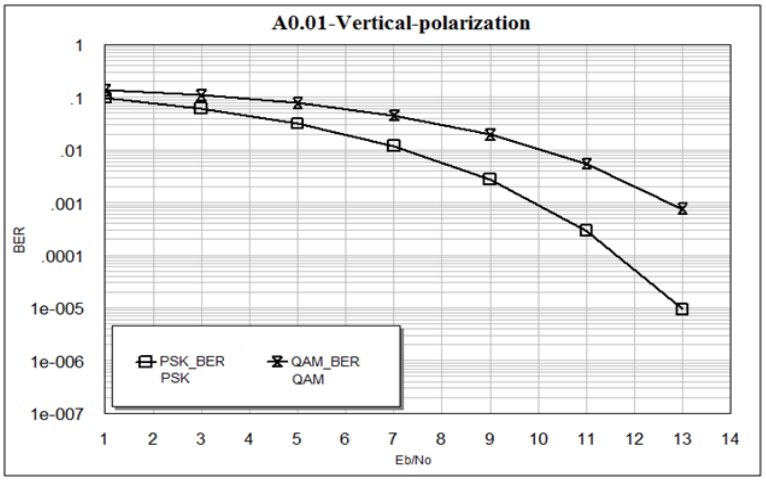

Figure 5.7: Vertical-polarization at $A_{0.01\%}$ for 16-PSK and16-QAM

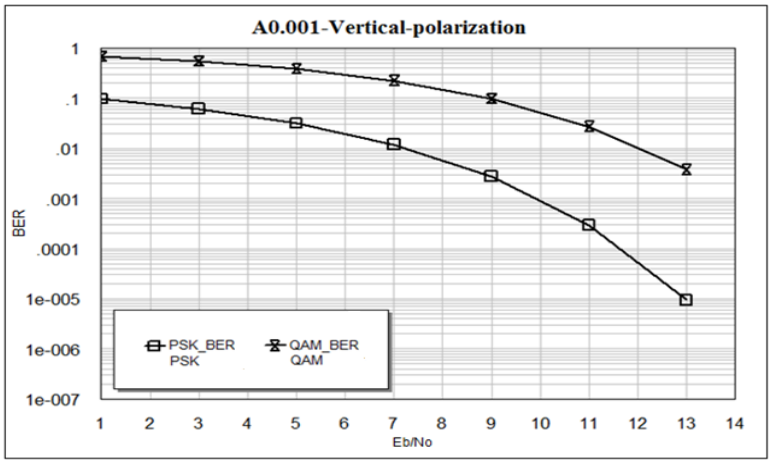

Figure 5.8: Vertical-polarization at $A_{0.001\%}$ for 16-PSK and16-QAM

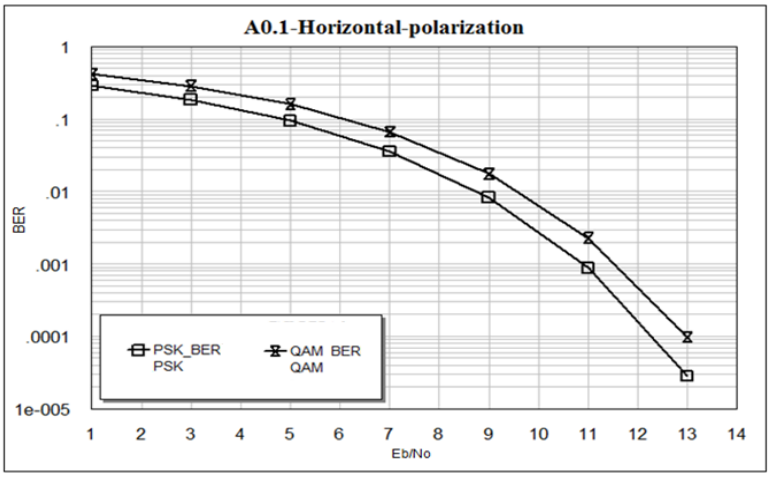

Figure 5.9: Horizontal-polarization at $A_{0.1\%}$ for 16-PSK and16-QAM

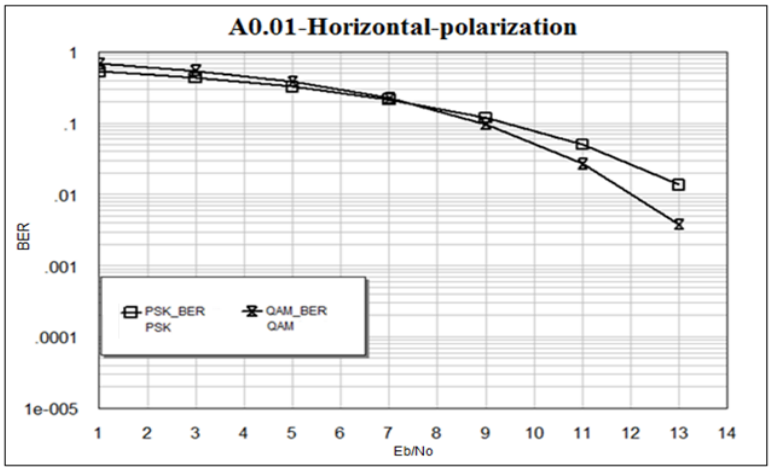

Figure 5.10: Horizontal-polarization at $A_{0.01\%}$ for 16-PSK and16-QAM

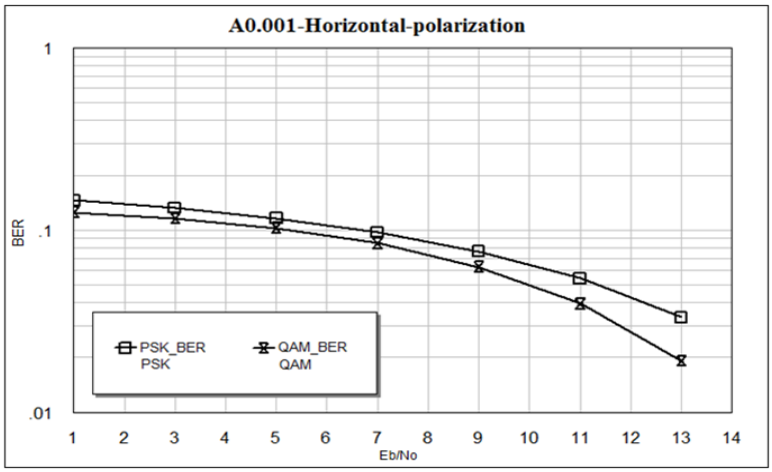

Figure 5.11: Horizontal-polarization at $A_{0.001\%}$ for 16-PSK and16-QAM

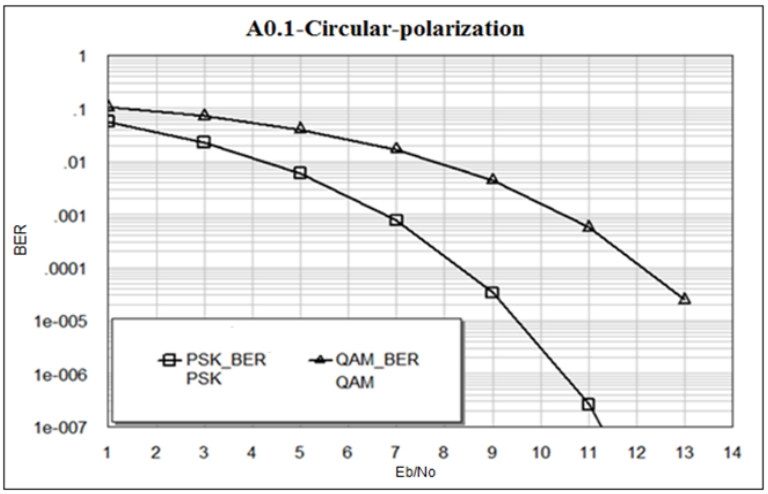

Figure 5.12: Circular-polarization at $A_{0.1\%}$ for 16-PSK and16-QAM

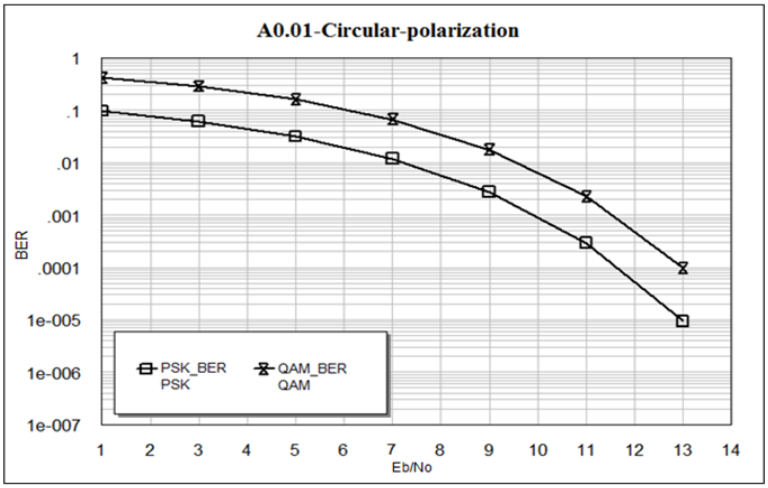

Figure 5.13: Circular-polarization at $A_{0.01\%}$ for 16-PSK and16-QAM

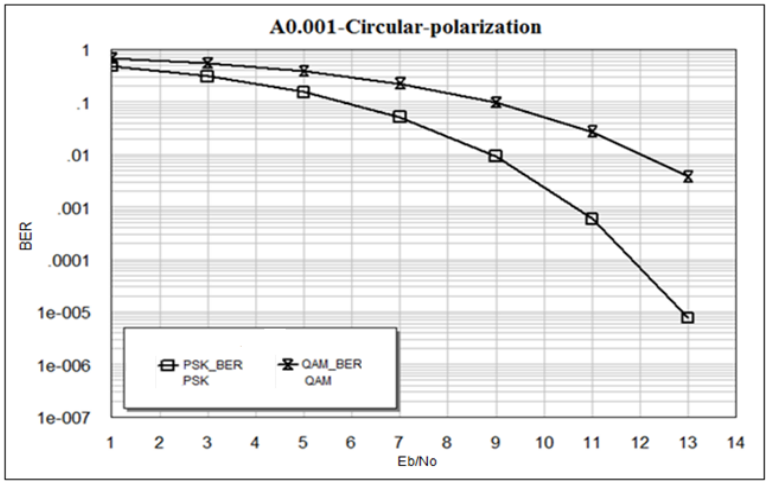

Figure 5.14: Circular-polarization at $A_{0.001\%}$ for 16-PSK and16-QAM

Table 5.1 shows the comparison between the 16-PSK and 16-QAM, and the comparison is successfully done. The table demonstrates that the 16-PSK values for the availability $A_{0.1\%}$, $A_{0.01\%}$, and $A_{0.001\%}$ in vertical polarization are better than the results in 16-QAM. At the same time, the values of the bit error rate are proportional with the availability.

Table 5.1
The 16-PSK and 16-QAM vertical polarization for $A_{0.1\%}$, $A_{0.01\%}$, and $A_{0.001\%}$ availability

Availability	**Transmission Loss**	**16-PSK**	**16-QAM**
$A_{0.1\%}$-Vertical-polarization	8.81436 dB	11.21dB1.0222e-007	12.98dB2.0406e-005
$A_{0.01\%}$-Vertical-polarization	20.0376dB	13dB6.7793e-006	12.97dB0.00010466
$A_{0.001\%}$-Vertical-polarization	31.54406 dB	13.2dB9.4169e-006	13.2dB0.0031069

Table 5.2 displays a comparison between the $A_{0.1\%}$, $A_{0.01\%}$, and $A_{0.001\%}$ availability for 16-PSK and 16-QAM in horizontal polarization. The results show that the value in 16-PSK is better than that of the 16-QAM for $A_{0.1\%}$ availability. But the results of BER at16-QAM are better than 16-PSK at $A_{0.01\%}$, and $A_{0.001\%}$ .In this table,

the $A_{0.1\%}$ availability is better than that of $A_{0.01\%}$ availability, and also $A_{0.01\%}$ availability is better than that of $A_{0.001\%}$ availability.

Table 5.2
The 16-PSK and 16-QAM horizontal polarization for $A_{0.1\%}$, $A_{0.01\%}$, and $A_{0.001\%}$ availability

Availability	**Transmission Loss**	**16-PSK**	**16-QAM**
$A_{0.1\%}$-Horizontal-polarization	10.1626 dB	13dB2.3214e-005	13dB9.2004e-005
$A_{0.01\%}$-Horizontal-polarization	22.87972 dB	12.96dB0.011917	12.97dB0.0031318
$A_{0.001\%}$-Horizontal-polarization	35.52207 dB	13.2dB0.03404	13.2dB0.020927

To make the comparisons very clear, Table 5.3 shows the same comparison for 16-PSK and 16-QAM as in Table 5.1 and Table 5.2 for the results, but the polarization is circular. In addition to that, the $A_{0.1\%}$ availability for vertical polarization is the best value among the $A_{0.1\%}$ circular and horizontal polarization. The $A_{0.01\%}$ availability circular polarization is in the middle (between $A_{0.1\%}$, and $A_{0.001\%}$), and the $A_{0.01\%}$ availability horizontal polarization is the worst result, and this comparison is applicable $A_{0.1\%}$, and $A_{0.001\%}$ for the three polarizations too, for 16-PSK either 16-QAM.

Table 5.3
The 16-PSK and 16-QAM at circular polarization for $A_{0.1\%}$, $A_{0.01\%}$, and $A_{0.001\%}$ availability

Availability	**Transmission Loss**	**16-PSK**	**16-QAM**
$A_{0.1\%}$-Circular-polarization	9.460446 dB	11.25dB1.1222e-007	13dB2.1406e-005
$A_{0.01\%}$-Circular-polarization	21.44257 dB	13dB9.0413e-006	13dB0.00075867
$A_{0.001\%}$-Circular-polarization	33.51535 dB	13.2dB1.0712e-005	13.2dB0.0032841

5.6.3 Simulation Results in Scintillation and XPD

Referring to Table 3.2 in Chapter Three, the value of transmission loss from Scintillation aspect was 0.0084dB, and this calculated value does not affect the received signals in transmitter-receiver design system, which means that there are no changes on the bit error rate in respect with E_b/N_0. For XPD aspect, the value of calculated loss was 20.91dB. Figure 5.15 shows the $A_{0.01\%}$ availability for XPD. Thus, the BER for XPD with 16-PSK is 0.019917 at13dB, and with 16-QAM is 0.0039318 at13dB. So, the BER with 16-QAM is better than the 16-PSK modulation.

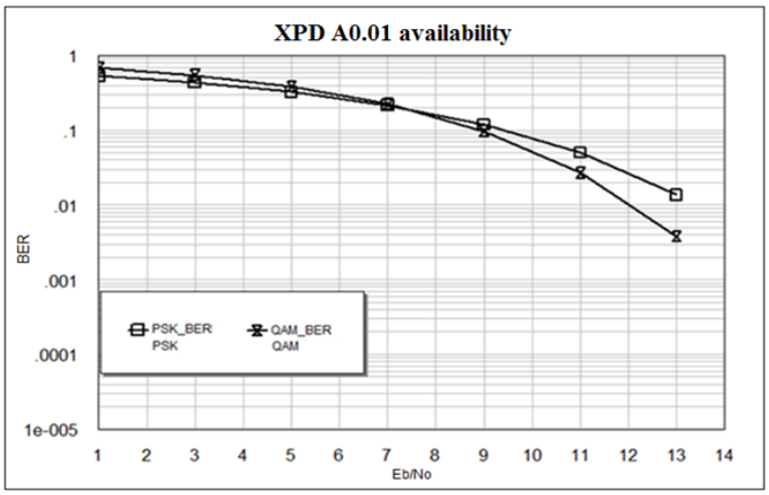

Figure 5.15: The XPD loss at $A_{0.01\%}$ for 16-PSK and16-QAM

5.6.4 Simulation Results for $A_{0.01\%}$ Availability at Different PSK Levels

To make this design a contributed one, Figure 5.16 shows the comparison between different levels of PSK modulation which are 2-PSK(BPSK), 4-PSK(QPSK), 8-PSK, 16-PSK, 32-PSK, and 64-PSK at $A_{0.01\%}$ availability where the transmission loss is 20.0376 dB. The BER for 2-PSK is $2.5158e^{-007}$at 11dB, 4-PSK is $5.0941e^{-007}$at 11dB, 8-PSK is $1.0743e^{-006}$at 13dB, 16-PSK is $1.3219e^{-005}$at 13dB, 32-PSK is 0.026898at

13dB, and 64-PSK is 0.096291at 13dB. The bit error rate for 2-PSK (BPSK) is the best and BER for 64-PSK is the worst.

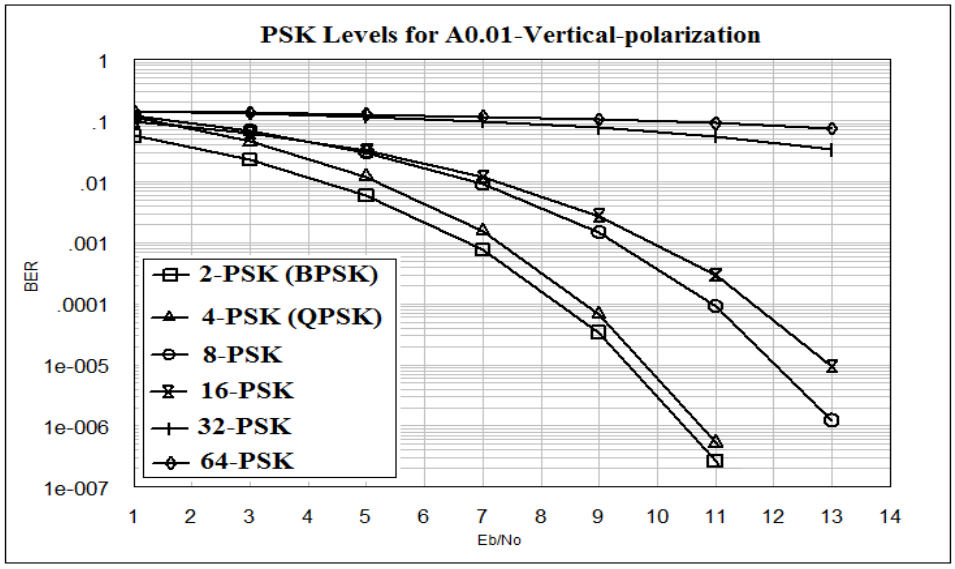

Figure 5.16: The PSK levels for $A_{0.01\%}$ in vertical polarization

5.7 SUMMARY

A transmitter-channel-receiver chain is designed and simulated with 16-PSK and 16-QAM modulators in VSS at different availabilities. The receiver is designed in Chapter Four, and the complete transmitter-channel-receiver chain is simulated to show the evaluation change of BER performance in clear air and with the atmospherical losses (rain attenuation) as calculated in Chapter Three. The simulated results for $A_{0.1\%}$, $A_{0.01\%}$, and $A_{0.001\%}$ availability in vertical, horizontal, and circular polarizations show the performance of bit error rate in transmission losses. The results show a perfect lower bit error rate for the proposed design of a satellite RF receiver at $A_{0.1\%}$ availability for 16-PSK and 16-QAM.

CHAPTER SIX

CONCLUSION AND FUTURE WORK

6.1 CONCLUSION

Heavy rainfall, high humidity, and high temperature are among many factors that affect the performance of a satellite receiver in tropical regions. The parameters that are examined in the calculation process for this design are scintillation, Cross-Polarization Depolarization (XPD), and rain fade attenuation. Attenuation by atmospheric losses, which is entirely caused by absorption, depends mainly on frequency, elevation angle, altitude above sea level and water vapour density. At frequencies below 10 GHz, it may normally be neglected. Its importance increases with frequency above 10 GHz. It becomes a critical issue at that frequency, especially for low elevation angles.

The components of the satellite receiver at 12GHz Ku-Band are designed. The receiver is optimized using AWR (Microwave Office Simulator) 2006 version. The LNA is designed with 8.90 dB gain and 2.188 dB noise figure, using the GaAs MESFET transistor on MMIC, with an area of 0.316mm^2. A new type of interdigital miniaturized bandpass filter at Ku-Band is also designed. The simulated filter occupies a chip area of 129.16mm^2 and has a center frequency of 12GHz with a -6.8415dB insertion loss, -10.053dB return loss, and bandwidth of 86MHz, covering the frequency ranges from 11.966GHz to 12.052GHz. A downconverter is also designed to convert 12GHz to 1GHz at Ku-Band downlink for satellite receiver. The downconverter is designed with bandwidth range 475MHz between 11.776GHz to 12.241GHz frequencies. The satellite receiver of all three designed components

(LNA, BPF, DC) is simulated with a transmitter in tropical environment by AWGN channel using Visual Simulation System (VSS). The simulation shows the evaluation changes of BER in clear air and in the atmospherically losses. The simulated results for $A_{0.1\%}$, $A_{0.01\%}$, and $A_{0.001\%}$ availability in vertical, horizontal, and circular polarizations show the performance of BER in transmission losses. The performance of the designed receiver at clear air and raining condition has been investigated using various modulation schemes. The performance during raining condition has also been investigated using vertical, horizontal, and the circular polarizations with different availabilities and presented in this thesis. A substantial development in the performance of the satellite receiver can be noted when using the proposed design.

This work achieves and receives till $A_{0.1\%}$ availability; by using multistage of this LNA design may solve the problems of rain fade at $A_{0.01\%}$ and $A_{0.001\%}$ availability. As targeted results for the proposed satellite receiver design, the simulated results in this thesis show a perfect lower bit error rate of the performance for this design, with a comparison between the 16-PSK and 16-QAM, and the comparison is successfully done. In order to achieve 10dB for the availability $A_{0.1\%}$ in vertical-polarization, the comparison demonstrates that the simulated value of 16-PSK is 1.9067e-006 in clear air and 3.1473e-006 with rain effect. The 16-QAM achieves 0.0023046 in clear air and 0.0027505 with rain effect. So the $A_{0.1\%}$ availability give better results for 16-PSK than the results in 16-QAM at vertical, horizontal, and circular polarizations. Furthermore, in rain condition and in order to achieve 10^{-4} BER for $A_{0.1\%}$ availability with vertical polarization, the 16-PSK modulation scheme needs 8.2dB, and for 16-QAM modulation scheme needs 12dB. But in horizontal polarization the 16-PSK needs 12.4dB, and for 16-QAM needs 13.2dB for $A_{0.1\%}$ availability with the same polarization.

6.2 FUTURE WORK

The simulated results in this thesis provide a strong foundation for future work in awareness the tropical regions factors. One recommended area for future work is in increasing the gain by using multi stage of the low noise amplifier design to reach until 20dB to cope with the different polarization at $A_{0.01\%}$ availability, in order to observe and test the design performance in tropical regions environment. Therefore, more refinement research should be done in the field of the satellite receiver design with different availabilities in RF microwave communications system, especially in tropical regions with high frequency.

This performance evaluation is based on simulation only. It is recommended to constructing the receiver and testing it in real environment.

BIBLIOGRAPHY

Abbas, T., and Bin Ihsan, M. (2005). "Design of a two stage Low Noise Amplifier at Ku Band," *Microelectronics, ICM. The 17th International Conference*, pp. 40.IEEE. Munich, Germany.

Ain, M.F., Hassan, S.I.S., Mandeep, J.S., Igarashi, K., Tanaka, K., and Iida, M. (2007, August). "Design of 11 GHz Ku-Band Amplifier," *Engineering Letters*, 15:1, EL_15_1_5, 15.

Anerao, V. M., Pillai, J.S., Chande , J.V., and Krishnan, S. (2009). "Parallel Coupled Microstrip Band Pass Filter," *Second International Conference on Emerging Trends in Engineering and Technology*, ICETET- IEEE, Nagpur.

Applied Wave Research, (2006, June) Inc, MWO/VSS/AO, *Element Help*.

Applied Wave Research, (2007, June) Inc, MWO/VSS/AO, *Getting Started Guid*e, Version 7.5.

Ayaki, N., Inoue, A., Katoh, T., Komaru, M., Noda, M., Kobiki, M., Nagahama, K., and Tanino, N. (1988). "A 12 GHz-band monolithic HEMT low-noise amplifier," *Gallium Arsenide Integrated Circuit (GaAs IC) Symposium. Technical Digest*, 10th Annual IEEE. Tech Dig, pp 101- 104, Nashville, TN.

Bazak, Jr., H. V., Hendrix, C. E., Naya, K. F., and Reinhardt, V. F. (1994). "A Simple Depolarization Compensator for Very Wideband Communication Links - An Experimental Evaluation", *Topical Meeting on Silicon Monolithic Integrated Circuits in RF Systems*. Digest of Papers, COM-42(5), 2073-2077. IEEE, Garmisch.

Boglione, L., Pollard, R. D., and Postoyalko, V. (1999). "12 GHz MMIC Series Feedback LNA Based on a Novel Analytical Design Procedure for Simultaneous Noise and Power Match," *The 29th European Microwave Conference*, IEEE, Munich,Germany.

Breed, G. (2003, January). "Bit Error Rate: Fundamental Concepts and Measurement Issues," *High Frequency Electronics*, Summit Technical Media, LLC.

Buettrich, S., and Pascual, A. E. (2005, September). "Itrainonline MMTK Radio Link Calculation Handout,".

Chang, D., Yom, I., and Lee, S. (2003). "Development of a Receiver Downconverter Module for Ka-band Satellite Payload," *Electronics and Telecommunications Research Institute*, Taejon, 305-350, IEEE, South Korea.

Dafalla, Z., David S., and Abdel Rahrnan, A. (2004). "Low Noise Amplifier Design for LEO Satellite Applications," *Information and Communication*

Technologies: From Theory to Applications, International Conference on Malaysia, IEEE, Malaysia.

Davis, W., Agarwal, K. (2001). *Radio Frequency Circuit Design*. New york: John Wiley & Sons.

Elbert, B.R. (2008). *Introduction to Satellite Communication*. Third Edition, London: Artech House, Boston.

Farag, I.S., Kotkata, M.F., Selim, M.M., Battisha I.K., and El- Rafaay, M.M. (2004). "Study of the Structural Characteristics of α- Alumina Doped with Different Cations," *J. Solids*, Vol. (27), No. 2, Egypt.

Gil, J., Han, K., and Shin, H. (2003, July). "13 GHz 4.67 dB NF CMOS low-noise amplifier," *Electron. Lett*, vol. 39, no. 14, pp. 1056–1058.

Gilbert, B. (2008, June). "Noise Figure and Logarithmic Amplifiers", *Analog Dialogue*,Vol 42.

Hao, Y. Zu, B. and Huang, P. (2008). "An Optimal Microstrip Filter Design Method Based on Advanced Design System for Satellite Receiver," *Proceedings of IEEE International Conference on Mechatronics and Automation*. Takamatsu.

Hori, S. Kamei, K. Shibata, K. Taematsu, M. Mishima, K. and Okano, S. (1983). "GaAs monolithic MICs for direct broadcast satellite receivers," *IEEE MTT-S International Microwave Symposium Digest* , pp. 59-64. Boston, MA, USA.

Hughes, B., Perdomo, J., and Kondoh, H. (1993, December). "12 GHz Low-Noise MMIC Amplifier Designed with a Noise Model that Scales with MODFET Size and Bias," *IEEE Transactions on Microwave Theory and Techniques*. Vol.41. No. 12. Santa Rosa.

Islam, Md. F., Ali, M. A. M., and Majlis, B. Y. (2007). "Miniaturized Bandpass Filter for Ku-band Applications," *The 5th Student Conference on Research and Development*, IEEE, Malaysia.

Itoh, H., Sugiura, T., TSUJI, T., Honjo, K., and Takayama, Y. (1983). "12- GHz band low-noise GaAs monolithic amplifier," *Electron Devices*, IEEE MTT-S Dig. pp 54-58.

Jeong, J. C., Lim, Y. H., Jang, B., Yom, I., and Lee, S. (2002). "Development of Ku-band Receiver/Downconverter for Satellite Transponders," *Communications Satellite Development Center ETRI-Radio & Broadcasting Technology Laboratory*, 305-350, IEEE,Korea.

Jia, X., Na, Y., Bingxia, S., and Quanming, Z. (2009). "The Miniaturization Design of Microstrip Interdigital Bandpass Filter," *2nd International Conference on Power Electronics and Intelligent Transportation System*, IEEE, China.

Lee, J., Lee, S., Lee, J. C., Kim, J. H., Lee, B., Jeon, S. H., Pa, J. W., and Kim, N. Y. (2004). "Low Power and Small Sized Ku-band MMIC Low Noise Block

Downconverter Design using InGaP/GaAs HBT Process," *Microwave Symposium Digest, MTT-S International*, IEEE, South Korea.

Lee, J., Shin, H., Park, C.H., and Kim, N.Y. (2005, April). "A Low-Power Ku-Band Downconverter in InGaP–GaAs HBT Technology," *Microwave and Wireless Components Letters*, VOL. 15, NO. 4, IEEE, South Korea.

Long, S. (2007). "Design of Low Noise Amplifiers," ECE145A/ECE218A.

Monstein, C. (2002). "Figuring noise figure," HB9SCT, Wiesenstrasse 13, CH-8807 Freienbach, Switzerland,

Moradian M., and Oraizi, H. (2007). "Optimum design of microstrip parallel coupled-line band-pass filters for multi-spurious pass-band suppression," *The Institution of Engineering and Technology*, pp. 488–495, IEEE,Iran.

Niclas, K.B., Gold, R. B., Wilser, W. T., and Hitchens, W. R. (1978, August). "A 12-18 GHz Medium-Power GaAs MESFET Amplifier," *IEEE Journal of Solid state circuits*, vol. SC-13, NO. 4.

Pearce, J. (2000). "Eb/N0 Explained," issue of Spread Spectrum Scene Online.

Pozar, D. (1998). *Microwave Engineering*. 2nd ed., New York: John Wiley and Sons.

Pozar, D.M. (2001). *Microwave and RF Design of Wireless systems*. 2nd ed., New York: John Wiley and Sons.

Pratt, T., Bostian, C. W. and Allnutt, C. W. (2003). *Satellite Communication*. Second Edition. New York: McGraw Hill.

Rahman, A.K., Anuar, M.S., Aljunid, S.A., and Junita, M.N. (2008, August 26-27). "Study of rain attenuation consequence in free space optic transmission," *Proceedings of IEEE 6th National Conference on Telecommunication Technologies and IEEE 2nd Malaysia Conference on Photonics*, Putrajaya, Malaysia.

Recommendation ITU-R P.453-9, (2003). "The Radio Refractive Index: Its Formula and Refractivity Data,".

Recommendation ITU-R P.618-8T, (2003). "Propagation data and prediction methods required for the design of Earth-space telecommunication systems,".

Recommendation ITU-R P.837-4, (2003). "Characteristics of precipitation for propagation modeling,".

Recommendation ITU-R P.838-2, (2003). "Specific attenuation model for rain for use in prediction methods,".

Recommendation ITU-R P.839-3, (2001). "Rain height model for prediction methods,".

Rene, T., Bruin, G., Wassink, B., and Zanen, B. (2001, 5-8 November). "*Preservation of Archives in Tropical Climates*", Jakarta.

Sahoolizadeh, H., Kordalivand, A., and Heidari, Z. (2009). "Design and Simulation of Low Noise Amplifier Circuit for 5 GHz to 6 GHz", *World Academy of Science, Engineering and Technology*. IEEE, Iran.

Sakuno, K., Yoshimasu, T., Matsumoto, N., Tsukao, T., Nakagawa, Y., Suematsu, E., and Tomita, T. (1992). "A Miniature Low Current GaAs MMIC Downconverter for KU-Band Broadcast Satellite Applications," *Central Research Laboratories,* SHARP Corporation Microwave and Millimeter-Wave Monolithic Circuits Symposium, IEEE, Japan.

Sakuno, K., Yoshimasu, T., Matsumoto, N., Tsukao, T., Nakagawa, Y., Suematsu, E., and Tomita, T. (1992, June). "A miniature low current GaAs MMIC downconverter for Ku-band broadcast satellite applications," *IEEE Microwave and Millimeter- Wave Monolithic Circuits Symp*. Dig, pp. 101-104. Albuquerque.

Scappaviva, F., Cignani, R., Florian, C., Vannini, G., Filicori, F., and Feudale, M. (2008, October). "10 Watt High Efficiency GaAs MMIC Power Amplifier for Space Applications," *Proceedings of the 3rd European Microwave Integrated Circuits Conference*, IEEE, Amsterdam.

Schad, K.-B., Erbent, U., Sacnmcz, E., Abele P., and Schuinaclier, H. (2000). "A Ku Band SiGe Low Noise Amplifier," *Topical Meeting on Silicon Monolithic Integrated Circuits in RF System, Digest of Papers*, D-89069, IEEE, Germany.

Shiga, N., Nakajima, S., Kuwata, N., Otobe, K., Sekiguchi, T., Matsuzaki, K., and Hayashi, H. (1992, October). "Monolithic pulse-doped MESFET LNA for DBS downconverter," *GaAs IC symp Tech Dig*, PP 127-130. Japan.

Shiga, N., Nakajima, S., Otobe, K., Sekiguchi, T., Kuwata, N., Matsuzaki, K., and Hayahi, H. (1991, Dec.). "X-band MMIC amplifier with pulsed-doped GaAs MESFETs," *Microwave and Millimeter-Wave Monolithic Circuits Symposium*. Microwave Theory Tech, Digest of Papers, vol 39, pp. 1987-1994. IEEE,Yokohama.

Stratakos, G. E., Uzunoglu N. K. (12-1 4 Sep 1995). "Design of a MMIC Low Noise Amplifier at 10GHz," *Proc. 20th International Conference Microelectronics (MIEC95)*, Vol 2, IEEE, Serbia.

Tsukada, H., Kanazawa, K., Oishi, Y., Takenaka, H., Nishiuma, M., Hagio, M., and Kazumura, M. (1990). "A 12-GHz-band MMIC low noise amplifier with low Rg and low Rn HEMT's," *The 3rd Asia-Pacific Microwave Conf. Proc*, pp 955-958, Tokyo.

Van de Kamp, M.M.J.L, Tervonen, J. K., Salonen, E. T., and Poiares Baptista, J.P.V. (1998, October). "Improved Models for Long-Term Prediction of Tropospheric Scintillation on Slant Paths", *First International Workshop on Radiowave*

Propagation Modelling for Sat Com Services at Ku-band and above, ESA/ESTEC, Noordwijk.

Wang, C. S., and Wang, C. K. (2006). "A90 nm CMOS Low noise amplifier using noise neutralizing for 3.1-10.6 GHz UWB System," *proceedings of the 32nd European Solid state circuits Conference*, pp. 251-4, IEEE, Montreux.

Wang, Y., Fu, Y., Cui, W., and Ma, W. (2008, March 24-28). "A Broadband Low Noise Amplifier Design," *National Key Laboratory of Space Microwave Technology Xi'an Institute of Space Radio Technology*, Xi'an 710100, China.

www.ecmwf.int/research/demeter/verification/maparea2.html#top

Xiong, F. (2006). "*Digital Modulation Techniques*," Boston.

Yamane, M., Mori, M., Takahashi, S., and Noda, M. (1990). "Low-noise 2DEGFET MMIC amplifier for DBS," *The 3rd Asia-Pacific Microwave Conf. Proc*, pp 951-954, Tokyo.

PUBLICATIONS

1. Md. Rafiqul Islam, A.H.M. Zahirul Alam, Sheroz Khan, & Arafat A. A Shabana. (11-13 May 2010) “Design of a Low Noise Amplifier with GaAs MESFET at Ku_Band,” International Conference on Computer and Communication Engineering (ICCCE), IEEE, Department of Electrical and Computer Engineering, Faculty of Engineering, International Islamic University Malaysia P.O. Box: 10, 50728 Kuala Lumpur, Malaysia.

2. Md. Rafiqul Islam & Arafat A. A Shabana (August 2009) “Link Budget and Rain Attenuation Calculations for the Transmission from MEASAT_2 and ARABSAT_2B (The differences between Malaysia and Palestine)”, Poster of Research for a Better Tomorrow, University of Nottingham Malaysia Campus.

3. IIUM Research, Invention and Innovation Exhibition IRIIE 2011, “Design of Satellite Receiver at Ku-Band for Tropical Region” Poster for Department of Electrical and Computer Engineering, Faculty of Engineering, International Islamic University Malaysia P.O. Box: 10, 50728 Kuala Lumpur, Malaysia.

APPENDIX A

LOW NOISE N76038a at Ku-BAND GaAs MESFET

FEATURES:

Low noise figure: 1.8 dB typical at 12 GHz.

High associated gain: 7.5 dB typical at 12 GHz.

L_G = 0.3 μm, W_G = 280 μm.

Low cost plastic packaging.

Tape & reel packaging option available.

DESCRIPTION:

N76038a is a high performance gallium arsenide metal semiconductor field effect transistor in a plastic package. Its low noise figure makes this device appropriate for use in the first or second stages of low noise amplifiers operating in the 1 - 14 GHz frequency range. The device is fabricated using ion implantation for improved RF and DC performance, reliability, and uniformity. These devices feature a recessed 0.3 micron gate and triple epitaxial technology.

NEC's stringent quality assurance and test procedures ensure the highest reliability and performance.

Electrical characteristics (T_A = 25°C)

PART NUMBER PACKAGE OUTLINE			N76038a		
SYMBOLS	PARAMETERS AND CONDITIONS	UNITS	MIN	TYP	MAX
NF_{OPT}[1]	Optimum Noise Figure at V_{DS} = 3 V, I_{DS} = 10 mA f = 4 GHz f = 12 GHz	 dB dB		 0.8 1.8	 1.2
G_A	Associated Gain at V_{DS} = 3 V, I_{DS} = 10 mA f = 4 GHz f = 12 GHz	 dB dB	 12.0	 13.0 7.5	
I_{DSS}	Saturated Drain Current at V_{DS} = 3 V, V_{GS} = 0 V	mA	15	30	50
V_P	Pinch-off Voltage at V_{DS} = 3 V, I_{DS} = 0.1 mA	V	-3.0	-0.8	-0.5
g_m	Transconductance at V_{DS} = 3 V, I_{DS} = 10 mA	mS	30	40	70
I_{GSO}	Gate to Source Leakage Current at V_{GS} = -3 V	µA			10

Note:

1. Typical values of noise figures are those obtained when 50% of the devices from a large number of lots were individually measured in a circuit with the input individually tuned to obtain the minimum value. Maximum values are criteria established on the production line as a "go-no-go" screening test with the fixture tuned for the "generic" type but not for each specimen.

ABSOLUTE MAXIMUM RATINGS[1] (T_A = 25°C)

SYMBOLS	PARAMETERS	UNITS	RATINGS
V_{DS}	Drain to Source Voltage	V	5
V_{GD}	Gate to Drain Voltage	V	-5
V_{GS}	Gate to Source Voltage	V	-3
I_{DS}	Drain Current	mA	I_{DSS}
P_{IN}	RF Input (CW)	dBm	+15
T_{CH}	Channel Temperature	°C	150
T_{STG}	Storage Temperature	°C	-65 to +150
P_T	Total Power Dissipation	mW	240
R_{TH}[2, 3]	Thermal Resistance	°C/W	1250

Notes:
1. Operation in excess of any one of these parameters may result in permanent damage.
2. R_{TH} for plastic package mounted on glass epoxy substrate is 965°C/W.
3. R_{TH} for chip mounted on copper heat sink is 190°C/W.

TYPICAL NOISE PARAMETERS (T_A = 25°C)

V_{DS} = 3 V, I_{DS} = 10 mA

FREQ. (GHz)	NF_{OPT} (dB)	G_A (dB)	Γ_{OPT}		Rn/50
			MAG	ANG[1]	
0.5	0.40	21.67	0.84	5	0.79
1.0	0.45	20.01	0.82	10	0.75
2.0	0.60	18.88	0.76	28	0.70
4.0	0.80	15.53	0.66	58	0.61
6.0	1.10	13.24	0.55	101	0.50
8.0	1.35	11.32	0.50	152	0.40
10.0	1.60	9.49	0.48	-166	0.31
12.0	1.80	8.15	0.54	-130	0.25
14.0	2.10	7.11	0.63	-105	0.20
16.0	2.30	6.54	0.70	-87	0.15
18.0	2.55	5.68	0.77	-75	0.12

Note:
1. Γ_{OPT} is referenced to the bend of the lead, as shown on back page.

TYPICAL PERFORMANCE CURVES (T_A = 25°C)

TOTAL POWER DISSIPATION vs. AMBIENT TEMPERATURE

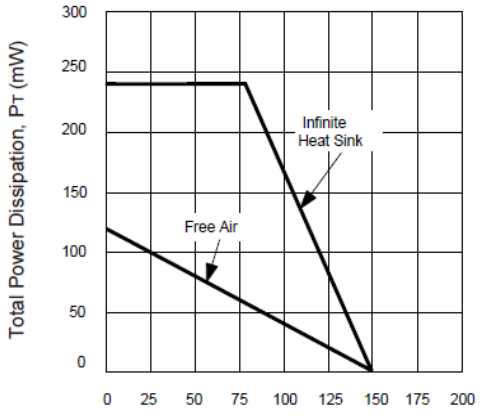

DRAIN CURRENT vs. GATE TO SOURCE VOLTAGE V_{DS} = 3 V

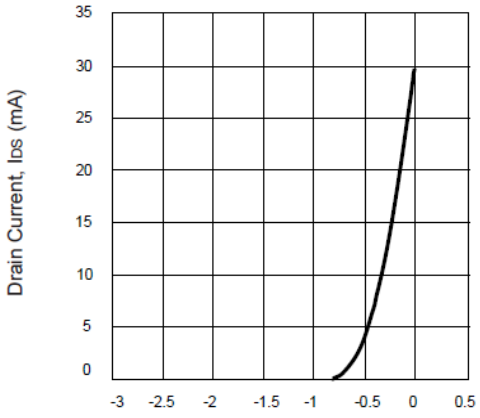

DRAIN CURRENT vs. DRAIN TO SOURCE VOLTAGE

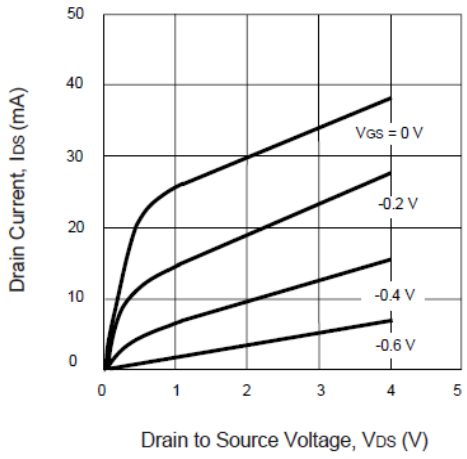

SCHEMATIC

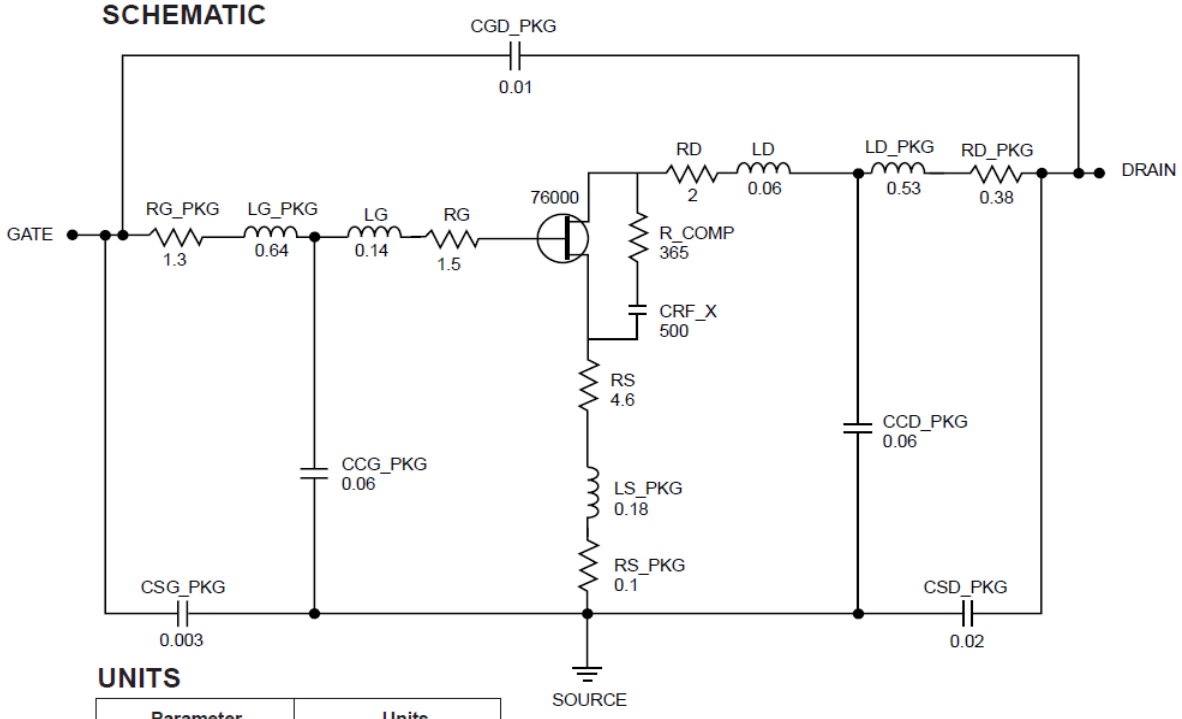

UNITS

Parameter	Units
capacitance	picofarads
inductance	nanohenries
resistance	ohms

MODEL RANGE
Frequency: 0.1 to 18 GHz
Bias: V_{DS} = 3 V, I_D = 10 mA to 30 mA

OUTLINE DIMENSIONS (Units in mm)

PACKAGE OUTLINE 38